Diagenetic History of the Lower Port au Port Group Carbonates in Western Newfoundland

by

©Noel Clement Shembilu

A thesis submitted to the

School of Graduate Studies

In partial fulfillment of the requirements for the degree of

Master of Science

Department of Earth Sciences

Memorial University of Newfoundland

August 2021

St. John's Newfoundland

ABSTRACT

The investigated Middle–Upper Cambrian carbonates span, from bottom to top, the uppermost Hawke Bay (40 m), the March Point (~83 m thick), and the lowermost Petit Jardin (~47 m) formations of the Port au Port Group (western Newfoundland, Canada). The deposits consist of dolomitized shallow-water carbonates ranging from microbial mudstones to oolitic grainstones. Petrographic examination of the March Point and Petit Jardin carbonates reveals three generations of dolomite: (i) micritic to near-micritic (D1, 4 µm −35 µm) fabric-retentive dolomite, (ii) coarse crystalline sucrosic (D2, 60 µm−150 µm) fabric-destructive dolomite (sub- to euhedral zoned rhombs with clear rim and cloudy core), and (iii) coarse anhedral (D3, >0.5 mm) fracture-filling saddle dolomite. The microthermometric measurements of primary two-phase fluid inclusions retained in D2, and D3 samples yielded homogenization temperatures (T_h) showing a general increase with burial. The mean values of T_h and salinity are 89.1 ± 6.4 ^{o}C vs 21.2 ± 2.2 eq. wt% NaCl, and 110 ± 8.2 ^{o}C vs 21.1 ± 4.7 eq. wt% NaCl, respectively. The dolomites show a decrease of Sr from D1 (90 ± 44 ppm) to D3 (47 ± 15 ppm), which reflects the influence of progressive burial. The estimated $\delta^{18}O$ values of the D1 parent fluid (−5 to −10‰ VSMOW) are bracketed by those suggested for the Middle Cambrian meteoric and seawaters. The fluid-inclusion gas analyses provided CO_2/CH_4 and N_2/Ar ratios coherent with the conclusions from the petrographic examination and geochemical compositions.

A multi-technique evaluation of the preservation of carbonates was applied by using several petrographic and chemical screening tools. The $\delta^{13}C$ and $\delta^{18}O$ values of dolomicrites (−1.2 ± 1.1 ‰ VPDB and −6.7 ± 1.3 ‰ VPDB, respectively) exhibit an insignificant correlation ($R^2 = 0.16$) and similarly, the $\delta^{13}C$ values with their Mn/Sr ratio ($R^2 = 0.02$). This supports the preservation of at least near-primary $\delta^{13}C$ signatures that can be utilized to construct a high-resolution $\delta^{13}C$ profile for reliable global correlations. The $\delta^{13}C$ profile exhibits two major negative excursions, the lower excursion (~4 ‰) immediately below the lower boundary of the March Point Formation (Hawke Bay/March Point boundary) and the upper excursion (~2 ‰) almost at the lower boundary of the Petit Jardin Formation where these excursions are likely associated with short-term sea level changes. The trilobite biozonation scheme suggests the correlation of the lower excursion with the DICE (Drumian Carbon Isotope Excursion) event and the upper excursion with the base of the SPICE (Steptoean Positive Carbon Isotope Excursion) counterpart and both events have been globally documented on different paleocontinents.

The variations in several proxies of bioproductivity (e.g., P, Ni, and Cu), input of weathering products (Mn, Fe, Al, and ∑REE), and paleoredox (e.g., Th/U) have been utilized to study the paleoenvironmental conditions during the investigated time interval. Distinct positive shifts in the profiles of Al, ∑REE, Mn, and Fe have been associated with the negative shifts recorded by the $\delta^{13}C$ profile and correlated with the DICE (Middle Cambrian) and base of the SPICE (lowermost Upper Cambrian) events.

They reflect contributions from detrital weathered material during sea level falls. Similar correlated positive shifts are also documented by the P, Ni, and Cu profiles, thus suggesting an increase in the riverine inputs of nutrients associated with the drop of sea level and increase of weathering activities. In addition, the changes in the bioproductivity and weathering proxies were associated with relative rising in the Th/U ratios (0.1 to 8.3), which reflects variations in the redox state towards relatively more oxidizing conditions.

ACKNOWLEDGEMENTS

I would like to express sincere appreciation to my supervisor Professor Dr. Karem Azmy for his management, guidance, support, critical reading and correcting of the thesis and the chance to pursue this research study. Special thanks also to Dr. Elliot Burden for his constructive comments on the thesis. This project was supported by funding (to Karem Azmy) from Petroleum Exploration Enhancement Program (PEEP) and Mitacs Canada.

The author also wishes to thank Allison Pye (Stable Isotope Lab) as well as Drs. Bleuenn Gueguen and Marie-Laure Rouget (Trace Element Lab, Institut Universitaire Europeen de la Mer, France) for technical assistance in chemical analyses.

Lastly, I would like to thank my family, especially my parents and brother, and friends for the encouragement and support that they gave me to study in a foreign country. I am very appreciative to everything they have done to help me.

TABLE OF CONTENTS

LIST OF TABLES

LIST OF FIGURES

LIST OF APPENDICES

Co-Authorship Statement

The thesis is constructed in manuscript format and consists of six chapters. Chapter I is an introduction that reviews the background literature and outlines the main objectives of the study. Chapters II and III represent the geologic settings, litho- and biostratigraphy, structured in three research papers (Chapters V), two of them have been already published in Marine and Petroleum Geology (Sections 5.1 and 5.2) and the third one has been also submitted to Marine and Petroleum Geology (section 5.3). The final chapter (Chapter VI) summarizes the overall conclusions of the three papers and the study significance.

The mainframe for the three research studies of the thesis was designed by Prof. Karem Azmy. As the primary author, I was responsible for all aspects of the research project, reviewing the literature, formulating the research questions, performing the laboratory work, analyzing and interpreting the data, and preparing the manuscripts. Meanwhile, the co-author (Prof. Karem Azmy) guided the research progress, offered advice for analysing and interpreting the data and corrected the manuscripts before submission. Dr. Nigel Blamey handled analyses of fluid-inclusion gas ratios and corrected the related part in the manuscript of the first paper (Section 5.1).

Section 5.1 (Chapter V) entitled “Origin of Middle-Upper Cambrian Dolomites on eastern Laurentia: a case study from Belle Isle Strait, western Newfoundland” has been published in the Journal of Marine and Petroleum Geology, volume 125, p. 104858. **Section 5.2 (Chapter V)** entitled “Carbon-isotope stratigraphy of the Middle–Upper

Cambrian in eastern Laurentia: Implications for global correlation” has been also published in the Journal of Marine and Petroleum Geology, volume 128, p. 105052., while **Section 5.3** entitled “Trace element variations across the Middle–Upper Cambrian carbonates: Implications for the paleoenvironment of eastern Laurentia” has been published in the Journal of Marine and Petroleum Geology, volume 135, p. 105385.

CHAPTER I

INTRODUCTION AND OVERVIEW

Dolomites have been the focus of many studies that discussed their origins including, environments (e.g., Azmy et al., 2008; Hu et al., 2012; Huang et al., 2014; Hou et al., 2015) and dolomitizing fluids (e.g., Zhang et al., 2008; Conliffe et al., 2009, 2010; Vandeginste et al., 2013; Jacquemyn et al., 2014) due to their scientific values in sedimentary geology and economic importance as potential reservoirs for hydrocarbons (Mazzullo and Chilingarian, 1996; Honarmand and Amini, 2012; Rong et al., 2012; Li et al., 2015a). Dolostones, in many cases, develop higher porosity than surrounding limestones because dolomitization is a significant diagenetic process that influences porosity development and hence the accumulation and flow of hydrocarbon in carbonate reservoirs (Allan and Wiggins, 1993; Sun, 1995; Wang et al., 2015).

Although many recent studies were directed towards the Lower Ordovician dolomites (St. George Group) of the eastern Laurentian margin in western Newfoundland (e.g., Haywick, 1984; Lane, 1990; Cooper et al., 2001; Lavoie et al., 2005; Azmy et al., 2008, 2009; Conliffe et al., 2009; Azmy and Conliffe, 2010; Azomani et al., 2013; Hou et al., 2015), the dolomitization of Middle-Upper Cambrian in the area has not been investigated in detail, particularly when dolomites are known to vary in different aspects including the texture, composition, and origin (Machel and Mountjoy, 1986; Machel, 2004).

In addition, the Cambrian Period holds a pivotal role in the evolution of Paleozoic biosphere, where carbonates record large variations of $\delta^{13}C$ reflecting global changes in the carbon isotopic compositions of the oceans, seawater oxygenation, atmospheric O_2, and biological innovation (e.g., Saltzman et al., 1998, 2000; Maloof et al., 2010). In the Port au Port Group of western Newfoundland, the Cambrian biostratigraphy is mainly based on a trilobite biozonation scheme that provided sufficient information to date various components of the sequence and can be correlated with the standard North American faunal zones (e.g., Lochman, 1938; Kindle and Whittington, 1965; Palmer, 1969; Levesque, 1977).

The globally correlated Drumian carbon isotope excursion (DICE) and Steptoean carbon isotope excursion (SPICE) are significant events that represent major perturbations of the global carbon cycle during the Late Cambrian. This is reflected by the major global physical and biological changes (e.g., Saltzman et al., 1998, 2000; Zhu et al., 2006; Maloof et al., 2005; Kouchinsky et al., 2008; Peng et al., 2009; Hammer and Svensen, 2017).

The Cambrian Period represents a critical stage of evolution of life in the oceans and the appearance of first shelly organisms in the Phanerozoic seawater. Lime mudstones are abundant in Cambrian carbonate successions and have been widely used in global stable isotope chemostratigraphic correlations (e.g., Derry et al., 1992; Kaufman et al., 1993; Veizer et al., 1999; Hill and Walter, 2000; McKirdy et al., 2001). Preservation of carbonates is the foundation for the reconstruction of paleoenvironmental conditions that dominated during the Earth's history (Wignall and Twitchett, 1996; Veizer et al., 1999). Micritic carbonates, including dolomicrites that are common in the currently Middle-Upper carbonates, have been found at times to retain their near primary $\delta^{13}C$ signatures (e.g., Land, 1992; Chang et al., 2021; Liang and Jones, 2021; Liyuan et al., 2021).

The Eustatic sea level variations during the Late Cambrian influenced the redox conditions and organic primary productivity as well as the terrestrial inputs of weathered material into the oceans. This also affected the contents of trace elements, including total rare-earth elements (∑REE), in the ocean water and the deposited marine carbonates (e.g., Wignall and Twitchett, 1996; Arnaboldi and Meyers, 2007). Therefore, these eustatic events result in variations in elemental compositions of the marine carbonates such as those of P, Si, Al, U, Ni, Cu and ∑REE (e.g., Arnaboldi and Meyers, 2007; Wignall et al., 2007; Azmy et al., 2015; Wang and Azmy, 2020) and also lead to changes in the redox conditions, which are reflected by the relative changes in the Th/U ratios (e.g., Sholkovitz and Shen, 1995; Wignall and Twitchett,1996; Kimura et al., 2005).

The March Point Formation, the lowermost part of the Port au Port Group is formed of mixed shales, sandstones, and carbonates (Chow and James, 1987, 1992). These sedimentary rocks might contain sufficient organic matter to become a source that can constitute a part of a hydrocarbon system if some of the carbonate interbeds are porous and sealed by non-porous overlying sediments particularly when shales from neighboring basins are, to some extent, organic rich (Weaver and Macko, 1988). However, no evaluation, even preliminary, of the organic contents of the Port au Port Group shales have been documented yet. Therefore, understanding the paleoenvironment and redox conditions during the precipitation of carbonates will shed light on the main conditions that dominated during the deposition of the entire succession.

1.1 Objectives

The main objectives of this study are:

- To investigate the origin and all diagenetic history of the dolomites of the Port au Port Group especially those of the Petit Jardin and March Point formations.
- To identify (petrographically and geochemically) the dolomitization phases that influenced the rocks and the origin and nature of the dolomitizing fluid of each phase to deduce the diagenetic controls on porosity development if applicable.

- To evaluate the impact of diagenesis on the petrography and geochemistry of micritic carbonates of the lower Port au Port Group at the Strait of Belle Isle (north-western Newfoundland), and
- To establish a reliable C-isotope profile that allows the identification of the SPICE and DICE events to enhance the global correlation of the Middle and Upper Cambrian of eastern Laurentia.
- To investigate the influence of sea level changes on trace element geochemistry of ocean water during Middle to Late Cambrian to better understand the paleoenvironmental conditions that dominated during that time interval.
- To understand the associated changes of paleoredox conditions.

CHAPTER II

GEOLOGIC SETTING AND STRATIGRAPHIC FRAMEWORK

2.1 Geologic settings

The Port au Port Group consists of mixed carbonate and siliciclastic sediments that crop out on the Port au Port Peninsula forming a belt approximately 400 km long and 75 km wide (Fig. 2.1; Williams, 1976, 1979; Chow and James, 1987a). These deposits are part of the autochthonous Cambro-Ordovician sequence (Upper Cambrian–Lower Ordovician: shallow water carbonates changing into basinal shales) that comprise the tectono-stratigraphic Humber Zone of the northern Appalachian Orogen (Williams, 1976, 1979; Chow and James, 1987a). The Port au Port Group is believed to represent shallow marine deposition on the outer part of a stable, low-latitude shelf that bordered the Iapetus Ocean and reflects the gradual transition from Early Cambrian siliciclastic sediments to Early Ordovician carbonates (Fig. 2.2; Williams, 1976, 1979; Chow and James, 1987a; Lavoie, 1994; Lavoie et al., 2008).

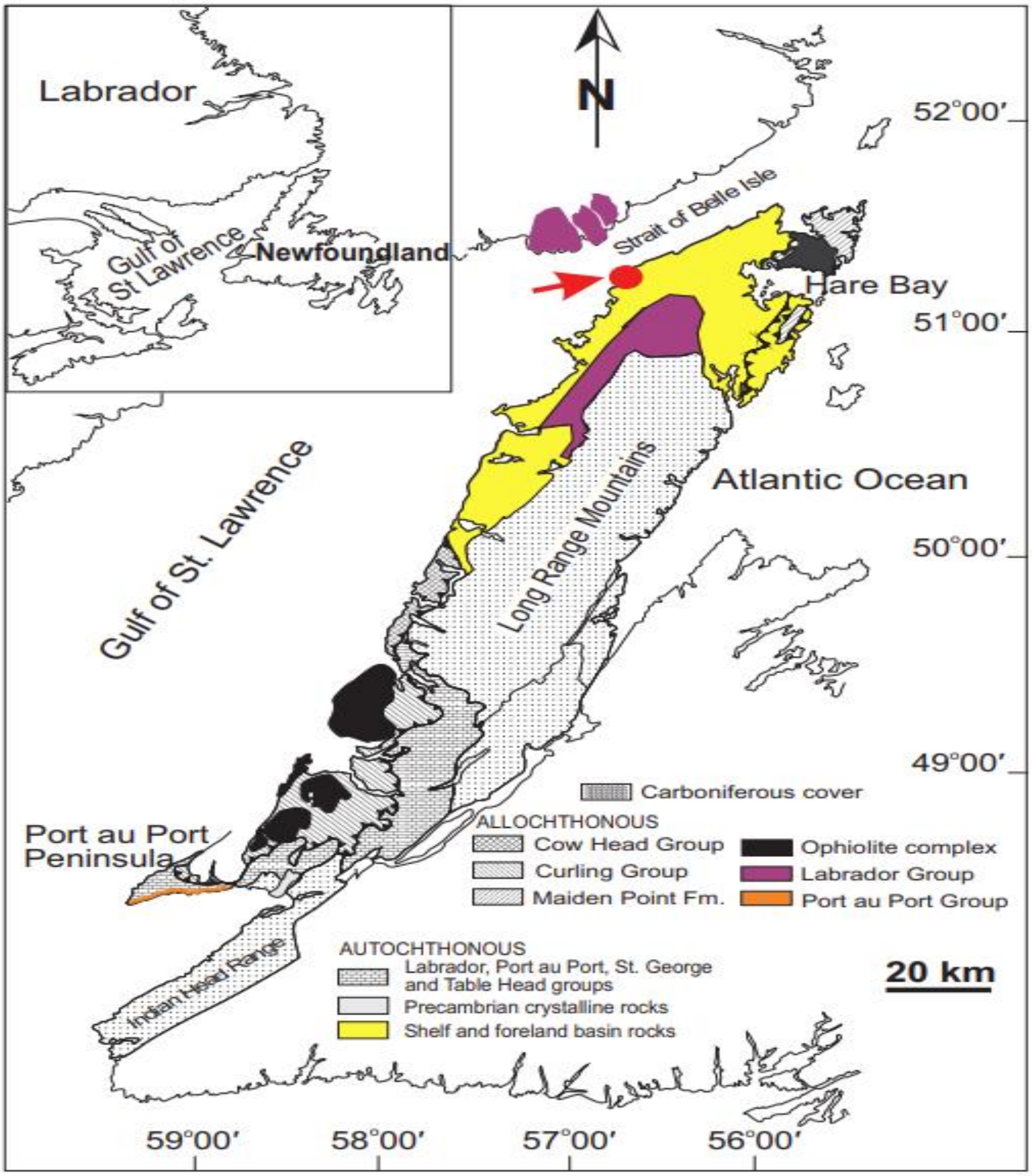

Fig. 2.1. Map of the study area showing the location (arrow) of the sampled core, NF-02 (Appendix 1) at the Strait of Belle Isle (51^{o}30’00.0” N; 56^{o}29’56.0” W), which spans the Port au Port Group carbonates in Western Newfoundland, Canada (modified from Zhang and Barnes).

Uplift, faulting, and exposure on the Port au Port Peninsula during the Late Devonian Acadian Orogeny resulted in the development of karst topography on the exposed Cambrian and Ordovician carbonates (Dix, 1981). The Middle and Upper Cambrian shallow-marine strata of this part of the tectono-stratigraphic Humber Zone of the Appalachian Orogen (Williams, 1976; 1979) records the growth and demise of a continental margin of Iapetus. The paleographic reconstructions suggest that sediments on the outer part of the stable shelf were located at approximately 25° S, within the sub-tropical climate zone (Scotese et al., 1979). They comprise a part of an eastward-thickening prism of Lower Cambrian to Middle Ordovician volcanics, siliciclastics and carbonates that rest uncomformably on the Grenvillian crystalline basement (Rodgers, 1968; Williams and Stevens, 1974; James and Stevens, 1982).

The eastern side of the outcrop belt is either covered by Carboniferous rocks or disappears into White Bay. The western side passes under the Gulf of St. Lawrence and is tectonically overlain by allochthonous rocks (Chow and James, 1987a). Equivalent strata in Quebec and Ontario (Canada) are predominantly sandstone and conglomerate.

2.2 Lithostratigraphy

The Port au Port Group carbonates vary between laminated lime mudstones to packstones and oolitic grainstones (Chow and James, 1987a).

However, they are almost entirely dolomitized in the subsurface beneath the Strait of Belle Isle (Fig. 2.1; Core NF-02), and dominated by microbial/peloidal lime mudstones, and occasionally interbedded with shales (Fig. 2.2). The dolomicrites in core NF-02 constitute the lower Port au Port Group that spans the March Point (~83 m thick) and the lowermost Petit Jardin (~47 m thick) formations. The Petit Jardin Formation is believed to rest conformably on the March Point Formation since no unconformity has yet been documented between the March Point and the Hawke Bay formations (Fig. 2.2). The lime mudstone consists mainly of laminated to massive gray dolomicrites that may have cemented vugs.

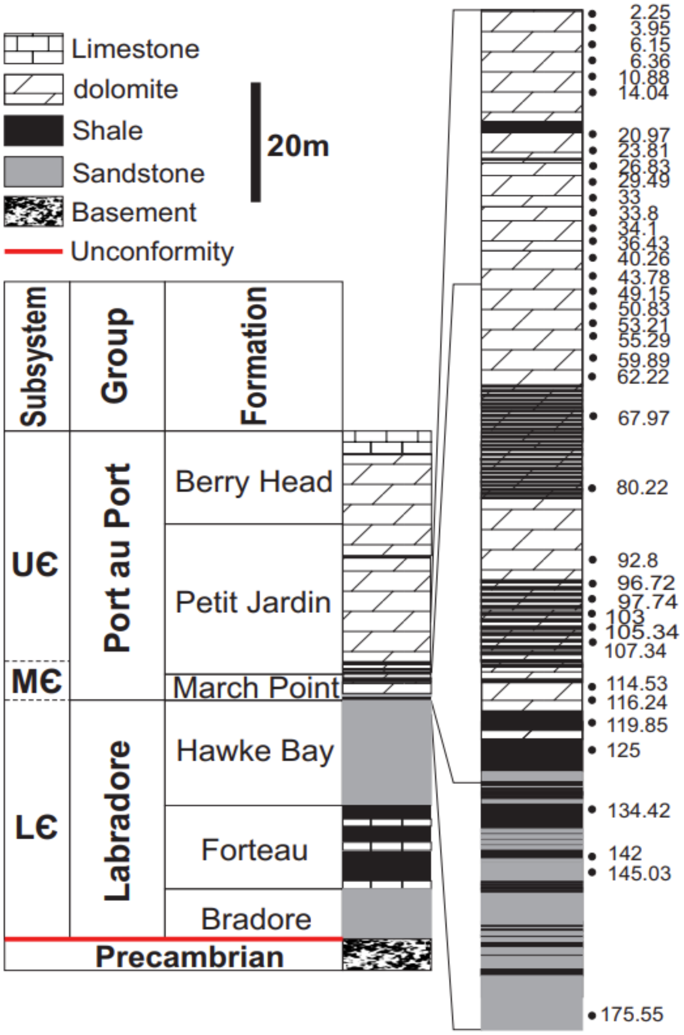

Fig. 2.2. Stratigraphic framework of the investigated dolomicrites from Strait of Belle Isle in western Newfoundland, showing the positions of investigated samples.

2.3 Biostratigraphy

Accordingly, the Cambrian system has been subdivided into three series, the Lower Cambrian (Hawke Bay Formation) marked by *Bathyuricus-Elthrina* and *Bonnia-Olenellus* trilobite zones, Middle (March Point Formation) spanning the

Bolaspidella, and Upper Cambrian (Petit Jardin Formation) having trilobites ranging from *Cedaria* to *Taenicephalus* (Lochman, 1938; Levesque, 1977).

The trilobite biozonation scheme of the Petit Jardin Formation (Fig. 2.3) includes the *Cedaria*, *Crepicephalus*, *Dunderbagia, Elvina* and *Taenicephalus* zones, which span the Dresbachian to early Franconian stages of Upper Cambrian (Lochman, 1938; Troelsen, 1947; Levesque, 1977). There are three zones (the *Aphelaspis*, *Dicanthopyge* and *Prehousia*; Levesque, 1977) compressed into a short stratigraphic interval between the *Crepicephalus* and the *Dunderbergia* zone (Fig. 2.3), indicating a possible depositional break and/or interval of condensed sedimentation near the Dresbachian-Franconian boundary (Fig. 2.3), although no surface unconformity has been physically recognized in the investigated core or documented in the earlier study of outcrops (Chow and James, 1987a,b; 1992). The March Point Formation contains trilobites of the *Bathyuriscus-Elrathina* and *Bolaspidella* zones indicating a late-Middle Cambrian age (Lochman, 1938; Levesque, 1977; Boyce, 1977). Trilobites gathered from the lower half of the underlying Hawke Bay Formation (*Bonnia-Olenellus* zone) indicate a latest Early Cambrian age (Boyce, 1977; Levesque, 1977). No fossils from the intervening *Plagiura-Poliella*, *Albertella* or *Glossopluera* zones (Early to Middle Cambrian) have been yet discovered, signifying that either the upper part of the Hawke Bay sandstones is partly of Middle Cambrian age, or a hiatus (the

Hawke Bay Event) may occur near the Hawke Bay-March Point contact as suggested by Palmer and James (1979).

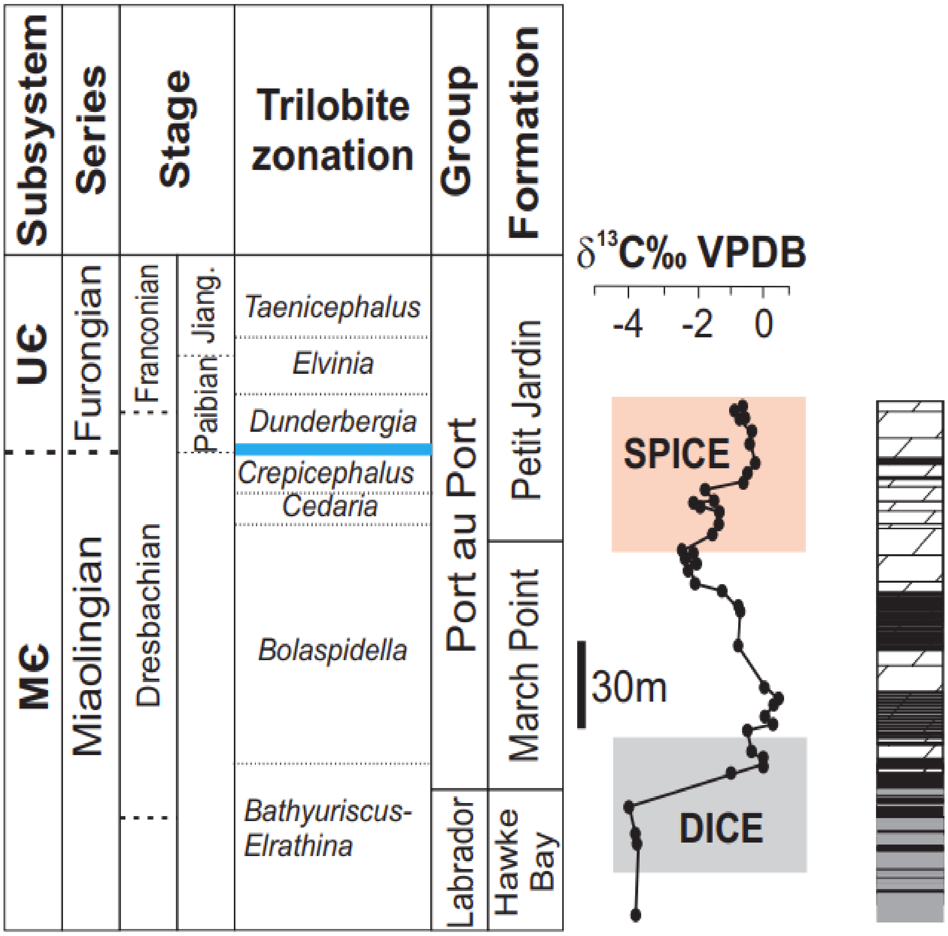

Fig. 2.3. The δ^{13}C profile of the investigated Middle–Upper Cambrian Belle Isle carbonates (from Shembilu and Azmy, 2021) and their trilobite biozonation scheme (after Lochman, 1938; Kindle & Whittington, 1965; Palmer, 1969; Levesque, 1977). The Blue line represents the compressed biozones (the Aphelaspis, Dicanthopyge, and Prehousia; Levesque, 1977). Legend as in Figure 2.2. Detail in text.

CHAPTER III

METHODOLOGY

3.1 Sampling and thin sections

Samples were collected from Core NF-02 (Appendix 1, Fig. 2.2) a geotechnical and engineering borehole drilled in the strait of Belle Isle (51°30’00.0” N, 56°29’56.0” W), western Newfoundland. The sampling interval was generally between 30 cm and 2 m (Fig. 2.2) but the frequent occurrences of shale and sandstone interbeds (Fig. 2.2) made, in some cases, the sampling interval wider. The sampled interval spans the uppermost part (40 m) of the Hawke Formation (uppermost Lower Cambrian) of the Labrador Group, the entire March Point Formation (83 m, Middle Cambrian) and the lowermost part (43 m) of the Petit Jardin Formation (uppermost Middle Cambrian) of the Port au Port Group (Fig. 2.2).

The thin sections were cut, stained with Alizarin Red-S and Potassium ferricyanide solutions (Dickson, 1966; Lindholm and Finkelman, 1972) and examined under standard polarizing microscope and cathodoluminoscope for petrographic features where the most micritic spots were identified. A mirror-image slab of each thin section was also polished and cleaned with de-ionized water prior to microsampling the different carbonate generations for geochemical analyses. Cathodoluminoscence (CL) was performed using a

Technosyn cold cathodoluminoscope operated at ~12kV accelerating voltage and ~0.7 mA gun current intensity.

3.2 Microthermometry

Fluid-inclusion microthermometry (Appendix 2) was conducted on double polished thick sections (wafers), using a calibrated Linkam THMSG 600 heating-freezing stage. Calibration with precision of ± 0.2 ^oC at −56.6 ^oC and ± 1^oC at 300 ^oC was established using synthetic H_2O and CO_2 fluid inclusion standards. The initial (T_i), final ice melting temperature ($T_{m(ice)}$) and the homogenization temperatures (T_h) were measured in primary two-phase fluid inclusions following the procedures outlined by Shepherd et al., (1985). Aqueous fluid salinities were calculated using $T_{m(ice)}$ and the equation of Bodnar (2003) and a program by Chi and Ni (2007) for the system of H_2O-NaCl-$CaCl_2$.

3.3 Stable isotope analyses

The polished slabs were washed with deionized water and dried overnight at 45°C. Approximately 10 mg were microsampled from the cleaned slabs under a binocular microscope using a low speed microdrill. For C- and O-isotope analyses (Appendix 1), about 200 µg of powder sample was reacted in inert atmosphere with ultrapure concentrated (100%) orthophosphoric acid at 70°C in a Thermo-Finnigan Gasbench II. The CO_2 produced from the reaction was automatically flushed through a Thermo-Finnigan Delta V plus isotope ratio mass spectrometer in a stream of Helium, where the gas was ionized and measured for isotope ratios. Uncertainties of better than 0.1‰ (2σ) for the analyses were determined by repeated measurements of NBS-19 ($\delta^{18}O$ = –2.20‰ and $\delta^{13}C$ = +1.95‰ vs. VPDB) and L-SVECS ($\delta^{18}O$ = –26.64‰ and $\delta^{13}C$ = –46.48‰ vs. VPDB) as well as internal standards during each run of samples.

3.4 Elemental analyses

For elemental analyses (Appendix 1), the sample powders were weighted in Teflon beakers, then a mix of HCl-HNO3 was added to the samples for digestion and an additional step of HF-HNO3 for the BHVO2 standard. The samples were dissolved in 5 mL HCl 6N for archiving, followed by a split of 1 mL (by weight) from the HCl 6N archive solution was evaporated to dryness. Lastly, a subset of a sample powder (~10 mg per sample) was digested in 2.5% (v/v) pure HNO_3 acid with Indium as the internal standard for 70-80 minutes and analyzed for Ca, Mg, Sr, Mn, and Fe as well as rare earth elements (REE) using HR-ICP-MS Thermo Scientific Element XR in which the internal standard indium was used to correct the signal drift. The analyses were done at European Institute for Marine Studies (IUEM) located in Brest, France. The relative uncertainties of the measurement are better than 5% using BHVO2 and internal standards. Calculations of major and trace element concentrations are based on an insoluble residue-free basis (100% soluble dolomite or calcite).

The Rare Earth Elements (REE) concentrations are normalized to the Post-Archean Australian Shale (PAAS, McLennan, 1989) and anomalies of Cerium $(Ce/Ce^*)_{SN} = Ce_{SN}/(0.5La_{SN} + 0.5Pr_{SN})$ and Lanthanum $(Pr/Pr^*)_{SN} = Pr_{SN}/(0.5Ce_{SN} + 0.5Nd_{SN})$ were calculated with the formulae of Bau and Dulski (1996). The latest calcite cement (C3) is very rare. It is not possible to extract sufficient material for geochemical analyses.

3.5 Fluid-inclusion gas analyses

The fluid-inclusion gas analysis protocol was described by Norman et al., (1996, 1997, 2002); Norman and Blamey (2001); Norman and Moore (2003) and Parry and Blamey (2010). Samples were gently crushed by hand and sieved in a 30-mesh sieve, where the smaller fraction was discarded. The +30 mesh size fraction was first washed in 20% KOH, agitated then decanted. The grains were washed repeatedly with deionized water and air-dried. Gas analyses were conducted with a dual quadrupole mass spectrometer system (two Prisma spectrometers) using the crush-fast scan method (Norman et al., 1996,1997, 2002; Norman and Blamey, 2001; Norman and Moore, 2003; Parry and Blamey, 2010). About 150 mg of prepared samples was incrementally crushed under vacuum (~10^{-8} Torr) to open multiple fluid inclusions thereby releasing gases, which are analyzed with the mass spectrometers. The measured volatiles include H_2, He, CH_4, H_2O, N_2, O_2, H_2S, Ar, CO_2, SO_2, C_2-C_4 alkanes and alkenes, and C_6H_6

(Appendix 3). The system was calibrated with commercial gas mixtures, in-house standards, and natural fluid inclusion standards following the protocol described by Norman and Blamey (2001), Azmy and Blamey (2013), and Blamey et al., (2015). Precision and accuracy vary with species. H_2 could be reliably detected at 50 ppm, He at <0.5 ppm. Precision for the major gas species CO_2, CH_4, N_2 and Ar is better than 5%, whereas it is ~10% for the minor species.

CHAPTER IV

RESULTS

4.1 Petrography

The investigated Port au Port carbonates are almost entirely dolomitized in the Belle Isle area (cf. Chow and James, 1987, 1992) and the crosscut relationships reveal a possible paragenetic sequence which is summarized in (Fig. 4.1). Petrographic examinations reveal 3 main generations of dolomite (D1, D2, and D3) and a very late phase of rare calcite cement (C3).

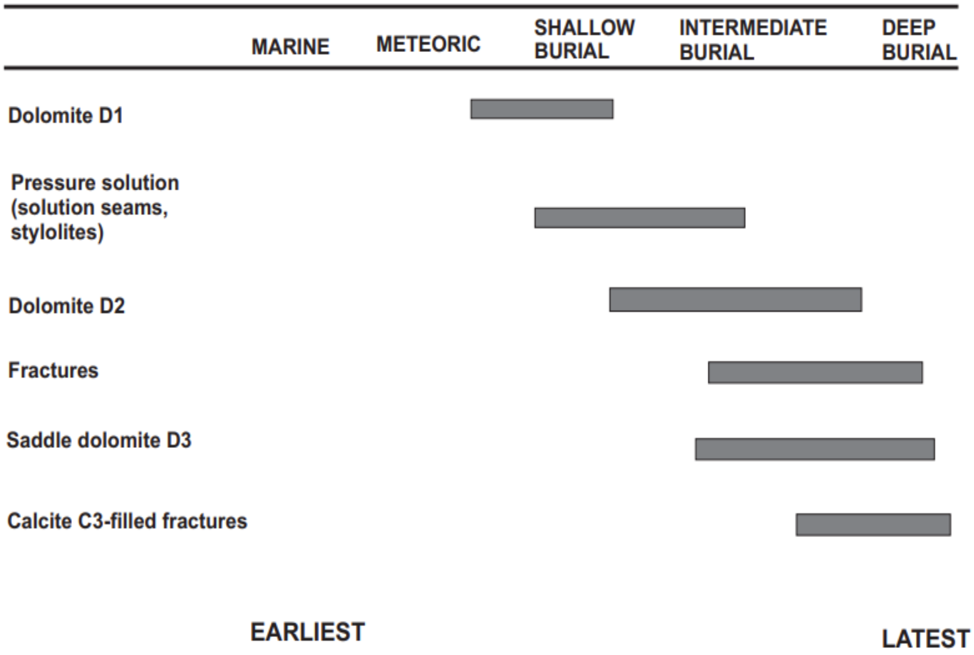

Fig. 4.1. Paragenetic sequence of the main diagenetic events that influenced the Strait of Belle Isle carbonates based on petrographic relationships.

Dolomite 1 (D1 – dolomicrite) is the most abundant type (ca. ~55%) and dominated by fabric-retentive micritic to near-micritic dolostones (dolomicrites) that have insignificant organic matter that ranges from 4 to 35 µm. It is generally mimetic (Sibley, 1982; Budd, 1997; Azomani et al., 2013; Olanipekun et al., 2014) and preserves sedimentary fabrics (Fig. 4.2a). Also, it is usually tightly packed (non-porous), non-planar mosaic crystals, with irregular intercrystalline boundaries and exhibit dull CL (Fig. 4.2b; Machel and Mountjoy, 1986; 1990) to non-CL (Fig. 4.3a–b).

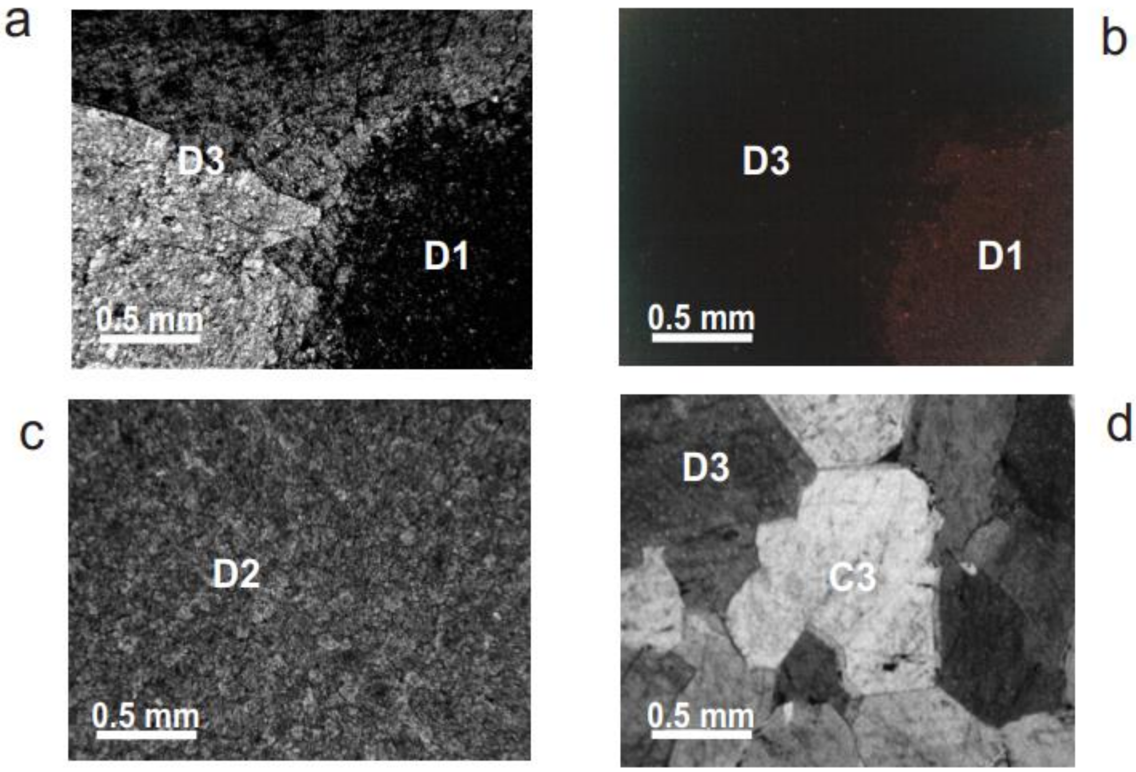

Fig. 4.2. Photomicrographs of petrographic features of the investigated dolomites. (a) Dolomite D1 and D3 (crossed polars: sample 33.8), (b) Cathodoluminescence image of (a) showing dull CL of D1 and D3 (c) Dolomite D2 in plane polarized (Sample 49.15), and (d) fracture- and vug-filling D3 and C3 in crossed polars (Sample 33.8).

Dolomite 2 (D2) is less abundant (ca. ~40%) but has coarser crystals than those of D1 and appears grey in hand specimens. It is replacive, fabric destructive, and easily distinguished from D1 by its tight (non-porous) sucrosic texture (e.g., Azomani et al., 2013; Olanipekun et al., 2014). It consists of inclusion-rich, sub- to euhedral zoned rhombs (clear rim and cloudy core; Fig. 4.2c) that are crosscut by microstylolites (e.g., Azmy et al., 2008) and range from

60 µm to up to 150 µm but may appear entirely non-CL under the cathodoluminoscope (Fig 4.2d). No intercrystalline porosity occurs in D2.

Rare vugs (25–130 µm) and late fractures (30–100 µm wide) crosscut D1 and D2 and are always filled with Dolomite 3 (D3; ca. ~5%), that appear distinctively milky-white in polished slabs. It is occasionally replacive and consists of coarse sub– to anhedral crystals (>0.5 mm, Fig. 4.2a). It displays undulose (sweeping) extinction and commonly has non-planar boundaries (Fig. 4.2b), typical features of saddle dolomite (Budd, 1997; Warren, 2000; Hou et al., 2016; Feng et al., 2017).

The dolomites are almost entirely non-porous. The vugs and late fractures are filled with calcite cement (C3) that postdates D3 (Fig. 4.2a) and exhibit non-CL (Fig. 4.2b). So too, they are occasionally replaced by quartz.

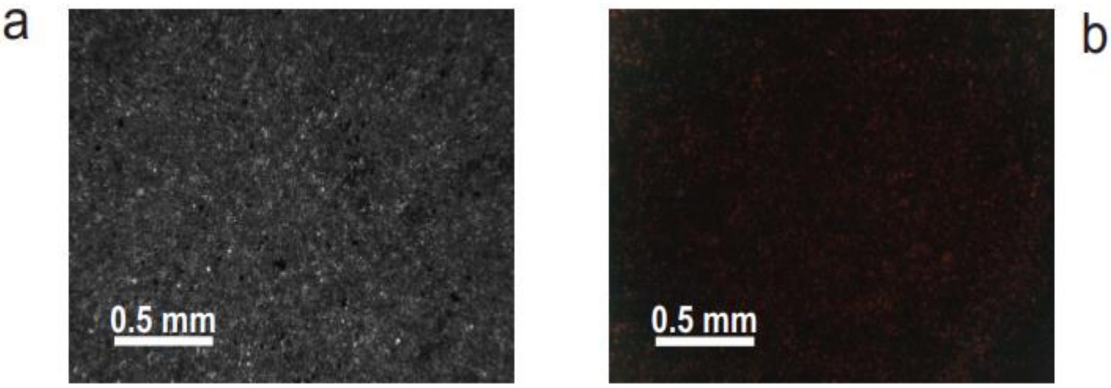

Fig. 4.3. Photomicrographs of (a) Dolomicrite (crossed polars: Sample 36.4), (b) CL image of (a).

4.2 Fluid Inclusions

Microthermometric measurements of primary aqueous two-phase (liquid-vapor) fluid inclusions from D2, D3 and C3 provide consistent melting (T_m) and homogenization temperatures (T_h) and estimates of salinity (Goldstein and Reynolds, 1994; Chi and Ni, 2007) for each cement phase. They are listed in Appendix 2 and their statistics are summarized in Table 4.1 and Figure 4.4a–d. The measured T_h provides an estimate of minimum entrapment temperatures. The examined inclusions were carefully selected (not stretched) to be parallel to crystal facets, and with the vapor bubble size within 10 to 15% of the total inclusion size (Goldstein and Reynolds, 1994). Fluid inclusions found within the D1 crystals were too small to be measured. The fluid inclusions in D2 yielded a range of T_h from 78.2 to 100.2 ^{o}C (89.1 ± 6.4 ^{o}C, *n* = 18; Fig. 4.4a) and final ice-melting temperatures (T_m) from −23.9 to −13.5 ^{o}C (−18.5 ± 3.0 ^{o}C, *n* = 18; Table 4.1), and salinities from 17.3 to 24.9 eq. wt.% NaCl (21.2 ± 2.2 eq. wt.% NaCl, *n* = 18; Fig. 4.4d). Those from D3 have T_h from 95.5 to 125.6 ^{o}C (110 ± 8.2 ^{o}C, *n* = 33; Fig 4.4b), final (T_m) from −32.8 to −5.6 ^{o}C (−18.9 ± 5.9 ^{o}C, *n* = 33; Table 4.1), and salinities from 8.7 to 30.5 eq. wt.% NaCl (21.1 ± 4.7 eq. wt.% NaCl, *n* = 33; Fig. 4.4b). The C3 crystals provided T_h values from 93.3 to 118.1 ^{o}C (105.3 ± 7.2 ^{o}C, *n* = 17; Fig. 4.4c), final (T_m) from −24.8 to −17.4 ^{o}C (−20.9 ± 2.1 ^{o}C, *n* = 17; Table 4.1), and salinities from 20.5 to 25.4 eq. wt.% NaCl (23.0 ± 1.4 eq. wt.% NaCl, *n* =

17; Fig. 4.4b). Despite a wider range of estimated salinity of D3 compared with that of D2 (Fig. 4.4d), their mean values are almost identical (Table 4.1) but that of C3 is slightly higher. The mean T_h values of D3 and C3 appear to be comparable but higher than that of D2.

Table 4.1. Summary of statistics of microthermometric measurements of the investigated Port au Port Group carbonates.

Host mineral		$T_{m(ice)}$(^{O}C)	Eq. Wt% NaCl	T_h(^{O}C)
D2	*n*	18	18	18
	Mean	-18.5	21.2	89.1
	S.D	3.0	2.2	6.4
	Max	-13.5	24.9	100.2
	Min	-23.9	17.3	78.2
D3	*n*	33	33	33
	Mean	-18.9	21.1	110.0
	S.D	5.9	4.7	8.2
	Max	-5.6	30.5	125.6
	Min	-32.8	8.7	95.5
C3	*n*	17	17	17
	Mean	-20.9	23.0	105.3
	S.D	2.1	1.4	7.2
	Max	-17.4	25.5	118.1
	Min	-24.8	20.5	93.3

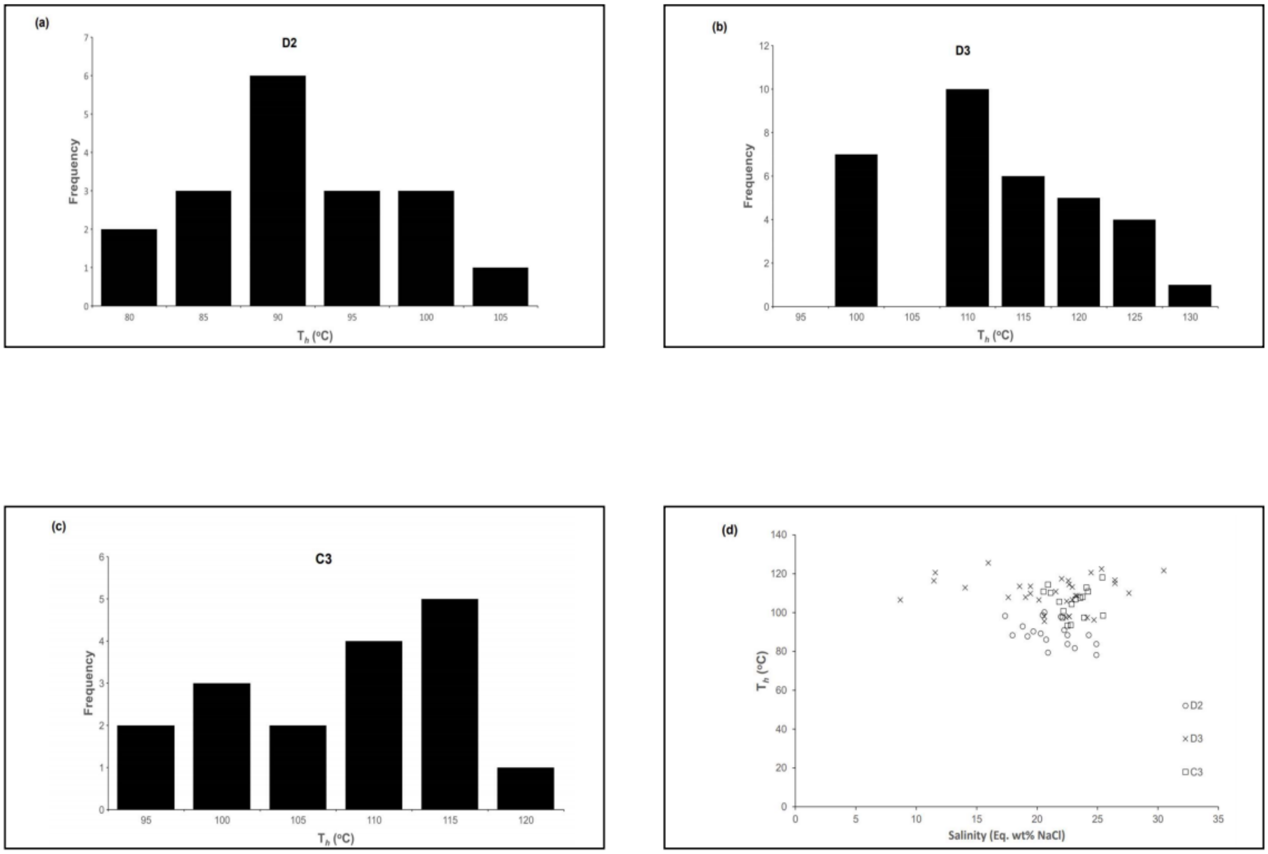

Fig. 4.4. Plot of microthermometric data from primary two-phase fluid inclusions of D2, D3, and C3 carbonated phases showing histograms of T_h values of (a) D2, (b) D3, and (c) C3, and (d) scatter diagram of estimated salinity (Bodnar, 2003) vs. T_h values of D2, D3 and C3.

4.3 Carbon and oxygen isotopes

Table 4.2 summarizes the statistics for the stable isotope composition of carbonates (Appendix 1). The mean $\delta^{13}C$ value of D1 is slightly lower than that of D3 (−1.2 ± 1.1 and −0.8 ± 0.7‰, respectively) but D2 (−1.6 ± 1.4‰) is relatively the lowest (Fig. 4.5b). However, the mean $\delta^{18}O$ values (Table 4.2) decrease from

−6.7 ± 1.3‰ (VPDB) in D1 to −9.7 ± 1.7‰ (VPDB) in D3. The mean δ^{18}O value of D2 (−7.6 ± 1.2‰ VPDB) is slightly higher than those of D3 (−9.7 ± 1.7‰ VPDB) and D1 (Table 4.2; Fig. 4.5b). Although the D1 and D2 δ^{18}O values show significant overlap, those from D3 are very distinct and mainly cluster outside (Fig. 4.5b).

Table 4.2. CaCO3, MgCO3, Fe, Mn, Sr, REE, δ18O, δ13C statistics for the investigated dolomites.

Phase		δ^{13}C‰ VPDB	δ^{18}O‰ VPDB	CaCO$_3$ %	MgCO$_3$ %	Fe	Mn	Sr	La	Ce	Pr	Nd	Sm	Eu	Gd	Tb
D1	*n*	38	38	33	33	33	33	33	33	33	33	33	33	33	33	33
	Mean	-1.2	-6.7	53.7	46.2	21465	857	90	8.69	20.05	2.28	8.64	1.48	0.35	1.42	0.18
	S.D.	1.1	1.3	2.9	2.8	19355	396	44	7.57	17.40	1.88	6.97	1.16	0.27	1.10	0.15
	Max	0.3	-4.1	57.0	53.6	83975	2261	264	31.14	77.59	7.40	25.86	4.54	1.07	4.39	0.57
	Min	-3.9	-10.9	46.1	43.0	4087	296	30	1.90	4.11	0.47	1.76	0.30	0.07	0.28	0.00
D2	*n*	14	14	9	9	9	9	9	9	9	9	9	9	9	9	9
	Mean	-1.6	-7.6	55.1	44.9	25199	1120	69	6.503	14.325	1.719	6.582	1.143	0.279	1.096	0.153
	S.D.	1.4	1.2	1.8	1.8	18039	589	22	4.379	10.022	1.273	4.846	0.869	0.214	0.836	0.117
	Max	0.3	-6.1	58	48	60803	2471	101	17.652	39.558	4.887	18.634	3.334	0.803	3.163	0.438
	Min	-4.2	-9.7	52	42	4523	334	40	2.099	4.360	0.465	1.769	0.302	0.068	0.282	0.042
D3	*n*	11	11	9	9	9	9	9	9	9	9	9	9	9	9	9
	Mean	-0.8	-9.7	56.0	44.0	17400	953	47	5.854	24.670	3.794	15.552	2.933	0.669	2.968	0.375
	S.D.	0.7	1.7	0.7	0.7	4253	276	15	4.595	19.484	3.333	14.632	3.441	0.941	3.310	0.483
	Max	-0.3	-6.4	57	45	22604	1583	82	15.767	66.270	11.947	52.981	12.352	3.286	11.529	1.710
	Min	-2.3	-11.7	55	43	11480	689	34	1.725	3.432	0.399	1.504	0.257	0.061	0.586	0.036

*All trace element concentrations are in ppm

Phase		Dy	Ho	Er	Tm	Yb	Lu	U	∑REE	Ce/Ce*	Pr/Pr*	Al (ppm)	P (ppm)	Ni (ppm)	Cu (ppm)	Th (ppm)	V (ppm)	Mo (ppm)
D1	*n*	33	33	33	33	33	33	33	33	33	33	33	33	33	33	33	33	33
	Mean	0.95	0.17	0.47	0.06	0.44	0.06	0.83	45.2	1.03	1.02	13133	280	12	7	2.14	18.79	1.05
	S.D.	0.67	0.13	0.33	0.05	0.32	0.05	0.60	37.3	0.07	0.04	17467	350	10	9	2.81	18.46	1.51
	Max	2.50	0.42	1.06	0.16	1.12	0.17	2.39	154.3	1.21	1.11	75238	1697	39	36	10.73	79.35	7.16
	Min	0.21	0.00	0.10	0.00	0.07	0.00	0.16	9.7	0.91	0.91	872	30	2	1	0.03	2.90	0.00
D2	*n*	9	9	9	9	9	9	9	9	9	9							
	Mean	0.795	0.157	0.410	0.060	0.387	0.058	1.120	33.7	0.99	1.03							
	S.D.	0.613	0.122	0.314	0.046	0.295	0.044	0.649	23.8	0.06	0.05							
	Max	2.238	0.434	1.094	0.154	0.965	0.138	2.354	93.5	1.11	1.11							
	Min	0.233	0.048	0.137	0.022	0.152	0.023	0.544	10.0	0.91	0.94							
D3	*n*	9	9	9	9	9	9	9	9	9	9							
	Mean	1.760	0.307	0.681	0.083	0.471	0.065	0.190	59.9	1.07	1.11							
	S.D.	2.276	0.379	0.783	0.085	0.435	0.056	0.225	52.9	0.08	0.04							
	Max	8.034	1.344	2.789	0.304	1.570	0.201	0.615	190.1	1.19	1.16							
	Min	0.181	0.037	0.099	0.014	0.092	0.015	0.006	7.9	0.94	1.03							

*All trace element

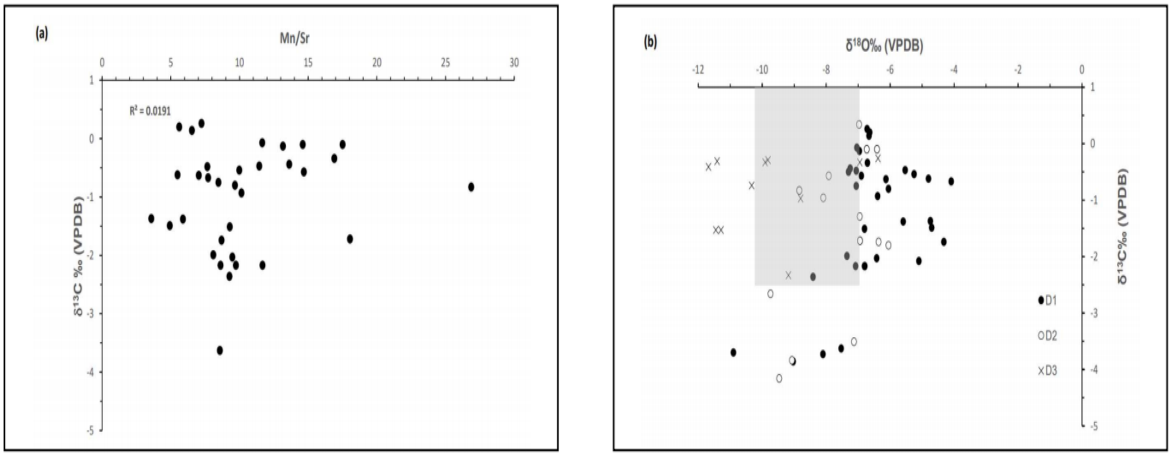

Fig. 4.5. Scatter diagrams showing correlations of (a) Mn/Sr and (b) δ^{18}O with δ^{13}C of dolomicrites from the Port au Port Group. The rectangle in (b) marks the isotopic composition of the best-preserved Middle–Upper Cambrian carbonates (Veizer et al., 1999).

The mean δ^{13}C and δ^{18}O values for carbonates (−1.2 ± 1.1 and −6.7 ± 1.3 ‰ VPDB, respectively; Table 4.2) are comparable to their counterparts of the Upper Cambrian carbonates in the neighboring basins (e.g., Green point and Martin Point in western Newfoundland; Azmy, 2019a,b). The δ^{13}C values almost fall entirely within the documented range for well-preserved Middle–Upper Cambrian marine carbonates (Fig. 4.5b; Veizer et al., 1999) but many of the $\delta^{18}O$ values are higher than those of the best-preserved carbonates (Fig. 4.2b). The $\delta^{13}C$ profile exhibits a smaller negative shift of ~4 ‰ and an upper one of ~2 ‰ (Fig. 2.1) that peaks at the base of a positive excursion and the global C-isotope chemostratigraphic correlations of the SPICE and DICE events documented in sections from different paleocontinents (Fig. 5.2). Additionally, the individual profiles of the paleoenvironmental proxies show also distinct and consistent positive shifts associated with those excursions on the $\delta^{13}C$ profile (Fig. 5.4).

The calculated $\delta^{18}O$ values for the D1 parent fluid range from approximately −5 to −10‰ VSMOW while the estimated $\delta^{18}O$ values of the parent fluids of D2 and D3 are from +1 to +2‰ VSMOW and from +2 to +4‰ VSMOW, respectively (Fig. 5.1).

4.4 Major and minor elements

The geochemical compositions of carbonates are listed in Appendix 1 and their statistics are summarized Table 4.2. The Calcium contents of dolomites are very comparable where the mean $CaCO_3$ % values of D1 (53.7 ± 2.9%, *n* = 33) and D2 (55.1 ± 1.8%, *n* = 9) are almost similar and that of D3 (56.0 ± 0.7%, *n* = 9) is only slightly higher. Despite the general overlap in the elemental compositions

(Fig. 4.6a–b), their statistical parameters (Table 4.2), particularly the mean values, may still reveal some trends. The Mn contents vary from 857 ± 396 ppm in D1 to 953 ± 276 ppm in D3 and those of Fe decrease from 21465 ± 19355 ppm to 17400 ± 4253 ppm, respectively whereas those of D2 are 1120 ± 589 ppm and 25199 ± 18039 ppm, respectively (Fig. 4.6a). The Sr concentrations (Table 4.2; Fig. 4.6b) decreases from 90 ± 44 ppm in D1 to 69 ± 22 ppm in D2 and drops to minimal a value of 47 ± 15 ppm in D3. The C3 cement is very rare and insufficient for microdrilling sample powder for C3 crystals geochemical analyses.

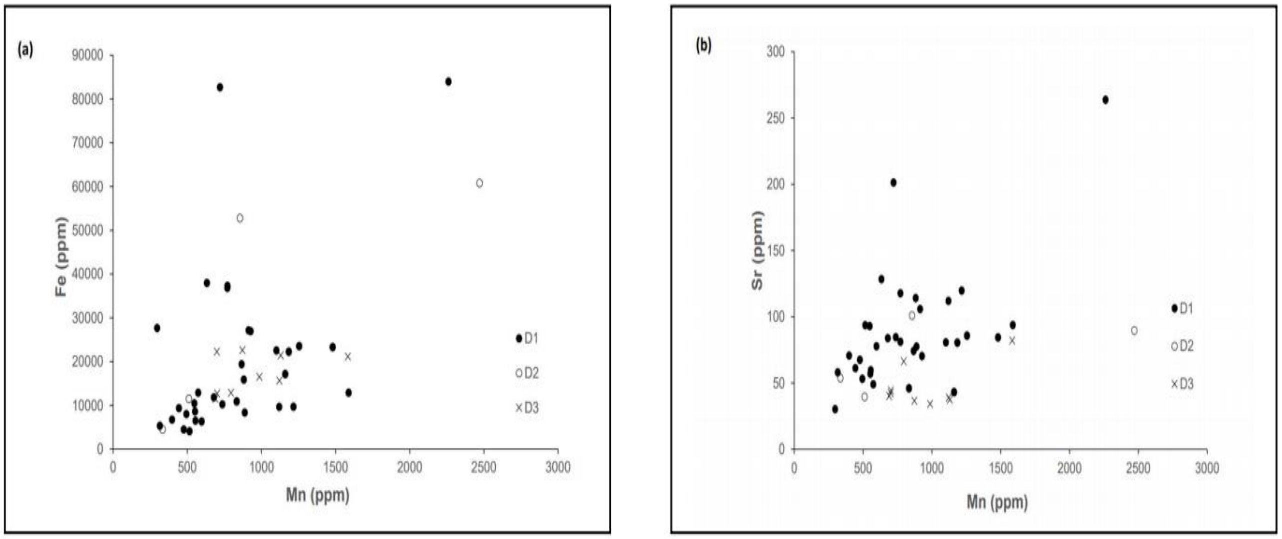

Fig. 4.6. Scatter diagrams of Mn vs (a)Fe and (b) Sr for dolomites.

The concentrations of the paleoenvironmental proxies (e.g., Śliwiński et al., 2010; Pattan et al., 2013; Acharya et al., 2015; Liyuan et al., 2021), including P, Ni, Cu (bioproductivity), Al, ∑REE, Mn, Fe (weathering), and Th/U, Mo, and V (paleoredox), are listed in Appendix 1 and their statistics are summarized in Table 4.2. Compared with the elemental compositions of the other slightly younger Upper Cambrian (Martin point; Wang and Azmy, 2020) and Cambrian-Ordovician boundary (GSSP, Green Point; Azmy et al., 2015) carbonates of neighboring basins in western Newfoundland, the Belle Isle carbonates have generally higher mean P, Ni, Th/U, Mn, and Fe concentrations but lower Sr although the mean ∑REE values are very comparable.

The Sr values (90 ± 44 ppm; Table 4.2; Appendix 1) have consistent positive correlations with their P (R^2=0.05), Ni (R^2=0.16), Cu (R^2=0.01), Al (R^2 = 0.57), total REE (∑REE; R^2=0.35), Th/U (R^2=0.20), Fe (R^2=0.60), and Mn (R^2=0.32) counterparts although some of the correlations seem week to insignificant (Fig. 5.3a–h). The Sr concentrations (Fig. 4.6b) decreases from 90 ± 44 ppm in D1 to 69 ± 22 ppm in D2 and drops to a minimal value of 47 ± 15 ppm in D3.

The geochemical characteristics of dolomicrite from Strait of Belle Isle are listed in Appendix 1 and their statistics are summarized in Table 4.2. The Sr concentrations appear to be lower than those documented by earlier studies (Azmy, 2019a,b) for Upper Cambrian Cow Head Group carbonates in the neighboring basins, spanning the SPICE and HERB (Hellnmaria-Red Tops Boundary) events (324 ± 192 ppm and 304 ± 144 ppm, respectively). However, the Mn contents of the Belle Isle dolomites (857 ± 396 ppm; Table 4.2) are higher than their neighboring basin counterparts (Azmy, 2019a,b; 360 ± 160 ppm and 291 ± 154 ppm, respectively). The Sr values have insignificant correlation with their $\delta^{13}C$ counterparts ($R^2 = 0.09$; Appendix 1) and similarly the Mn ($R^2 = 0.009$; Appendix 1). The Mn/Sr ratio shows a very poor correlation with their $\delta^{13}C$ values ($R^2 = 0.02$; Fig. 4.5a).

4.5 Rare Earth Elements (REE)

Table 4.2 summarizes the statistics of the REE concentrations and the calculated Ce and Eu anomalies of samples from the Petit Jardin, March Point, and a few from the uppermost Hawke Bay formations of the Port au Port Group at the Strait of Belle Isle. The mean ∑REE values of dolomites show the lowest in D2 (33.7 ± 23.8 ppm, *n* = 9) and the highest in D3 (59.9 ± 52.9 ppm, *n* = 9). The D1 has a middle value (45.2 ± 37.3 ppm, *n* = 33). The variations in the REE compositions of carbonates are also reflected by their shale normalized patterns (Fig. 4.7). The D1 and D2 patterns are very similar although that of D3 is different.

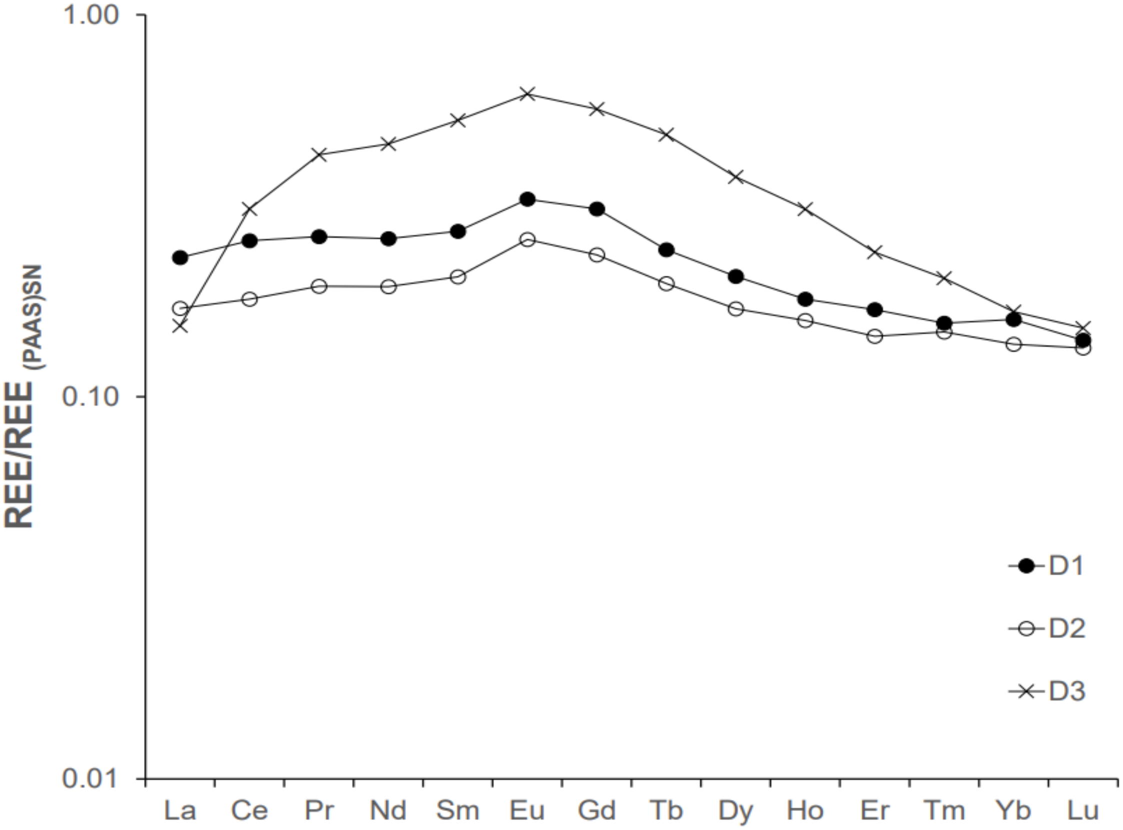

Fig. 4.7. Patterns of mean shale-normalized REE concentrations of the investigated dolomites.

The Ce and Eu anomaly calculations (Bau and Dulski, 1996) show D2 having the lowest mean Ce anomaly (0.99 ± 0.06), whereas D3 has the highest (1.07 ± 0.08; Table 4.2). The mean Ce anomaly value of D1 lies between these end-member values (Fig. 4.8). The mean Eu anomalies (Fig. 4.8) range from 1.02 ± 0.04 in D1 to 1.11 ± 0.04 in D3.

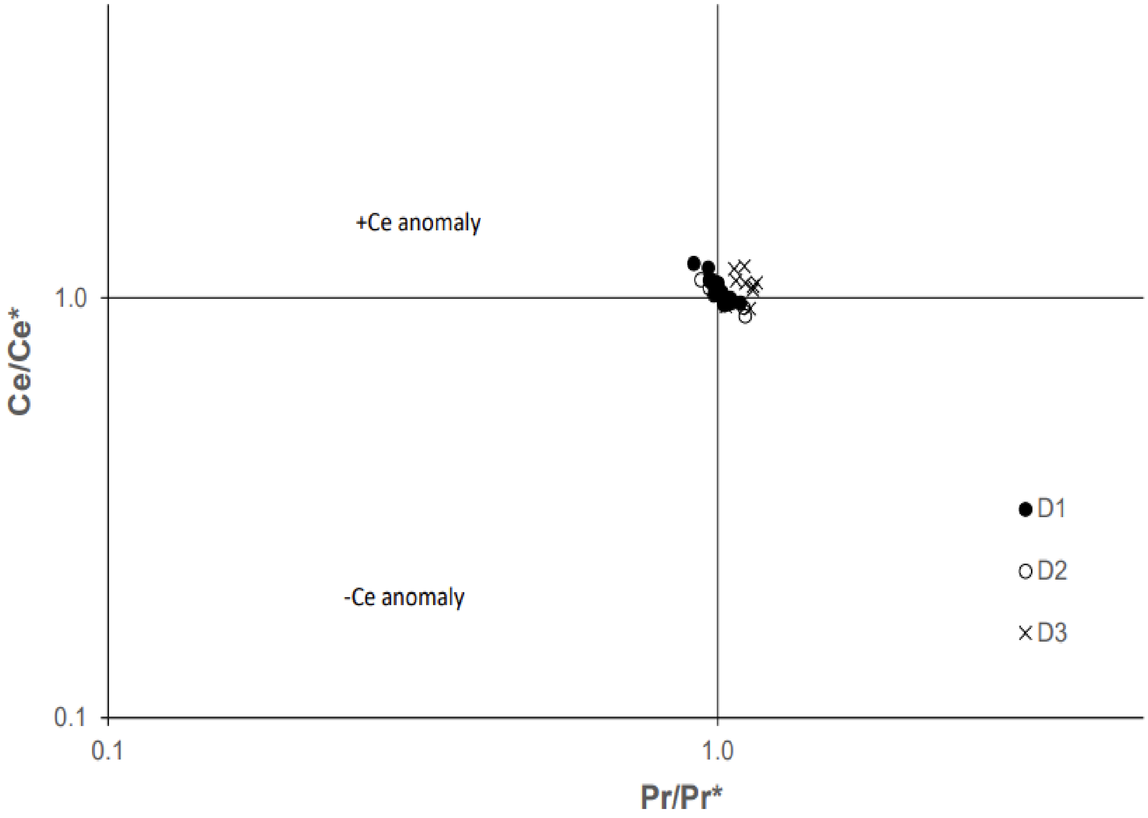

Fig. 4.8. Scatter diagram of Ce (Ce/Ce*) vs La (Pr/Pr*) anomalies for the samples.

4.6 Fluid-Inclusion gas analysis

Results of fluid inclusion gas analysis display the weighted averages of all analyses carried out on carbonates at the Strait of Belle Isle and tabulated in Appendix 3. The statistics of the CO_2/CH_4 and N_2/Ar ratios are summarized in Table 4.3. The weighted mean ratio of N_2/Ar (Fig. 4.9) varied from 6.1 to 82.7 in D1, 60.9 to 232.4 in D2, and 131.5 to 231.1 in D3, while the weighted mean ratio of CO_2/CH_4 varied from 0.15 to 3.2 in D1, 0.04 to 7.4 in D2, and 0.06 to 0.10 in D3.

Table 4.3. Summary of quantitative fluid-inclusion gas analyses (in mol) of the investigated Strait of Belle Isle dolomites.

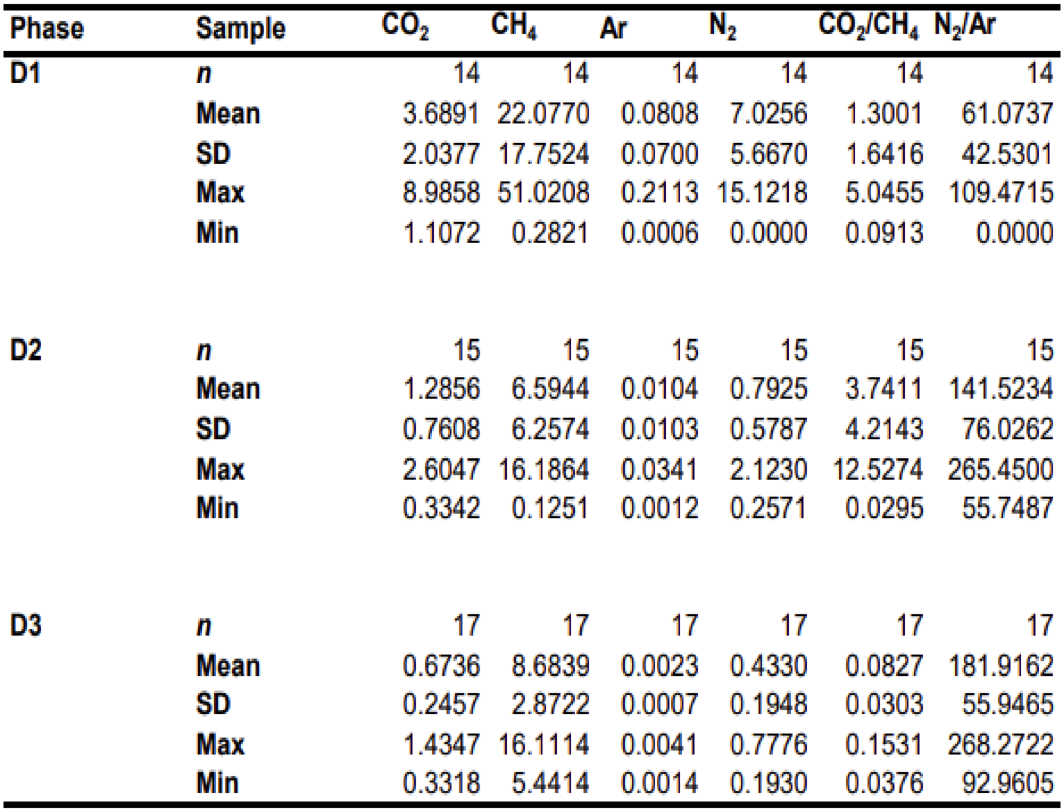

Phase	Sample	CO_2	CH_4	Ar	N_2	CO_2/CH_4	N_2/Ar
D1	***n***	14	14	14	14	14	14
	Mean	3.6891	22.0770	0.0808	7.0256	1.3001	61.0737
	SD	2.0377	17.7524	0.0700	5.6670	1.6416	42.5301
	Max	8.9858	51.0208	0.2113	15.1218	5.0455	109.4715
	Min	1.1072	0.2821	0.0006	0.0000	0.0913	0.0000
D2	***n***	15	15	15	15	15	15
	Mean	1.2856	6.5944	0.0104	0.7925	3.7411	141.5234
	SD	0.7608	6.2574	0.0103	0.5787	4.2143	76.0262
	Max	2.6047	16.1864	0.0341	2.1230	12.5274	265.4500
	Min	0.3342	0.1251	0.0012	0.2571	0.0295	55.7487
D3	***n***	17	17	17	17	17	17
	Mean	0.6736	8.6839	0.0023	0.4330	0.0827	181.9162
	SD	0.2457	2.8722	0.0007	0.1948	0.0303	55.9465
	Max	1.4347	16.1114	0.0041	0.7776	0.1531	268.2722
	Min	0.3318	5.4414	0.0014	0.1930	0.0376	92.9605

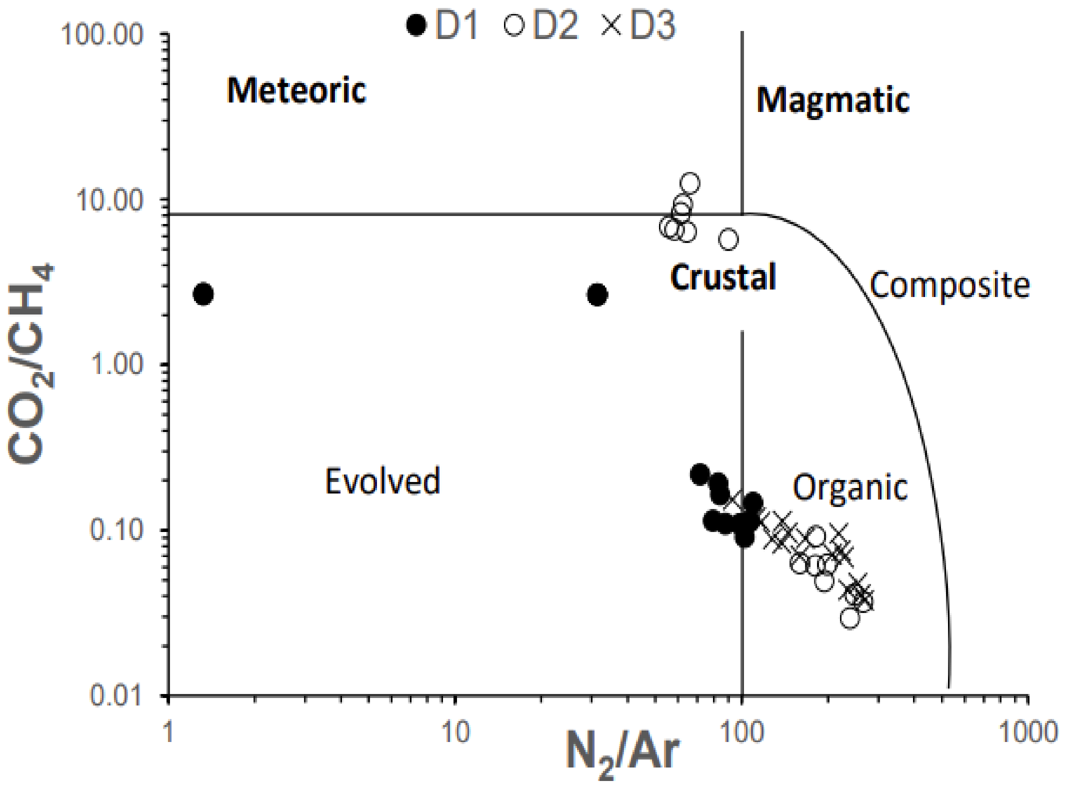

Fig. 4.9. Scatter diagram of the CO_2/CH_4 vs N_2/Ar ratios of the investigated dolomites.

CHAPTER V

DISCUSSION

5.1 Origin of Middle-Upper Cambrian Dolomites on eastern Laurentia: a case study from Belle Isle Strait, western Newfoundland (Published in the Journal of Marine and Petroleum Geology, volume 125, p. 104858)

5.1.1 Dolomite Petrography

The micritic grain-size, fabric-retention and dull CL of the D1 (Fig. 4.2a–b) suggest dolomitization of marine lime mud during an early stage of diagenesis in shallow burial settings and under near-surface conditions. This is consistent with the microstylolites crosscutting through D1 (e.g., Lane, 1990; Azomani et al., 2013; Olanipekun et al., 2014; Hou et al., 2016). This may also reflect some insignificant meteoric alteration of the precursor lime mudstone (e.g., Azmy et al., 2008, 2009; Hou et al., 2016), a process which is supported by the relatively enriched $\delta^{18}O$ values (−6.7 ± 1.3‰ VPDB; Table 4.2) of D1 compared to those of D2 and D3. In addition, the lack of evaporitic layers (cf. Chow and James, 1992) suggests dolomitization by diagenetic fluids that were possibly modified seawater, such as a mixture of marine and meteoric waters (e.g., Hein et al., 1992), rather than evaporated brines. The visual estimates of insignificant porosity (<0.5%) reflect extensive dolomitization.

Unlike D1, the larger crystal sizes of D2 (60 µm – 150 µm), and fabric destructive textures (Fig. 4.2c) as well as the high mean T_h (89.1 ± 6.4 °C, *n* = 18;

Table 4.1) suggest a later stage of replacement dolomitization in deeper burial, higher temperature setting compared with that of D1 (e.g., Warren, 2000; Azmy et al., 2009). Some of the D2 crystals show cloudy cores with clear rims indicating progressive dolomitization during burial and resulted in replacement of precursor carbonates (the cloudy core) followed by a later cement as a clear rim (e.g., Olanipekun et al., 2014; Hou et al., 2016; Olanipekun and Azmy, 2016). This is consistent with the non-CL images by D1, petrographic examination indicates that D2 has insignificant porosity.

Vugs seem to have formed in D1 and D2 due to dissolution from acidic fluids, leaving irregular voids that were filled with cements during the latest stages of diagenesis.

The latest phase of dolomitization yielded D3 (saddle dolomite) that fills vugs and late fractures (Fig. 4.2b, d) crosscutting the earlier phases (D1 and D2). This is consistent with the higher mean T_h (110 ± 8.2 ^oC, n = 33; Table 4.1) of the associated primary aqueous two-phase fluid inclusions of D3. The anhedral crystals and undulose (sweeping) extinction of D3 are consistent with precipitation from hot saline brines and crystal growth at high temperatures (>60 ^oC) of deep burial settings (e.g., Lohmann and Walker, 1989; Gregg and Sibley, 1984; Warren, 2000; Al-Aasm et al., 2002; Lonnee and Machel, 2006; Ramiel, 2008; Hou et al., 2016; Feng et al., 2017). The non-CL images of D3 (Fig. 4.2b) support the precipitation in deep burial settings under reducing conditions

(Warren, 2000; Lonnee and Machel, 2006; Haeri-Ardakani et al., 2013; Olanipekun et al., 2014; Hou et al.,2016). The higher mean T_h of fluid inclusions and lowest $\delta^{18}O$ values of D3 are key features of saddle dolomites (e.g., Radke and Mathis, 1980; Gregg, 1983; Kretz, 1992; Al-Aasm and Azmy, 1996; Al-Aasm et al., 2002; Zhang et al., 2009). A very rare vug-filling calcite (C3) postdates D3 (Fig. 4.2d).

The overlap in salinity ranges (Fig. 4.4d) and close mean T_h values of the dolomite phases, particularly those of D2 and D3 (Table 4.1), suggest that they might have developed from the same dolomitizing fluid composition evolved through circulation in basin sediments.

Saddle dolomites, comparable to D3, have been documented in other massive dolostones, but those were associated with hydrothermal mineralization. An example may be seen in the Ordovician Ogdensburg Formation, New York, USA and in strata believed to be related to the Taconic Orogeny (Benison and Lowenstein, 1997; Landing, 2007). Also, comparable Cambrian–Middle Ordovician hydrothermal dolostones occur in eastern New York and western Vermont (USA) with minor mineralization (Landing, 2007; Landing et al., 2009).

5.1.2 Major and minor Elements

The Ca concentrations in the Strait of Belle Isle dolomites appear to vary throughout the dolomite phases and the mean values of $CaCO_3$ contents are between 53.7% and 56.0% (Table 4.2), thus reflecting their calcian and non-stoichiometric compositions (Budd, 1997; Sperber et al., 1984). The non-stoichiometric dolomites are believed to be formed in a relatively closed and rock-buffered diagenetic systems (Sperber et al., 1984; Kırmacı and Akdağ, 2005) due to less fluid mobility and/or relatively inadequate supply of Mg^{2+} (e.g., Sperber et al., 1984; Azomani et al., 2013).

The mean Sr values of the dolomites Table 4.2 exhibit a trend of gradual decrease from the earliest D1 (90 ± 44 ppm) to the latest D3 (47 ± 15 ppm), which reflects the influence of diagenesis with progressive burial (Veizer, 1983; Al-Aasm et al., 2002; Conliffe et al., 2009; Olanipekun et al., 2014). The low Sr contents of the dolomicrite (D1 <550 ppm) do not support a sabkha or bacterial origin (Tucker and Wright, 1990; Sanchez-Roman et al., 2011; Azmy et al., 2013; Hou et al., 2016). It is well established that during burial diagenesis of carbonates some elements, such as Sr, are depleted in the diagenetic carbonate phase whereas others, such as Mn and Fe, are enriched (Veizer, 1983).

The Sr/Ca molar ratio of dolomites may also provide clues about the origin and nature of their parent dolomitizing fluids in a particular diagenetic environment (cf. Vahrenkamp and Stewart, 1990; Banner, 1995; Budd, 1997; Azomani et al., 2013; Olanipekun et al., 2014; Hou et al., 2016) when the estimates of the Sr distribution coefficient (D_{Sr}) value between the parent fluid and the precipitated dolomite are established. The Sr/Ca molar ratio of the dolomitizing fluid can be calculated from the following equation:

$$({}^{m}Sr/{}^{m}Ca)_{\text{dolomite}} = D_{sr}({}^{m}Sr/{}^{m}Ca)_{\text{fluid}}$$

Where D_{sr} is the distribution coefficient (0.05 to 0.06; Banner, 1995), whereas ${}^{m}Sr$ and ${}^{m}Ca$ are the molar concentrations of Sr and Ca in dolomites, respectively. The calculated Sr/Ca molar concentrations for D1 range from 0.0056 to 0.0047, are lower than that modern seawater 0.0086 (Drever, 1988). This may suggest that the parent dolomitizing fluid of D1 was a modified marine water, possibly a mixture of marine and meteoric waters (e.g., Azmy et al., 2001).

Iron (Fe) and Manganese (Mn) are good proxies of redox conditions (Table 4.2) since they become enriched in carbonates with enhanced reducing conditions associated with the increase of depth by progressive burial (e.g., Eriksson et al., 1975; Land, 1986; Zhang et al., 2017). However, this is also influenced by the concentrations of those elements in the diagenetic fluid (e.g., Azomani et al., 2013; Olanipekun et al., 2014). The dolomites exhibit a clear increase in the mean values of Fe and Mn concentrations with progressive burial from D1 to D2 (Table 4.2), but the trend does not continue with D3 (latest vug- and fracture-filling dolomite). This suggests that the geochemistry of the dolomitizing fluid evolved during the course of dolomitization or D3 possibly formed from a different fluid although the results from the estimated salinities support the former scenario.

In oxidizing environments, uranium ions remain soluble and higher oxidation state (U^{+6}) whereas in reducing conditions, they retain the insoluble lower oxidation state (U^{+4}) (Wignall and Twitchett, 1996). The mean U concentration (Table 4.2) of D3 (0.19 ± 0.23 ppm) is significantly lower than those of D1 (0.83 ± 0.60 ppm) and D2 (1.12 ± 0.65 ppm) and thus suggesting that D3 might have precipitated from a different dolomitizing parent fluid although the salinity estimates does not support this scenario.

The Rare Earth Elements (REE) group is composed of 15 elements that range in atomic number from 57 (Lanthanum) to 71 (Lutetium) on the periodic table of elements and are officially referred as the Lanthanoids although they are commonly referred to as the Lanthanides. The REE are classified into three groups: (i) the Light Rare Earth Elements (LREE) from La to Nd, (ii) the Medium Rare Earth Elements (MREE) from Sm to Dy, and the Heavy Rare Earth Elements (HREE) from Ho to Lu. The REE are generally trivalent, except for Ce (e.g., Ce^{4+} in some environments – redox sensitive) and Eu (Eu^{2+} in hydrothermal waters), and they have similar ionic radii nonetheless their chemical characteristics tend to change systematically along the series (Sholkovitz and Shen, 1995). Their comparable distribution coefficient values, when incorporated in carbonates, make their shale-normalized distribution pattern a proxy of the variations in the geochemistry of the parent fluid (Sholkovitz et al., 1994; Zhong and Mucci, 1995). Recent studies indicated that diagenesis of carbonates at low water/rock interaction ratios (insignificant recrystallization) does not alter their REE compositions significantly (e.g., Banner et al., 1988; Webb and Kamber, 2000; Nothdurft et al., 2004; Barton et al., 2006; Webb et al., 2009). Therefore, the REE compositions of carbonates have been used as a tool to understand the nature and origin of diagenetic fluids and the redox conditions (e.g., Azmy et al., 2013; Azomani et al., 2013; Xiong et al., 2015; Hou et al., 2016)

The shale-normalized patterns (Fig. 4.7) of the REE mean values of the dolomites (D1 and D2) are similar and exhibit insignificant differences, which suggests that they developed likely from the same dolomitizing fluid that its elemental composition varied slightly during dolomitization rather than from different fluids. However, D3 shows a different pattern, from those of D1 and D2. The D3 parent dolomitizing fluid had a different composition and one that might be due to extensive circulation from the surrounding basinal rocks. This is also consistent with comparable ∑REE mean values (Table 4.2) and with the conclusions from microthermometric measurements (T_h values and salinities) of entrapped primary two-phase fluid inclusions.

The Ce/Ce* anomaly in carbonates is utilized as proxy for redox conditions (Bau and Dulski, 1996; Barton et al., 2006). The mean Ce/Ce* values of the dolomites (Table 4.2) are almost or around 1 (Fig. 4.8) and the lack of a negative

Ce anomaly, a characteristic of seawater, suggests possible reducing (anoxic and dysoxic) conditions. This is consistent with the diagenetic settings of D2 and D3. However, the preservation of micritic to near-micritic grainsize and sedimentary fabric of D1 supports dolomitization during early diagenetic stages close to near-surface conditions. The general and slight enrichment in Ce could be caused by changes in the geochemistry of the parent dolomitizing fluids due to mixing with fluids from REE-rich siliciclastic rocks in the basin e.g., the co-occurrence shales and sandstones (Shields and Stille, 2001; Abanda and Hannigan, 2006; Xiong et al., 2015, 2016). This is consistent with the slight positive Eu/Eu* anomaly (Fig. 4.8), which is usually associated with dissolution of plagioclase feldspars in clastic rocks such as sandstones (Lee et al., 2003; Bau et al., 2010)

5.1.3 Stable Isotopes

5.1.3.1 Carbon and Oxygen isotopes

Most of the $\delta^{13}C$ values of D1 (dolomicrites) lay within the documented range for the best-preserved Cambrian marine carbonates (Fig. 4.5b; Veizer et al., 1999), and reflects preservation of at least their near-primary c-isotope compositions. In addition, many of the $\delta^{18}O$ values of D1 are located within the range documented for the best-preserved Cambrian marine carbonate, also suggesting that the dolomitizing parent fluid likely had a marine-water component, which is part with their Sr/Ca molar ratios.

The O-isotope composition of carbonates is influenced by that of the parent fluid from which it precipitated and by the temperature of precipitation (Urey et al., 1951). Therefore, the $\delta^{18}O$ of dolomites is influenced by that of the dolomitizing fluid, and particularly because dolomitization requires large volumes of Mg-rich fluids (Land, 1983, 1992). Accordingly, estimates of the $\delta^{18}O$ composition of a dolomitizing fluid can be calculated using the T_h values of primary two-phase fluid inclusions entrapped into the dolomite crystals (Land, 1992; Goldstein and Reynolds, 1994) and the $\delta^{18}O$ values of dolomites.

The fabric retention and near-micritic grain size of D1 suggests dolomitization occurred in shallow burial settings and near-surface conditions ($T < 50$ °C, Goldstein and Reynolds, 1994). The precursor carbonate was likely a Cambrian lime mud from a tropical, warm, shallow water settings (Chow and James, 1987), similar to our present-day environment (25 to 30 °C). The calculated $\delta^{18}O$ values for the D1 parent fluid range from approximately −5 to −10‰ VSMOW (Fig. 5.1). The documented $\delta^{18}O$ values of the Cambrian best-preserved marine carbonates (−7 to −11‰ VPDB; Veizer et al., 1999) suggest Cambrian seawaters with $\delta^{18}O$ values between −4 and −7‰ VSMOW (Friedman and O'Neil, 1977). Assuming that the difference between the $\delta^{18}O$ values of Cambrian meteoric water and seawater in a tropical zone is similar to that of present-day environment (~4‰; Clark and Fritz, 1997), the estimated $\delta^{18}O$ of Cambrian meteoric water is possibly between −8 to −11‰ VSMOW. Thus, estimates of Cambrian most enriched $\delta^{18}O$

of seawater (−4‰ VSMOW) and most depleted $\delta^{18}O$ of meteoric water (−11‰ VSMOW) bracket the range of D1 $\delta^{18}O$ values (−4 to −10‰ VSMOW). This suggests dolomite origin from a dolomitizing fluid that was a mixture marine and meteoric water, a phenomenon which is consistent with the conclusions from the Sr/Ca molar ratio estimates.

The estimated $\delta^{18}O$ values for the parent fluids of D2 and D3 are from +1 to +2‰ VSMOW and from +2 to +4‰ VSMOW, respectively (Fig. 5.1). Both fluids are more enriched in ^{18}O, which is expected for fluids of deep burial settings with high temperatures due to the enrichment of ^{18}O in the fluid phase with increasing temperature during dolomite precipitation (Faure and Mensing, 2004). Comparable enrichment in $\delta^{18}O$ estimates of parent fluids of mid-to deep burial dolomites of similar temperature settings have been documented in neighboring basins of western Newfoundland (e.g., Azomani et al., 2013; Olanipekun et al., 2014) and other areas (e.g., Hou et al., 2016; Feng et al., 2017; Berra et al., 2020). This may suggest that the parent fluids of D2 and D3 might have been different from that of D1, or they evolved from the earlier D1 fluid that was circulated through the basin sediments, which resulted in the modification in its o-isotope composition. However, earlier evidence from microthermometry and elemental chemistry favors the latter scenario.

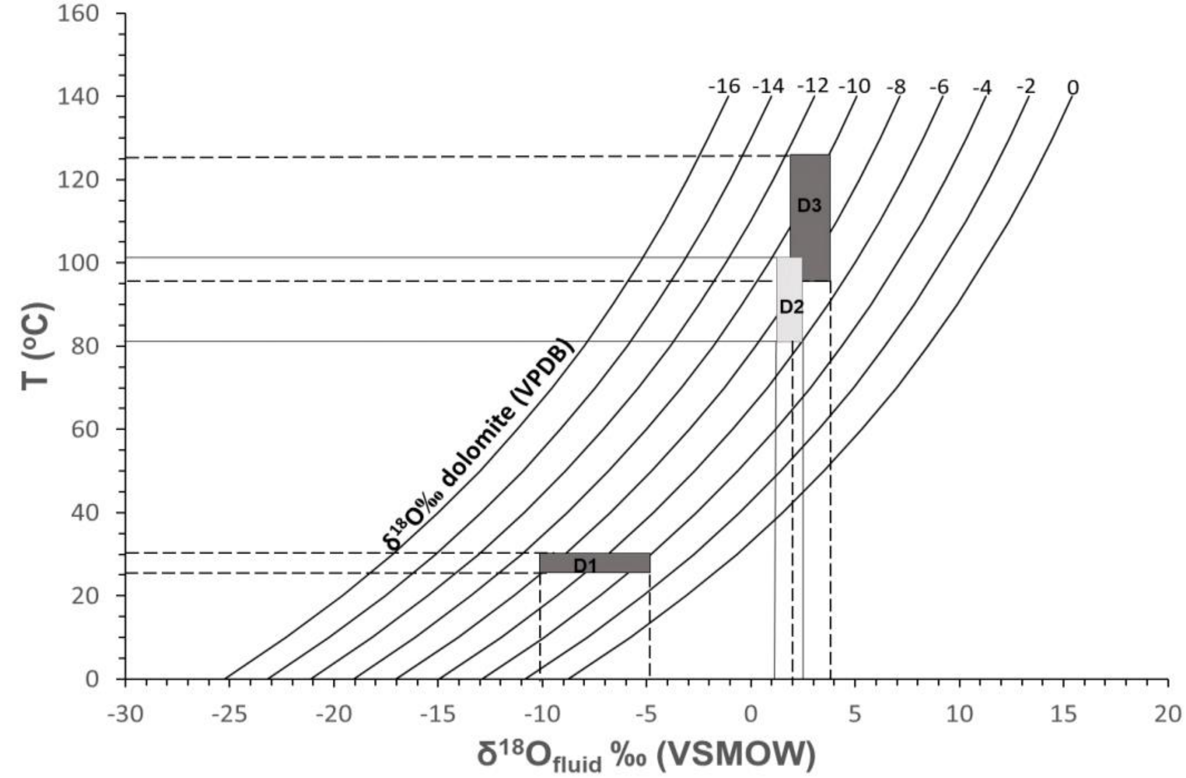

Fig. 5.1. Temperature (T) vs $\delta^{18}O_{\text{diagenetic fluid}}$ for various $\delta^{18}O_{\text{dolomite}}$ values that were reconstructed from the following equation: $10^3\ln\alpha = 3.2 \times 10^6 T^{-2} - 3.3$ (Land, 1983). The vertical bars indicate the ranges of $\delta^{18}O$ fluid, based on the ranges of $\delta^{18}O$ values and homogenization temperature (T_h) of each identified dolomite phase.

5.1.4 Fluid-inclusion gas analysis

Fluid-inclusion gas analysis is a well-established proxy for the origin of diagenetic fluids. Ratios of N_2-Ar-He and N_2-Ar-CH_4 are utilized to identify the source for volatiles in geothermal fluids (Giggenbach, 1986; Blamey and Norman, 2002; Blamey, 2012) such as the sources, and including dolomitizing fluids (e.g., Azmy and Blamey, 2013; Azomani et al., 2013; Hou et al., 2016).

Figure 4.9 shows that most of the N_2/Ar and CO_2/CH_4 ratios (Appendix 3) are within the organic and some within the meteoric zone, which excludes contributions from magmatic fluids as dolomitizing agents. This may reflect an evolution of the meteoric fluids, possibly through mixing with seawater (source of Mg for dolomitization) and circulation in the basin sediments. Some of the samples, particularly those of D3, plot within the organic field, with elevated CH_4 and N_2 producing a negative correlation between N_2/Ar and CO_2/CH_4. This is attributed to N_2 released from the decay of protein compounds, especially at deeper burial settings, is also consistent with the higher CH_4 contents as reflected by their lower CO_2/CH_4 ratios (Norman and Moore, 1999; Lowenstern and Janik, 2003). The general overlap in the gas ratios of the Port au Port dolomites suggests that they were likely deposited from the same fluids that were circulated in the basin sediment with progressive burial, which is consistent with conclusions from corresponding stable isotope and trace element compositions and salinity estimates from microthermometric measurements (e.g., Azomani et al., 2013).

5.2 Carbon-isotope stratigraphy of the Middle-Upper Cambrian in eastern Laurentia: implications for global correlation (Published in the Journal of Marine and Petroleum Geology, volume 128, p. 105052)

5.2.1 Preservation of the $\delta^{13}C$ signatures

Combined petrographic and geochemical techniques have been utilized to evaluate the degree of preservation of the Cambrian carbonates of the Port au Port Group (e.g., Azmy et al., 2006; Azmy and Lavoie, 2009; Azmy, 2019a,b). The degree of alteration depends mainly on the water/rock interaction ratio and the extent of reset of the retained proxy signal (Veizer, 1983; Banner and Hanson 1990). The dominant micritic to near-micritic grainsize and insignificant recrystallization of the Strait of Belle Isle carbonates as well as their retention of sedimentary fabrics (Fig. 4.3a) argue for a high degree of petrographic preservation (Shembilu et al., 2021), is consistent with their non-CL image (Fig. 4.3b). Luminescence in carbonates is mainly activated by high concentrations of Mn but quenched by high concentrations of Fe (Marshall, 1988; Machel and Burton, 1991; Budd et al., 2000). Although some dull and non-CL images, at times, reflect preservation of primary geochemical signatures (e.g., Veizer et al., 1999), diagenetic carbonates, such as late-burial cements, may still exhibit dull to non-CL images due to their high Fe contents (Rush and Chafetz, 1990). Therefore, CL images have to be taken with caution and complemented by additional screening tests (Brand et al., 2011).

Diagenetic alteration of carbonates leads to depletion in the Sr contents and δ^{18}O values but enrichment of Mn in the altered phase (Veizer, 1983) and the Mn/Sr ratio can be therefore employed as a tool for the evaluation of degree of preservation (e.g., Derry et al., 1992; Kaufman and Knoll, 1995; Azmy et al., 2010). Few samples of the dolomites have Mn > 1000 ppm, but their Sr contents are generally higher than those with lower Mn contents, which is against the diagenetic trend and might be attributed to minor contaminations from hidden microrhombic bacterial pyrite during microsampling. The poor correlation of the Mn/Sr ratios of the carbonates with their δ^{13}C counterparts ($R^2 = 0.02$; Fig. 4.5a) argues for a high degree of preservation (at least near-primary) of the δ^{13}C signatures (e.g., Veizer et al., 1999). This is also consistent with the insignificant argillaceous inclusions in the micritic carbonates, which argue against any considerable contributions from weathered terrestrial organic matter. The preservation of at least near-primary signatures is strongly supported by the localization of almost the entire suite ofδ^{13}C values from the Strait of Belle Strait carbonates within the range documented for best-preserved Middle–Upper Cambrian carbonates (Fig. 4.5b; Veizer et al., 1999). The impact of diagenesis on $\delta^{13}C$ signatures of carbonates is relatively less than that on their $\delta^{18}O$ counterparts. Diagenetic fluids, in most, do not normally contain enough CO_2 to reset the C-isotope composition of carbonates, is and reflected by the poor correlation of the $\delta^{18}O$ with the $\delta^{13}C$ values (Fig. 4.5b; $R^2 = 0.16$). Therefore, the $\delta^{13}C$ signature reset requires a high water/rock interaction ratio and is usually associated with significant recrystallization and aggrading neomorphism, but this is not the case for the micritic to near-micritic grainsizes of the carbonates (Fig. 4.5a). The lack of significant organic contents revealed by petrographic exams and micritic grainsize argue also against remineralization of organic matter during diagenetic alteration (Lanz et al., 2021).

Some of the samples have higher $\delta^{18}O$ values than those of the best-preserved Middle-Upper Cambrian marine carbonates (Fig. 4.5; Veizer et al., 1999). This runs counter to simple diagenesis but may, perhaps, be attributed to dolomitization (Land, 1983, 1992).

Recently published work by Shembilu et al (2021) indicated that the Belle Isle carbonates are entirely dolomitized. The early phase of dolomitization was at/near-surface conditions and resulted in the preservation of micritic sedimentary fabrics whereas the later phases of dolomitization at deeper burial settings by hot diagenetic fluids led to the deposition coarser fabric destructive and fracture-/vug-filling (saddle) dolomite. Therefore, the current study targeted micritic interbeds that provide the best material for C-isotope stratigraphy.

In summary, the retention of at least near-primary C-isotope compositions in the Strait of Belle Isle carbonates is supported by petrographic and geochemical evidences that make their δ^{13}C values reliable for high-resolution global chemostratigraphic correlation.

5.2.2 Carbon-Isotope stratigraphy

Earlier studies suggest that the Cambrian Period may carry evidence in support of significant eustatic sea level changes (e.g., James and Steven, 1986; Cooper et al., 2001; Landing, 2007, 2013; Azmy, 2019a, b) that contained variations in the redox conditions, organic debris in sediments, and nutrient inputs (e.g., Cooper et al., 2001; Landing, 2013; Wang and Azmy, 2020). The variations in ocean chemistry are reflected in the C-isotope compositions of marine carbonates that their profiles exhibit distinct δ^{13}C excursions (e.g., Schmid, 2017; Pulsipher et al., 2021).

The δ^{13}C profile of the currently interval of Strait of Belle Isle (Fig. 2.3) shows a long-term pattern of ^{13}C enrichment, is consistent with the general direction of sea level rise during the Cambrian (Landing, 2007; 2012a,b; Landing et al., 2010, 2011).

The profile also exhibits two major negative excursions (Fig. 2.3), a lower negative excursion (~4 ‰) that peaks near the bottom of the section, immediately blow the Hawke Bay-March Point formation boundary and an upper negative shift (~2 ‰), almost at the March Point-Petit Jardin formation boundary, and which inflects into a positive excursion through the Petit Jardin Formation. These shifts were possibly caused by short-term sea level falls that brought oxygenated water into contact with buried organic carbon and led to the release of ^{13}C-depleted CO_2. Other comparable negative δ^{13}C excursions (SPICE, post-SPICE, HERB, and Cambrian-Ordovician boundary; Fig. 5.2) have been also recorded by C-isotope profiles of Upper Cambrian sections in the neighboring continental slope successions (Martin Point sections and the Cambrian-Ordovician boundary GSSP in Green Point) in western Newfoundland (e.g., Miller et al., 2011; Azmy et al., 2014, 2015; Barili et al., 2018; Azmy, 2019a,b) and are deemed to have marked short-term sea level falls (Azmy 2019a,b; Wang and Azmy, 2020).

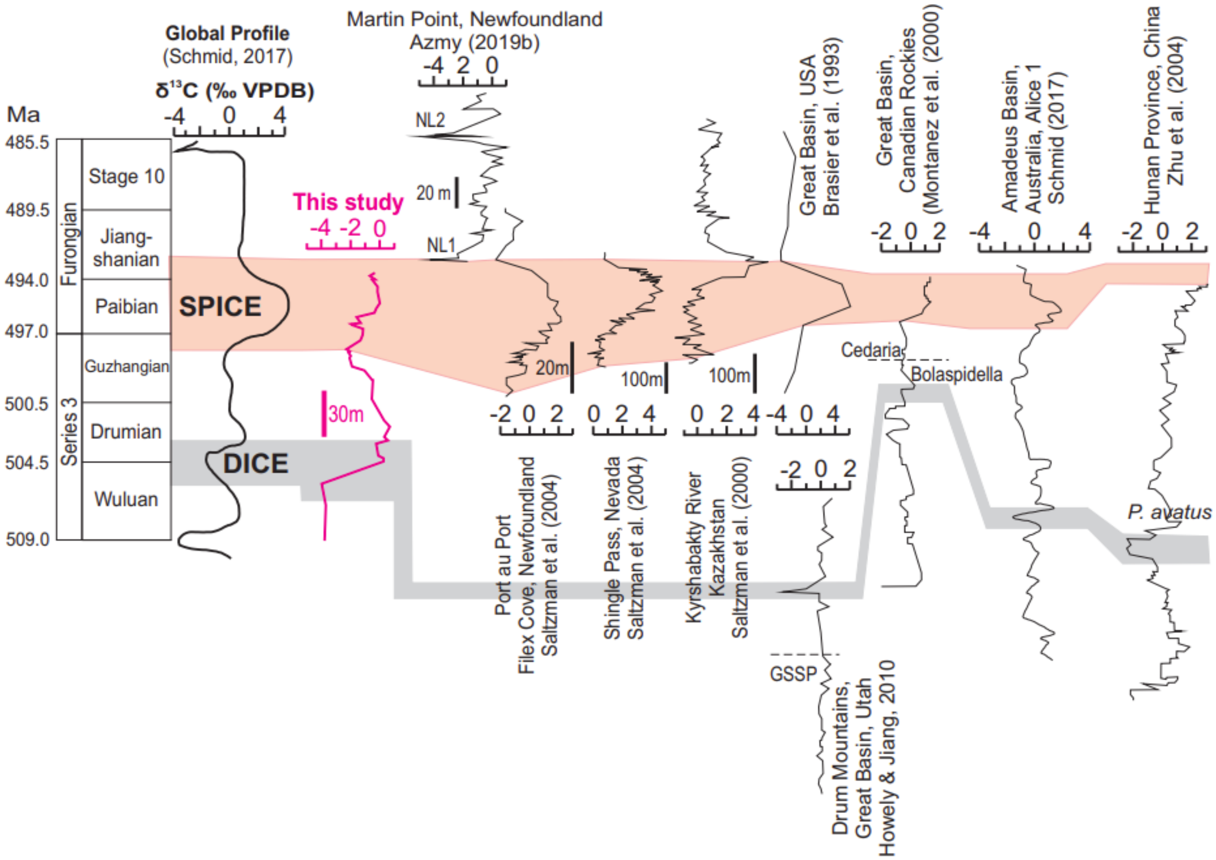

Fig. 5.2. Global C-isotope chemostratigraphic correlations of the SPICE and DICE events documented in sections from different paleocontinents (modified from Pages and Schmid, 2016; Schmid, 2017; Azmy, 2019b). The highlighted gray and red bands mark the mark the suggested covered intervals of the DICE and SPICE, respectively.

The global Cambrian δ^{13}C profile exhibits distinct negative shifts from sections in basins on different paleocontinents (e.g., Brasier, 1993; Hurtgen et al., 2009; Fan et al., 2011; Miller et al., 2011; Woods et al., 2011; Li et al., 2017; Azmy, 2019a,b; Schmid, 2017; Pulsipher et al., 2021) and correlated with the Middle Cambrian (e.g., DICE, Drumian Carbon

Isotope Excursion) and the base of the Upper Cambrian (e.g., SPICE, Steptoean Positive Carbon Isotope Excursion). The correlations of those C-isotope shifts were consistent with the global biostratigraphic schemes.

The SPICE reflects a global oceanographic event characterized by a distinct enhancement of oxygenation of the Cambrian seawater, which affected the atmosphere (e.g., Brasier, 1993; Hurtgen et al., 2009; Fan et al., 2011; Miller et al., 2011; Woods et al., 2011; Li et al., 2017; Azmy 2019a,b) and also marked a change from solely microbial forms to taxonomically diverse multicellular organisms in the ocean water (Rowell and Brady, 1976; Maruyama et al., 2014).

The trilobite biozonation scheme of the interval (Whittington and Kindle, 1969; Boyce, 1977, 1979; Levesque, 1977; Stouge and Boyce, 1983) suggests that the uppermost part of the Strait of Belle Isle δ^{13}C profile, where the positive excursion spans the *Cedaria* to *Elvina* zones and its base is marked by the peak of the upper negative δ^{13}C shift (Fig. 2.3), is correlated with the SPICE event.

The DICE event marks the base of the Middle Cambrian Drumian Stage (Howley and Jiang, 2010) and the first appearance datum (FAD) of the agnostid trilobite *Ptychagnostus atavus* (Pagès and Schmid, 2016) and the polymerid trilobite *Balospidella* of the Laurentian scheme (Levesque, 1977). Therefore, the lower negative δ^{13}C excursion of the

Belle Isle profile (Fig. 2.3; within the *Bolaspidella* Zone) can be attributed to the DICE event.

Azmy (2019b; his figures 5–6) and Pulsipher et al. (2021; their figures 4–7) discussed in detail and summarized the global correlations of the SPICE event as documented by earlier studies of carbonate sections from Laurentia (including western Newfoundland, Canada), Argentina, France, South Korea, China, Kazakhstan, Russia, Australia, and Sweden. The global positive SPICE excursion has been documented in many cases to be preceded by a small pre-SPICE negative shift, immediately at the base of the excursion, inflecting from the rising limb (Pulsipher et al., 2021). Therefore, the peak of the upper negative δ^{13}C shift of the Belle Isle Strait profile (Fig. 5.2) can be correlated with the pre-SPICE shift, which is supported by the trilobite biozonation scheme. However, it is not possible to confirm that the overlying positive excursion reaches fully the top of the SPICE event since the core does not seem to reach the upper boundary of the event. The three compressed zones (the *Aphelaspis*, *Dicanthopyge* and *Prehousia*; Levesque, 1977) between the *Crepicephalus* and *Dunderbergia* zones reflect an interval of condensed sedimentation near the Dresbachian-Franconian boundary (Fig. 2.3) or possibly a minor sedimentary hiatus although no recognizable surface of unconformity has been documented yet. Therefore, it is appropriate to place the peak of the upper negative $\delta^{13}C$ shift at the base of SPICE for correlation with its counterparts from other locations (Fig. 5.2).

The positive $\delta^{13}C$ excursion of the global SPICE event varies in magnitude (0.6 to 8.0 ‰; Pulsipher et al., 2021) and is generally ~ 4 ‰ in western Newfoundland (Saltzman et al., 2004). However, the positive $\delta^{13}C$ shift at the top of the Belle Isle $\delta^{13}C$ profile is only ~ 2 ‰. This might be attributed to the fact that the core does not cover the entire SPICE event particularly the upper part and also the trilobite biozonation scheme suggests a possible hiatus and/or interval of condensed sedimentation near the Dresbachian-Franconian boundary (Fig. 2.3). On the other hand, a comparable SPICE excursion (< 3 ‰) has been recorded by the March Point section on the Port au Port Peninsula in western Newfoundland (Barili et al., 2018).

The DICE negative $\delta^{13}C$ excursion has been documented in basins on different paleocontinents (Fig. 5.2) from sections in the USA (Howley and Jiang, 2010), Canada (Canadian Rockies, Montañez et al., 2000), China (Hunan Province, Zhu et al., 2004; Li et al, 2020) and Australia (Amadeus Basin, Schmid, 2017). Thus, the peak of the lower negative $\delta^{13}C$ excursion of the Belle Isle $\delta^{13}C$ profile can be therefore correlated with its global DICE counterparts (Fig. 5.2), particularly when supported by the trilobite biozonation.

5.3 Trace element variations across the Middle–Upper Cambrian carbonates: Implications for the paleoenvironment of eastern Laurentia (Published in the Journal of Marine and Petroleum Geology, volume 135, p. 105385)

5.3.1 Evaluation of sample preservation

Petrographic examinations of the Belle Isle carbonates reveal fabric-retentive textures and micritic (4 µm) to near-micritic grainsize (< 35 µm) (Fig. 4.3a–b). The degree of alteration depends mainly on the water/rock interaction ratio and the extent of reset of the retained proxy signal (Veizer, 1983; Banner and Hanson, 1990). The dominant micritic to near-micritic grainsize and insignificant recrystallization of the dolomicrites as well as their retention of sedimentary fabrics (Fig. 4.3a) argue for insignificant alteration (Shembilu and Azmy, 2021), which is consistent with their exhibited non-CL image (Fig. 4.3b). Luminescence in carbonates is mainly activated by high concentrations of Mn but quenched by high concentrations of Fe (Marshall, 1988; Machel and Burton, 1991; Budd et al., 2000). Although dull and non-CL images, at times, reflect preservation of primary geochemical signatures (e.g., Veizer et al., 1999), diagenetic carbonates such as late-burial cements may still exhibit dull to non-CL images due to their high Fe contents (Rush and Chafetz, 1990). Therefore, the CL results have to be taken with caution and confirmed by additional screening tests (Brand et al., 2011).

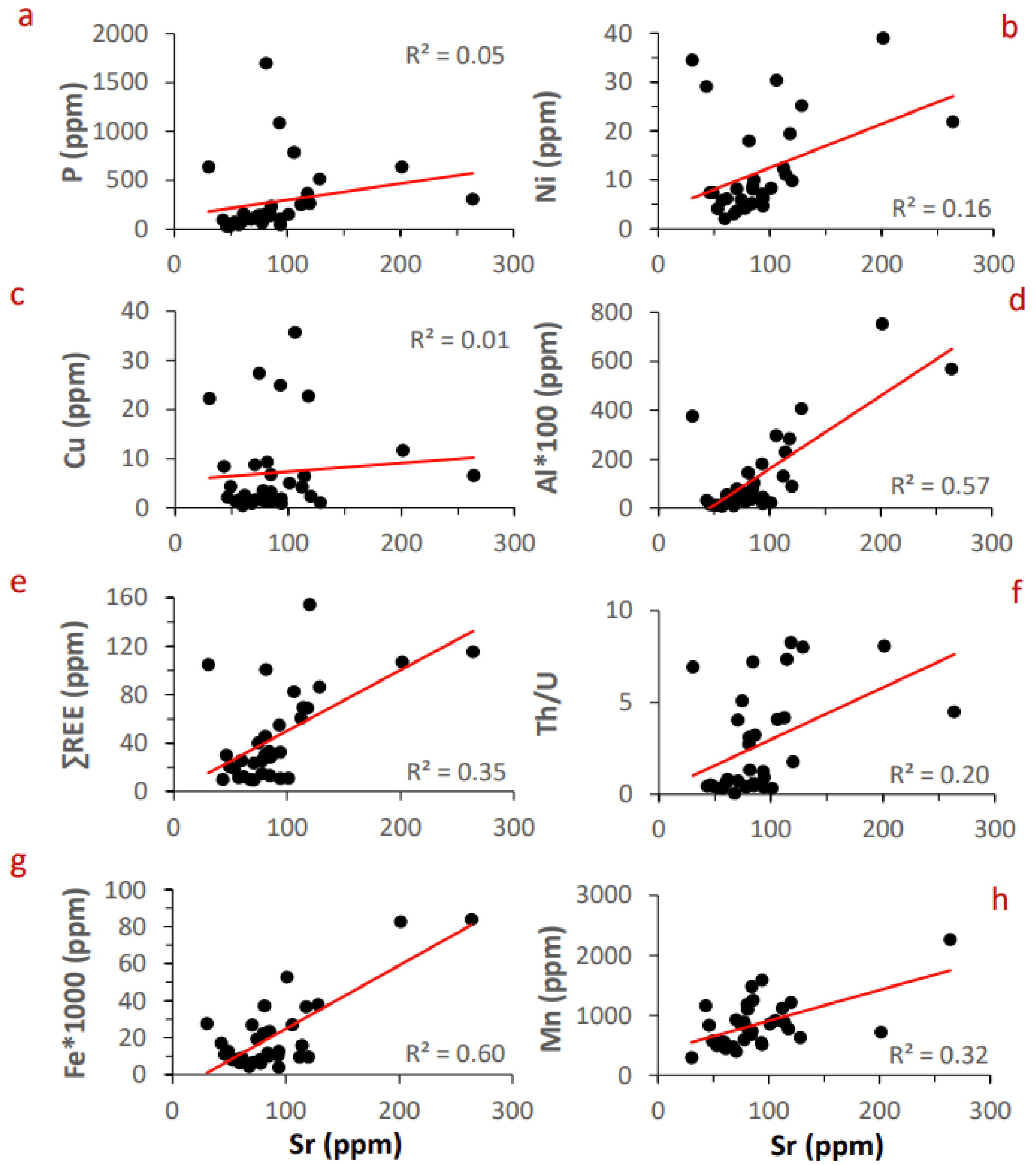

Fig. 5.3. Scatter diagrams showing correlations of Sr with (a) P, (b) Ni, (c) Cu, (d) Al, (e) ∑REE, (f) Th/U, (g) Fe, and (h) Mn of the investigated dolomicrites from the Port au Port Group.

Burial Diagenesis of carbonates leads to a significant depletion in the Sr contents but enrichment of other elements such as Mn, Fe (Veizer,

1983) and ∑REE (Azmy et al., 2011) in the altered phase. However, The Sr concentrations of the Belle Isle carbonates exhibit positive correlations with Mn, Fe, and ∑REE as well as the other paleoenvironmental proxies (Fig. 5.3a–h), which are opposite to the expected trends caused by diagenetic alteration.

Earlier studies suggested that diagenetic alteration of carbonates, under low water/rock interaction conditions (insignificant recrystallization/aggrading neomorphism), has insignificant influence on the contents of paleoenvironmental proxies such as P, Ni, Cu, Th and U (e.g., Veizer, 1983; Śliwiński et al., 2010; Pattan et al., 2013; Acharya et al., 2015; Wang and Azmy, 2020). Thus, the lack of correlations between diagenetic proxies is consistent with the petrographic preservation and supports the retention of at least near-primary geochemical signatures of the paleoenvironmental proxies (e.g., Wang and Azmy, 2020).

This is also supported by the proxies’ profiles (Fig. 5.4) that show distinct and consistent positive shifts associated with the negative excursions on the $\delta^{13}C$ profile (Fig. 5.4) since no diagenetic process has been known yet to cause such consistent changes.

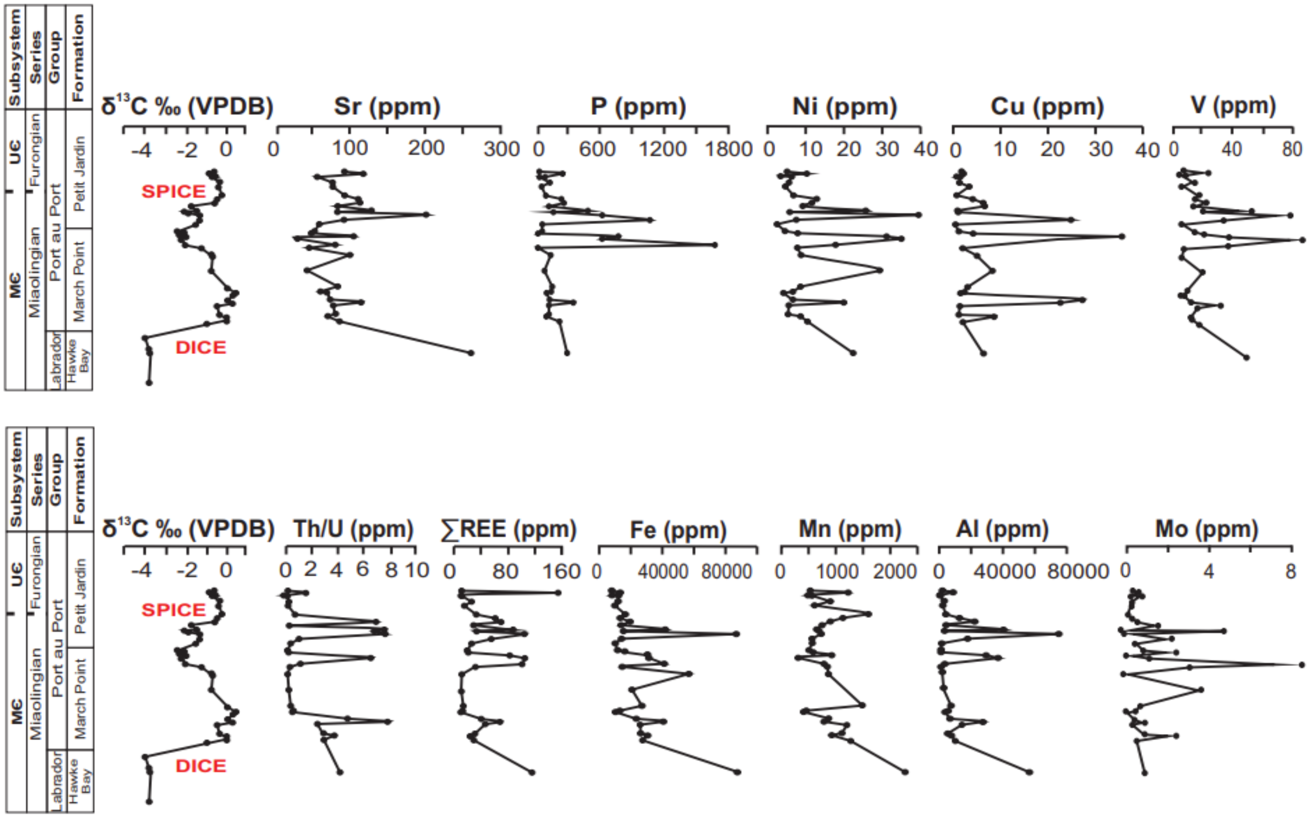

Fig. 5.4. The profiles of δ^{13}C, Sr, P, Ni, Cu, Th/U, ∑REE, Fe, Mn, and Al across the investigated Core NF-02 from the Strait of Belle Isle succession.

5.3.2 Paleoenvironmental proxies

Variations in eustatic sea level, particularly those related to time events, are commonly associated with changes in the δ^{13}C signatures and trace element concentrations of the marine carbonates due to changes in primary productivity, redox conditions, and impact of terrestrial material and nutrients inputs into the ocean (e.g., Wignall and Twitchett, 1996;

Murphy et al., 2000; Kimura et al., 2005; Wignall et al., 2007; Piper and Calvert, 2009; Śliwiński et al., 2010; Dickson et al., 2011).

The C-isotope profile of the Belle Isle carbonates (Shembilu and Azmy, 2021; Fig. 2.3) records a lower negative excursion (~ 4 ‰) that correlates with the Middle Cambrian global DICE (Drumian Carbon Isotope Excursion) event (Schmidt, 2017) and an upper negative counterpart (~ 2 ‰) that correlates with the base of the lowermost Upper Cambrian global SPICE (Steptoean Positive Carbon Isotope Excursion) event (Pulsipher et al., 2021). The negative shift at the base of SPICE inflects into the positive SPICE excursion (Shembilu and Azmy, 2021). The correlations of these excursions were supported by the Middle–Upper Cambrian trilobite biozonation scheme and the negative shifts are deemed to have been caused by brief sea level falls that likely brought down surface oxygenated water to oxidize buried organic matter and release light CO_2 enriched in ^{12}C (Shembilu and Azmy, 2021) although some earlier studies (e.g., Li et al., 2019) suggested that the DICE negative $\delta^{13}C$ excursion has been caused by inputs of upwelling anoxic deep waters into oxic shallow water column during transgression.

Aluminum and REE are enriched in crustal rocks and therefore reflect the impact of the terrestrial inputs in oceans (e.g., Veizer, 1983;

Śliwiński et al., 2010; Tripathy et al., 2014; Azmy et al., 2011; Wang and Azmy, 2020), which is confirmed by their considerable positive correlation (R^2=0.57; Appendix 1). The drop in sea level exposed more land areas for weathering that enhanced the inputs of terrigenous material into ocean water and caused the positive shifts in the Al and ∑REE profiles, which are associated with both of the main negative $\delta^{13}C$ excursions (Fig. 5.4).

Phosphorus, Ni, and Cu are among the constituents of nutrients and known to be reliable proxies for bioproductivity (e.g., Tribovillard et al., 2006; Arnaboldi and Meyers, 2007; Morel et al., 2004; Śliwiński et al., 2010). Their profiles reconstructed from the carbonates (Fig. 5.4) exhibit similar positive shifts associated with the negative $\delta^{13}C$ excursions, thus suggesting a relative increase in nutrient inputs from land sources likely through riverine discharge during the drop in sea level. This is consistent with the increase of terrigenous inputs during those periods, which is shown by the weathering (Al and ∑REE proxy profiles (Fig. 5.4). However, the effect of oxidation of organic matter and release of light $^{12}CO_2$ might have overprinted enhancement of primary productivity particularly during short-term sea level drops along the general long-term trend of sea level rise during the Cambrian (Landing, 2007, 2012a,b; Landing et al., 2010, 2011; Babock et al., 2015). Although the enhanced input of nutrients triggered the increase in primary productivity after a short-time lag, which is reflected by the positive $\delta^{13}C$ inflections following the negative shifts (e.g., the positive SPICE excursion). A eustatic sea level drop is associated with global cooling and well-mixed oceans, which suggests that input of nutrients was not restricted to land sources (riverine inputs of weathered material) but had contributions from upwelling. This is consistent with the steady enrichments of Mo and V, as well as Ni, associated with the negative $\delta^{13}C$ excursions (Fig. 5.4) since these elements are known to be enriched in anoxic seawater (Pagès and Schmid, 2016).

Sea level changes influence the oxygenation of water column and consequently the oxidation state of redox-sensitive elements and their solubility in seawater, which control their degree of enrichment in marine sediments (e.g., Wignall and Twitchett, 1996; Kimura et al., 2005; Arnaboldi and Meyers, 2007; Wignall et al., 2007). In oxidizing environments, uranium ions occur as [U^{6+}] that form uranyl carbonate, which is soluble in water whereas in reducing conditions, they retain the lower oxidation state [U^{4+}] and form an insoluble uranous fluoride which is trapped in marine carbonates (Wignall and Twitchett, 1996). In contrast, thorium is not affected by redox conditions in the water column and occurs permanently in the insoluble [Th^{4+}] state. Thus, sediments of anoxic environments are richer in uranium and have lower Th/U than those of oxic environments. Therefore, the Th/U ratio has been used as a proxy for environmental redox conditions. The Th/U profile of the Belle Isle carbonates also exhibits positive shifts associated adjacent to the negative $\delta^{13}C$ excursions of both of the DICE and base of SPICE events. This implies a relative increase in oxygenation of water column, a phenomenon consistent with a drop in sea level (Shembilu and Azmy, 2021) and an increase of inputs of terrigenous material due to an increase of land exposed to weathering. However, the correlated enrichment in Th/U also does not support a suggested scenario of rising sea level and attributing the negative $\delta^{13}C$ to upwelling of deep anoxic waters (rich in organic matter) onto an oxic shallow inner shelf environment during transgression (e.g., Li et al., 2019) particularly when U is expected to be enriched in the upwelling material (such as organic matter) and this would lead to negative Th/U shifts, which is not the case.

The relative variations in Fe and Mn content may reflect changes in the redox conditions. They are more soluble and enriched in seawaters in their lower oxidation state (Mn^{+2} and Fe^{+2}, respectively). Specifically, this is under dysoxic/anoxic conditions, when compared with oxic shallow water settings (Veizer et al., 1983; Landing and Bruland, 1987). The Mn and Fe contents from Belle Isle carbonates vary from 296 to 2261 ppm and 4087 to 83975 ppm, respectively (Table 4.2) and are significantly higher than those of modern warm shallow-water marine carbonates (Mn = 5.4–30 ppm and Fe = 1–20 ppm, respectively; Ichikuni, 1973; Lorens, 1981; Brand et al., 2003). Manganese and Fe are also known to be diagenetic proxies and become enriched with diagenetic alteration during progressive burial. However, the Mn and Fe profiles of the carbonates exhibit unexpectedly consistent positive correlation with Sr (Figs. 5.3 and 5.4) and also positive shifts correlated with the primary negative $\delta^{13}C$ excursions on the Belle Isle profile (Figs. 5.3 and 5.4). In total the enrichment in those elements is very unlikely to be a diagenetic overprint. These elements are common in siliciclastic crustal rocks (e.g., feldspars) and the increase in inputs as terrigenous materials are weathered during lower sea levels, caused by active weathering raised their concentrations in water. This is supported by the consistent positive shifts exhibited by the profiles of weathering (e.g., Al and ∑REE) and nutrient (P, Ni and Cu) proxies.

Viewed from a different perspective, Mn and Fe concentrations may still be used as redox proxies when normalized by Al to eliminate the influence of detrital fractions (Clarkson et al., 2014). The Belle Isle carbonates have mean ratios of Mn/Al (0.20 ± 0.16; Table 4.2) and Fe/Al (3.7 ± 4.2; Table 4.2), are significantly higher than those of the upper continental crust (0.0075 and 0.44, respectively; McLennan, 2001). This may reflect Fe-Mn oxy-hydroxides (Pattan et al., 2013) that cannot form in anoxic environment but may be either oxic, or at least dysoxic, conditions (cf. Landing et al., 2002; Pattan et al., 2013).

Although the [Sr^{2+}] concentrations for dolomicrites are low (30–264 ppm) and comparable with those of the micritic carbonates in the neighboring basins (e.g., Azmy and Lavoie, 2009; Azmy, 2019a,b), the Sr profile still shows a consistent enrichment thought to be the negative $\delta^{13}C$ excursions of the DICE and base of SPICE, and correlated positive shifts from weathering (Al and ∑REE), bioproductivity (P, Ni, and Cu), and redox (Th/U, Mn, and Fe) profiles. This is opposite to the trend expected from simple diagenetic alteration (Veizer, 1983). The Sr behavior may reflect the influence of another factor such as the source of precursor lime mudstone that might have generated contributions from primitive Cambrian aragonitic shells or alternations between aragonitic and calcitic seas.

A similar pattern of [Sr] has been documented in association with the younger uppermost Cambrian HERB event in the area (Wang and Azmy, 2020). The suggested sea level falls (Shembilu and Azmy, 2021) could reflect brief global cooling events that led to conditions of relatively more oxygenated and cooler well–mixed waters than those dominated during the Cambrian long-term rising sea level. These conditions favored the precipitation of some aragonitic mud (Neilson et al., 2016), which is richer in Sr (Kitano and Oomori, 1971; Tucker and Wright, 2009) than calcite. Aragonite loses U during alteration (Chen et al., 2018), which might have contributed to the Th/U ratios (redox proxy). However, the geochemical evidence from the poor (positive) correlation of Sr with U contents ($R^2 = 0.15$; Appendix 1), the diagenesis proxies (Fig. 5.3a–h), and petrographic preservation (Fig. 4.3a–b) argues against any influence of carbonate mineralogy through U contributions to the Th/U ratios but supports at least near-primary Th/U ratios.

On the other hand, the Sr enrichment cannot be reconciled with the consistent greenhouse during the Cambrian that was suggested by some earlier studies (e.g., Berner and Kothavala, 2001; Landing et al., 2010; Wotte et al., 2019). Earlier few studies on the ice free Cretaceous suggested that variations in global groundwater reservoir, by alternations between humid and arid climates, might cause eustatic sea level fluctuations (Hay and Leslie, 1990; Wendler and Wendler, 2016; Wendler et al., 2016a,b), which may explain the sea level changes but yet cannot be reconciled with the oxic cooling intervals suggested by the Sr enrichments. Therefore, it is suggested that the interpretation of the correlated Sr enrichment has to be taken with caution till further studies may reveal the nature of those variations.

An alternative scenario that might reconcile the consistent variations of the paleoenvironment proxies in the Belle Isle carbonates with the assumed continuous sea level rise during greenhouse Cambrian is that the enrichment of Al, ∑REE, Mn, and Fe was caused by active chemical weathering during very humid (wet) climate intervals while that of P, Ni, Cu, V, and Mo was upwelling, which might have also placed light organic carbon into the shallow oxic environment and caused the negative δ^{13}C shifts (e.g., Li et al., 2019). Possible contributions from the weathered organic matter might have also contributed to those negative shifts. A comparable scenario of humid climates, which resulted in high inputs of weathered crustal material, has been suggested for the Late Permian (e.g., Li et al., 2020). However, this scenario might not explain the correlated enrichments of Sr or the high Mn/Al and Fe/Al ratios (0.20 ± 0.16 and 3.7 ± 4.2, respectively; Table 4.2).

CHAPTER VI

CONCLUSIONS

- Petrographic, microthermometric, and geochemical studies of Strait of Belle Isle carbonates reveal three generations of dolomite: an early fabric-retentive dolomicrite (D1), later fabric-destructive coarse crystalline sucrosic dolomite (D2) with cloudy cores and clear rims, and the latest fracture-filling saddle dolomite (D3). The dolomites are almost non-porous with very rare vuggy pores (<0.5%) and late fractures that are entirely occluded.
- The fabric-retentive, micritic to near-micritic grainsize of D1 was formed at near-surface conditions from fluids that were possibly mixed sea and meteoric waters. This is supported the estimates of $\delta^{18}O$ values of D1 parent fluid (−4 to −10‰ VSMOW), which is consistent with the conclusions from the estimated Sr/Ca molar ratios of those fluids and with the lack of evaporite layers that eliminate an origin from evaporated brines. However, the petrographic, microthermometric (T_h values and salinities), and geochemical attributes of D2 and D3 (more depleted $\delta^{18}O$ values and enriched Mn and Fe contents) suggest formation at mid to deep burial settings at higher temperatures and salinities during later stages of diagenesis.

- The shale-normalized patterns of REE mean values of dolomites suggest that the D1 and D2 developed from the same dolomitizing fluids that determine their elemental geochemistry, but D3 varied and evolved during dolomitization, by circulation through basinal sediments, rather than from different fluids.
- Fluid-inclusions gas ratios also fall within the meteoric and crustal field suggesting an origin from crustal fluids and supporting a scenario of origin of dolomites from the same fluids, circulating in the basinal sediments rather than from entirely different fluids. Although, the trace element contents suggest significant modification of the element geochemical composition of the parent fluid, the latest D3 is likely due to intense circulation in the surrounding siliciclastic rocks in the basin.
- The petrographic and geochemical examination of samples indicates insignificant influence of diagenesis on the $\delta^{13}C$ signatures for Upper Cambrian dolomicrites of the Strait of Belle Isle in western Newfoundland and preservation of at least near-primary signatures.
- The $\delta^{13}C$ profile shows two main negative excursions, a lower excursion (~4 ‰) that can be correlated with global DICE event (*Bolaspidella* Zone) and an upper one (~2 ‰) with the base of the global SPICE event (*Crepicephalus−Taenicephalus* zones).

- Those distinct C-isotope excursions provide a reliable tool for global correlations of the Upper−Middle Cambrian in eastern Laurentia with equivalent sections on the same paleocontinent and beyond.
- Although no radiometric age measurements have been performed on the Belle Isle succession, its $\delta^{13}C$ profile provides clues on the age of the March Point and Petit Jardin formation carbonates.
- The petrographic and geochemical examinations of the dolomicrites from the Strait of Belle Isle reveal the preservation of at least near-primary trace element signatures that can be utilized as proxies to reconstruct paleoenvironmental conditions (weathering, bioproductivity, and redox) during the Middle Cambrian DICE event and lowermost Upper Cambrian SPICE events.
- The correlated positive shifts on the Sr profile with their counterparts on paleoenvironmental proxies argue for preservation of at least near-primary geochemical signatures.
- The profiles of weathering (Al and ∑REE), bioproductivity (P, Ni, and Cu), and redox (Th/U) proxies show consistent positive shifts associated with the negative $\delta^{13}C$ excursions, which apparently correlate with the DICE and base of the SPICE events documented in earlier studies. These apparently reflect enhancement in the riverine inputs of weathered crustal rocks due to possible active weathering

while the enrichment in the P, Ni, Cu, V, and Mo was likely by upwelling.

- The associated positive shifts exhibited by the Mn and Fe profiles reflect the influence of terrigenous inputs rather than diagenesis, which is supported by the associated enrichment in the Mn/Al values and consistent with the positive Th/U shift.

REFERENCES

Abanda, P.A., Hannigan, R.E., 2006. Effects of diagenesis on trace element partitioning in shales. Chemical Geology 230(1-2), 42–59.

Acharya, S. S., Panigrahi, M. K., Gupta, A. K., Tripathy, S., 2015. Response of trace metal redox proxies in continental shelf environment: The Eastern Arabian Sea scenario. Continental Shelf Research 106, 70–84. https://doi.org/10.1016/j.csr.2015.07.008

Al-Aasm, L.S., Azmy, K., 1996. Diagenesis and evolution of microporosity of Middle-Upper Devonian Kee scarp reefs, Norman Wells, N.W.T, Canada: Petrographic and chemical evidence. American Association of Petroleum Geologists Bulletin 80, 82–100.

Al-Aasm, L.S., Lonnee, J., Clarke, J., 2002. Multiple fluid flow events and the formation of saddle dolomite: Case studies from Middle Devonian of the Western Canada sedimentary basin: Marine and Petroleum Geology 19(3), 209–217.

Allan, J.R., Wiggins, W.D., 1993. Dolomite reservoirs: Geochemical techniques for evaluating origin and distribution. American Association of Petroleum Geologists, Continuing Education Course Notes, Series No. 36, 129.

Arnaboldi, M., Meyers, P.A., 2007. Trace elements indicators of increased primary production and decreased water-column ventilation during deposition of latest Pliocene sapropels at five locations across the Mediterranean Sea. Palaeogeography, Palaeoclimatology, Palaeoecology 249, 425–443. http://doi.org/10.1016/j.palaeo.2007.02.016

Azmy, K., 2019a. Carbon-isotope stratigraphy of the uppermost Cambrian in eastern Laurentia: implications for global correlation. Geological Magazine 156(5), 759–771.

Azmy, K., 2019b. Carbon-isotope stratigraphy of the SPICE event (Upper Cambrian) in eastern Laurentia: implications for global correlation and a potential reference section. Geological Magazine 156(8), 1311–1322.

Azmy, K., Lavoie, D., 2009. High-resolution isotope stratigraphy of the Lower Ordovician St. George Group of western Newfoundland, Canada: implications for global correlation. Canadian Journal of Earth Sciences 46(6), 403–423.

Azmy, K., Blamey, N.J.F., 2013. Origin of diagenetic fluids inferred from fluid inclusion gas rations. Chem. Geol. 347, 246–254.

Azmy, K., Conliffe, J., 2010. Dolomitization of the lower St. George Group on the Northern Peninsula in western Newfoundland: implications for lateral distribution of porosity. Bulletin of Canadian Petroleum Geology 58(4), 361–374.

Azmy, K., Veizer, J., Misi, A., de Oliveira, T.F., Sanches, A.L., Dardene, M.A., 2001. Dolomitization and isotope stratigraphy of the Vazante formation, Sao Francisco Basin, Brazil. Precambrian Res. 112 (3), 303–329.

Azmy, K., Kaufman, A. J., Misi, A., de Oliveira, T. F., 2006. Isotope stratigraphy of the Lapa formation, São Francisco basin, Brazil: implications for late Neoproterozoic glacial events in South America. Precambrian Research 149(3-4), 231–248.

Azmy, K., Lavoie, D., Knight, I., Chi, G., 2008. Dolomitization of the Aguathuna Formation carbonates of Port au Port Peninsula in western Newfoundland, Canada: implications for a hydrocarbon reservoir. Canadian Journal of Earth Sciences 45, 795–813.

Azmy, K., Knight, I., Lavoie, D., Chi, G., 2009. Origin of Boat Harbour Dolomites of St. George Group in Western Newfoundland, Canada: implications of porosity controls. Bulletin of Canadian Petroleum Geology 57, 81–104.

Azmy, K., Stouge, S., Christiansen, J.L., Harper, D.A.T., Knight, I., Boyce, D., 2010. Carbon-isotope stratigraphy of the Lower Ordovician succession in Northeast Greenland: implications for correlations with St. George Group in western Newfoundland (Canada) and beyond. Sedimentary Geology 225, 67–81.

Azmy, K., Brand, U., Sylvester, P., Gleeson, S., Logan, A., Bitner, M.A., 2011. Biogenic low Mg calcite (brachiopods): proxy of seawater-REE composition, natural processes and diagenetic alteration. Chem. Geol. 280, 180–190.

Azmy, K., Lavoie D., Wang, Z., Brand, U., Al-Aasm, I., Jackson, S., Girard, I., 2013. Magnesium -isotope and REE compositions of Lower Ordovician carbonates from eastern Laurentia: Implications for the origin of dolomites and limestones. Chemical Geology 356, 64–75.

Azmy, K., Stouge, S., Brand, U., Bagnoli, G., Riiperdan, R., 2014. High-resolution chemostratigraphy of the Cambrian-Ordovician GSSP in western Newfoundland, Canada: enhanced global correlation tool. Palaeoegeography, Palaeoclimatology, Palaeoecology 409, 135–44.

Azmy, K., Kendall, K., Brand, U., Stouge, S., Gordon, G.W., 2015. Redox conditions across the Cambrian-Ordovician boundary: elemental and isotopic signatures retained in the GSSP carbonates. Palaeoegeography, Palaeoclimatology, Palaeoecology 440, 440–54.

Azomani, E., Azmy, K., Blamey, N., Brand, U., Al-Aasm, I., 2013. Origin of Lower Ordovician dolomites in eastern Laurentia: Controls on porosity and implications from geochemistry. Marine and Petroleum Geology 40, 99–114.

Babcock, L.E., Peng, S.C., Brett, C.E., Zhu, M.Y., Ahlberg, P., Bevis, M. and Robison, R.A., 2015. Global climate, sea level cycles, and biotic events in the Cambrian Period. Palaeoworld 24(1-2), 5-15.

Banner, J.L., Hanson, G.N., Meyers, W.J., 1988. Rare earth element and Nd isotopic variations in regionally extensive dolomites from the Burlington-Keokuk Formation

(Mississippian): implications for REE mobility during carbonate diagenesis. J. Sediment. Petrol. 58, 415–432.

Banner, J. L., and Hanson, G. N. 1990. Calculation of simultaneous isotopic and trace element variations during water-rock interaction with applications to carbonate diagenesis. Geochimica et Cosmochimica Acta 54(11), 3123–3137.

Banner, J.L., 1995. Application of the trace element and isotope geochemistry of strontium to studies of carbonate diagenesis. Sedimentology 42, 805–824.

Barili, R., Neilson, J. E., Brasier, A. T., Goldberg, K., Pastro Bardola, T., De Ros, L. F., and Leng, M. 2018. Carbon isotopes, stratigraphy, and environmental change: The Middle–Upper Cambrian Positive Excursion (SPICE) in Port au Port Group, western Newfoundland, Canada. Canadian Journal of Earth Sciences, 55(11), 1209–1222.

Barton, E.D., Bau, M., Alexander, B. 2006. Preservation of primary REE patterns without Ce anomaly during dolomitization of Mid-Paleoproterozoic limestone and the potential re-establishment of marine anoxia immediately after the 'Great Oxidation Event'. South African Journal of Geology 109, 81–86.

Bau, M., and Dulski, P. 1996. Distribution of yttrium and rare-earth elements in the Penge and Kuruman iron-formations, Transvaal Supergroup, South Africa. Precambrian Research, 79(1-2), 37–55.

Bau, M., and Alexander, B. 2006. Preservation of Primary REE patterns without Ce anomaly during dolomitization of Mid-Paleoproterozoic limestone and the potential re-establishment of marine anoxia immediately after the ‘Great Oxidation Event’. South Afr. J. Geol. 109: 81–86.

Bau, M., Balan, S., Schmidt, K., and Kouchinsky, A. 2010. Rare earth elements in mussel shells of the Mytilidae family as tracers for hidden and fossil high-temperature hydrothermal systems. Earth Planet. Sci. Lett. 299 (3): 377–390.

Berner, R.A., Kothavala, Z., 2001. GEOCARB III: a revised model of atmospheric CO_2 over Phanerozoic time. American Journal of Science 301, 182–204.

Blamey, N.J.F., 2012. Composition and evolution of crustal, geothermal and hydrothermal fluids interpreted using quantitative fluid inclusion gas analysis. Journal of Geochemical Exploration 116, 17–27.

Blamey. N.J.F., Norman, D.I., 2002. New interpretations of geothermal fluid inclusion volatiles: Ar/He and N_2/Ar ratios-a better indicator of magmatic volatiles, and equilibrium gas geothermometry. In: Proceedings: Twenty-seventh workshop on Geothermal Reservoir Engineering. Stanford University, Stanford, California

Blamey, N.J.F., Parnell, J., McMahon, S., Mark, D., Tomkinson, T., Lee, M., Shivak, J., Izawa, M., Banerjee, M., Flemming, R., 2015. Evidence for methane in Martian meteorites. Nature Communications 6, 7399, doi:10.1038/ncomms8399

Bodnar, R.J., 2003. Interpretation of data from aqueous-electrolyte fluid inclusions. In: Samson, I., Anderson, A., Marshal, D. (Eds.), Fluid Inclusions: Analyses and Interpretation. Mineralogical Associations of Canada, Short Course Series 32, 81–100.

Boyce, W.D., 1977. New Cambrian trilobites from western Newfoundland: unpublished B.Sc. thesis, Memorial University of Newfoundland, 66.

Boyce, W.D., 1979. Further developments in western Newfoundland biostratigraphy: in Mineral Development Division, Department of Mines and Energy, Government of Newfoundland and Labrador Report 79-1, 7–10.

Brand, U., Logan, A., Hiller, N., Richardson, J., 2003. Geochemistry of modern brachiopods: Applications and implications for oceanography and paleoceanography. Chemical Geology 198, 305–334. http://doi.org/10.1016/S0009-2541(03)00032-9

Brand, U., Logan, A., Bitner, M.A., Griesshaber, E., Azmy, K., Buhl, D., 2011. What is the ideal proxy of Paleozoic seawater? Memoirs of the Association of Australasian Palaeontological Society Memoirs 41, 9–24.

Brasier, M.D., 1993. Towards a carbon isotope stratigraphy of Cambrian System: potential of the Great Basin succession. In High Resolution Stratigraphy (eds E.A., Hailwood and R.B., Kidd). Geological Society of London, Special Publication no. 70, 341–50.

Brasier, M.D., Khomentovksy, V.V., Corfield, R.M., 1993. Stable isotopic calibration of the earliest skeletal fossil assemblages in eastern Siberia (Precambrian-Cambrian boundary): Terra Nova 5, 225–232.

Budd, D.A., 1997. Cenozoic dolomites of carbonate islands: their attributes and origin. Earth-Science Reviews 42, 1–47.

Budd, D.A., Hammes, U., Ward, W.B., 2000. Cathodoluminiscence in calcite cements: New insights on Pb and Zn sensitizing, Mn activation and Fe at low trace-element concentration. Journal of Sedimentary Research 70(1), 217–226.

Chang, X., Hou, M., Woods, A., Chen, Z.Q., Liu, X., Liao, Z., Liu, Y., Chao, H., 2021. Late Ordovician paleoceanographic change: Sedimentary and geochemical evidence from Northwest Tarim and Middle Yangtze region, China. Palaeogeography, Palaeoclimatology, Palaeoecology 562, 110070.

Chen, X., Romaniello, S.J., Herrmann, A.D., Hardisty, D., Gill, B.C., Anbar, A.D., 2018. Diagenetic effects on uranium isotope fractionation in carbonate sediments from the Bahamas. Geochimica et Cosmochimica Acta 237, 294–311.

Chi, G., Ni, P., 2007. Equations for calculation of $NaCl/(NaCl+CaCl_2)$ ratios and salinities from hydrohalite-melting and ice-melting temperatures in the H_2O-NaCl-$CaCl_2$ system. Acta Petrologica Sinica, 22, 33–37.

Chow N., James, N.P., 1987a. Cambrian Grand Cycles: a northern Appalachian perspective. Geological Society of America Bulletin 98, 418–429.

Chow N., James N.P., 1987b. Facies-specific, calcitic and bimineralic ooids from Middle and Upper Cambrian platform carbonates, western Newfoundland, Canada. Journal of Sedimentary Petrology 57, 907–921.

Chow N., James, N.P., 1992. Synsedimentary diagenesis of Cambrian peritidal carbonates: evidence from hardgrounds and surface paleokarst in the Port au Port Group, western Newfoundland. Bulletin of Canadian Petroleum Geology 40(2), 115–127.

Chow N., James, N.P., 1992. Synsedimentary diagenesis of Cambrian peritidal carbonates: evidence from hardgrounds and surface paleokarst in the Port au Port Group, western Newfoundland. Bulletin of Canadian Petroleum Geology 40(2), 115–127.

Clark, I.D., Fritz, P., 1997. Environmental Isotopes in Hydrogeology. Lewis Publisher, 325.

Clarkson, M. O., Poulton, S. W., Wood, R. A., 2014. Assessing the utility of Fe/Al and Fe-speciation to record water column redox conditions in carbonate-rich sediments. Chemical Geology 382, 111–122. https:// doi.org/10.1016/j.chemgeo.2014.05.031

Conliffe, J., Azmy, K., Knight, I., Lavoie, D., 2009. Dolomitization of the Lower Ordovician Watts Bight Formation of the St. George Group, western Newfoundland: Evidence of Hydrothermal fluid alteration: Canadian Journal of Earth Sciences 46(4), 247–261.

Conliffe, J., Azmy, K., Gleeson, S.A., Lavoie, D., 2010. Fluids associated with hydrothermal dolomitization in St. George Group, western Newfoundland, Canada. Geofluids 10, 422–437.

Conliffe, J., Azmy, K., Greene, M., 2012. Dolomitization of the Lower Ordovician Catoche Formation: implications for hydrocarbon exploration in western Newfoundland. Marine and Petroleum 30, 161–173.

Cooper, M., Weissenberger, J., Knight, I., Hostad, D., Gillespie, D., Williams, H., 2001. Basin evolution in western Newfoundland: new insights from hydrocarbon exploration. American Association of Petroleum Geologists (AAPG) Bulletin 85, 393–418.

Cooper, R.A., Nowlan, G.S., Williams, S.H., 2001. Global stratotype section and point for base of the Ordovician system. Episodes 24, 19–28.

Dardene, M.A., 2001. Lithostratigraphic sedimentary sequences of the Vazante Group. IGCP 450 Proterozoic sediment-hosted base metal deposits of western Gondwana (Abstr.). Belo Horizonte, Brazil, 48-50.

Derry, L. A., Kaufman, A. J., Jacobsen, S. B., 1992. Sedimentary cycling and environmental change in the Late Proterozoic: evidence from stable and radiogenic isotopes. Geochimica et Cosmochimica Acta 56(3), 1317–1329.

Dickson, A.J., Cohen, A.S., Coe, A.L., 2011. Seawater oxygenation during the Paleocene-Eocene Thermal Maximum. Geology 40(7), 639–642.

Dickson, J.A.D., 1966. Carbonate identification and genesis as revealed by staining. Journal of Sedimentary Research 36(2), 491–505.

Dix, G.R., 1981. The Codroy Group (Upper Mississippian) on the Port au Port Peninsula, western Newfoundland: stratigraphy, paleontology, sedimentology and diagenesis: unpublished M.Sc. thesis, Memorial University of Newfoundland, 218.

Dixon, J., 1976. Pattern carbonate – a diagenetic feature: Bulletin of Canadian Petroleum Geology 24, 450–456.

Drever, J.I., 1988. The Geochemistry of Natural Waters. Prentice Hall Inc., Englewood Cliffs, N. J., 437.

Eriksson, K.A., McCarthy, T.S., Truswell, J.F., 1975. Limestone formation and dolomitization in Lower Proterozoic succession from South Africa. Journal of Sedimentary Petrology 45(3), 604–614.

Fan, R., Deng, S., Zhang, X., 2011. Significant carbon isotope excursions in the Cambrian and their implications for global correlations. Sci China Earth Sci. 54, 1686–1695.

Friedman, I., O'Neil, J. R., 1977. Compilation of stable isotope fractionation factors of geochemical interest (Vol. 440). US Government Printing Office.

Fritz, W.H., 1972. Corner of the Beach Formation: in St. Julian, Appalachian Structure and Stratigraphy in Quebec, Excursion A56-C56, XXIV International Geological Congress, Montreal, 72–74.

Giggenbach, W. F., 1986. The use of gas chemistry in delineating the origin of fluids discharged over the Taupo Volcanic Zone. In Proceedings of Symposium 5, Int. Volc. Congress, Auckland, 47–50.

Goldstein, R.H., Reynolds, T.J., 1994. Systematics of fluid inclusions in diagenetic minerals. Society for Sedimentary Geology (SEPM) Short Course, Tulsa, Okla.

Gregg, J. M., 1983. On the formation and occurrence of saddle dolomite: discussion. Journal of Sedimentary Research 53(3), 1025–1026.

Gregg, J.M., Sibley, D.F., 1984. Epigenetic dolomitization and the origin of xenotopic dolomite texture. Journal of Sedimentary Research 54(3), 908–931.

Haeri-Arkadani, O., Al-Aasm, L., Coniglio, M., Samson, I., 2013. Diagenetic evolution and associated mineralization in Middle Devonian carbonates, southwestern

Ontario, Canada. Bulletin for Canadian Petroleum and Geology 61, 41-58.Hammer, O., Svensen, H.H., 2017. Biostratigraphy and carbon and nitrogen geochemistry of the SPICE event in Cambrian low-grade metamorphic black shale, Southern Norway. Palaeogeography, Palaeoclimatology, Palaeoecology 468, 216–227.

Hay, W.W., Leslie, M.A., 1990. Could possible changes in global groundwater reservoir cause eustatic sea-level fluctuations? Sea-level change, pp.161–170.

Haywick, D.W., 1984. Dolomite within the St. George Group (Lower Ordovician), western Newfoundland. Unpublished M.Sc. thesis, Memorial University of Newfoundland, St. John’s, Newfoundland.

Hein, J.R., Gray, S.C., Richmond, B.M., and White, L.D. 1992. Dolomitization of quaternary reef limestone, Aitutaki, Cook Islands. Sedimentology. 39, 645-661.

Hill, A.C., Walter, M.R., 2000. Mid-Neoproterozoic (~830–750 Ma) isotope stratigraphy of Australia and global correlation. Precambrian Res. 100, 181–211.

Honarmand, J., Amini, A., 2012. Diagenetic processes and reservoir properties in the ooid grainstones of the Asmari Formation, Cheshmeh Khush Oil Field, SW Iran. J. Pet. Sci. Eng. 81, 70–79.

Hou, Y., Azmy, K., Berra, F., Jadoul, F., Blamey, N.J.F., Gleeson, S.A., Brand, U., 2015. Origin of the Breno and Esino dolomites in the western Southern Alps (Italy): Implications for a volcanic influence. Marine and Petroleum Geology 69, 38–52.

Howley, R.A., Jiang, G., 2010. The Cambrian Drumian carbon isotope excursion (DICE) in the Great Basin, western United States. Palaeoegeography, Palaeoclimatology, Palaeoecology 296, 138–150.

Hu, Z.W., Huang, S.J., Li, Z.M., Qing, H.R., Fang, M., Lan, Y.F., 2012. Temperatures of dolomitizing fluids in the Feixianguan Formation from the Northeastern Sichuan Basin. Sci. China-Earth Sci. 55, 1627–1640.

Huang, S.J., Huang, K.K., Lu, J., Lan, Y.F., 2014. The relationship between dolomite textures and their formation temperature: a case study from the Permian-Triassic of the Sichuan Basin and the lower Paleozoic of the Tarim Basin. Pet. Sci. 11, 39–51.

Hurtgen, M.T., Pruss, S.B., Knoll, A.H., 2009. Evaluating the relationship between the carbon and sulfur cycles in the later Cambrian ocean: an example from the Port au Port Group, western Newfoundland, Canada. Earth and Planetary Science Letters 281, 288–97.

Ichukuni, M., 1973. Partition of strontium between calcite and solution: Effect of substitution by manganese. Chemical Geology 11, 315–319. http://doi.org./10.1016/0009-2541(73)90102-2

Jacquemyn, C., Desouky, H.E., Hunt, D., Casini, G., Swennen, R., 2014. Dolomitization of the Latemar platform: fluid flow and dolomite evolution. Mar. Pet. Geo. 55, 43–57.

James, N.P., Steven, R.K., 1982. Anatomy and evolution of a lower Paleozoic continental margin, western Newfoundland: 11th International Congress on Sedimentology, Field Guidebook 2B, Hamilton, 75.

James, N.P., Stevens, P.K., 1986. Stratigraphy and correlation of the Cambro–Ordovician Cow Head Group, western Newfoundland. Geological Survey of Canada Bulletin 366, 1–143.

Kaufman, A.J., Knoll, A.H., 1995. Neoproterozic variations in the C-isotopic composition of seawater: stratigraphic and biogeochemical implications. Precambrian Res. 73, 27–49.

Kaufman, A.J., Jacobsen, S.B., Knoll, A.H., 1993. The Vendian record of Sr and C isotopic variations in seawater: implications for tectonics and paleoclimate. Earth Planet. Sci. Lett. 120, 409–430.

Kimura, H., Azmy, K., Yamamuro, M., Zhi-Wen, J., Cizdziel, J.V., 2005 Intergrated stratigraphy of the Upper Proterozoic succession in Yunnan of South China: Re-evaluation of global correlation and carbon cycle. Precambrian Research 138, 1–36. http://doi.org/10.1016/j.precamres.2005.02.002

Kindle, C.H., Whittington, H.B., 1965. New Cambrian and Ordovician fossil localities in western Newfoundland: Geological Society of America Bulletin 76, 683–688.

Kırmacı, M.Z., Akdağ, K., 2005. Origin of dolomite in the Late Cretaceous-Paleocene limestone turbidites, eastern Pontides, Turkey. Sedimentary Geology 181(1-2): 39–57.

Kitano, Y., Oomori, T., 1971. The coprecipitation of uranium with calcium carbonate. Journal of Oceanographical Society of Japan 27(1), 34–42.

Knight, I., Azmy, K., Boyce, W.D., Lavoie, D., 2008. Tremadocian carbonate rocks of the lower St. George group, Port au Port peninsula, western Newfoundland: lithostratigraphic setting of diagenetic, isotopic and geochemical studies. In Current research. Newfoundland and Labrador Department Mines and Energy, Geological Survey Report 08-1, 115–149.

Kouchinsky, A., Bengston, S., Gallet, Y., Korovnkikov, I., Pavlov, V., Runnegar, B., Shields, G., Veizer, J., Young, E., Zeigler, K., 2008. The SPICE carbon isotope excursion in Siberia: A combined study of the upper Middle Cambrian–lowermost Ordovician Kulyumbe River section, northwestern Siberian Platform: Geological Magazine 145, 609–622. doi:10.1017/S0016756808004913.

Kretz, R., 1992. Carousel model for the crystallization of saddle dolomite. Journal of Sedimentary Petrology 62, 190–195.

Land, L.S., 1983. The application of stable isotopes to studies of the origin of dolomite and to problems of diagenesis of clastic sediments. In: Arthur, M.A., Anderson, T.F., Kaplan, I.R., Veizer, J., Land, L.S. (Eds.), Society for Sedimentary Geology (SEPM) Short Course Notes 10, 4.1–4.22.

Land, L.S. 1986. Environments of limestone and dolomite diagenesis: some geochemical considerations. In: Longman MW (ed) Carbonate diagenetic textures from nearshore diagenetic environments, vol 64, 1980. American Association of Petroleum Geologists Bulletin, 461–487.

Land, L.S., 1992. The dolomite problem: stable and radiogenic isotope clues. In: Isotopic signatures and sedimentary records, Lecture Notes in Earth Sciences 43, 49–68.

Landing, E., 2007. Ediacaran–Ordovician of east Laurentia—geologic setting and controls on deposition along the New York Promontory. In S. W. Ford Memorial Volume: Ediacaran–Ordovician of East Laurentia (ed. E. Landing), New York State Museum Bulletin no. 510, 5–24.

Landing, E., 2012a.Time-specific black mudstones and global hyperwarming on the Cambrian–Ordovician slope and shelf of the Laurentia palaeocontinent. Palaeogeography, Palaeoclimatology, Palaeoecology 367–368, 256–72.

Landing, E., 2013. The Great American Carbonate Bank in northeast Laurentia: its births, deaths, and linkage to continental slope oxygenation (Early Cambrian–Late Ordovician). In The Great American Carbonate Bank, Essays in Honor of James Lee Wilson (eds J. R. Derby, R. D. Fritz, S. A. Longacre, W. A. Morgan and C. A.

Sternbach). American Association of Petroleum Geologists Bulletin, Memoir 98, 451–92.

Landing, E., Geyer, G., Bartowski, K. E., 2002. Latest Early Cambrian small shelly fossils, trilobites, and Hatch Hill dysaerobic interval on the east Laurentian continental slope. Journal of Paleontology 76, 285–303

Landing, E., Westrop, S.R., Miller, J.F., 2010. Globally practical base for the uppermost Cambrian (Stage 10): FAD of the conodont Eoconodontus notchpeakensis and the Housian [sic, read 'Lawsonian' as the abstract text] Stage. In The 15th Field Conference of the Cambrian Stage Subdivision Working Group. Abstracts and Excursion Guide, Prague, Czech Republic and South-eastern Germany (eds O. Fatka and P. Budil), Prague: Czech Geological Survey, 18.

Landing, E., Westrop, S.R., Adrain, J.M., 2011. The Lawsonian Stage – the Eoconodontus notchpeakensis FAD and HERB carbon isotope excursion define a globally correlatable terminal Cambrian stage. Bulletin of Geosciences 86, 621–40.

Landing, W. M., Bruland, K. W., 1987. The contrasting biogeochemistry of iron and manganese in the Pacific Ocean. Geochimica et Cosmochimica Acta 51(1), 29–43. https://doi.org/10.1016/00167037(87)90004-4

Lane, T.E., 1990. Dolomitization, Brecciation and Zinc Mineralization and Their Paragenetic Stratigraphic and Structural Relationships in the Upper St. George

Group (Ordovician) at Daniel’s Harbour, Western Newfoundland. Unpublished Ph.D. thesis, Memorial University of Newfoundland, St. John’s, Nfld.

Lavoie, D., 1994. Diachronous tectonic collapse of the Ordovician continental margin, eastern Canada: comparison between the Quebec Reentrant and St. Lawrence Promontory. Canadian Journal of Earth Sciences 31(8), 1309–1319.

Lavoie, D., 2008. Appalachian foreland basin of Canada. 1-Canada. In: Sedimentary basins of the United States and Canada. A.D. Miall (ed). Elsevier Science Publishing, 63–105.

Lavoie, D., Chi, G., Brennan-Alpert, P., Betrand, R., 2005. Hydrothermal dolomitization in the Lower Ordovician Romaine Formation of the Anticosti Basin: significance for hydrocarbon exploration. Bulletin of Canadian Petroleum Geology 53, 454–471.

Lee, S.G., Lee, D.H., Kim, Y., Chae, B.G., Kim, W.Y., Woo, N.C., 2003. Rare earth elements as indicators of groundwater environment changes in a fractured rock system: evidence from fracture-filling calcite. Appl. Geochem. 18, 135–143.

Levesque, R.J., 1977. Stratigraphy and sedimentology of Middle Cambrian to Lower Ordovician shallow water carbonate rocks, western Newfoundland: unpublished M.Sc. thesis, Memorial University of Newfoundland, 276.

Li, D., Zhang, X., Chen, K., Zhang, G., Chen, X., Huang, W., … Shen, Y., 2017. High-resolution C-isotope chemostratigraphy of the uppermost Cambrian stage (Stage 10) in South China: implications for defining the base of stage 10 and palaeoenvironmental change. Geological Magazine 1, 1–12.

Li, P.P., Hao, F., Guo, X.S., Zou, H.Y., Yu, X.Y., Wang, G.W., 2015. Processes involved in the origin and accumulation of hydrocarbon gases in the Yuanba gas field, Sichuan Basin, southwest China. Mar. Pet. Geol. 59, 150–165.

Liang, T., and Jones, B., 2021. Characteristics of primary rare earth elements and yttrium in carbonate rocks from the Mesoproterozoic Gaoyuzhuang Formation, North China: Implications for the depositional system. Sedimentary Geology 415, 105864.

Lindholm, R.C and Finkelman, R.B., 1972. Calcite staining: semiquantitative determination of ferrous iron. Journal of Sedimentary Petrology 42, 239–242.

Liyuan, W., Qingjun, G., Changqiu, Z., Rongfei, W., Yinan, D., Xiaokun, H., Liyan, T., Jing, K., Xi, Y., 2021. Trace and rare earth elements geochemistry of sedimentary rocks in the Ediacaran-Cambrian transition from the Tarim Basin, Northwest China: Constraints for redox environments. Precambrian Research 352, 105942.

Lochman, C. 1938. Middle and Upper Cambrian fauna from western Newfoundland: Journal of Paleontology 12, 461–477.

Lohmann, K.C., Walker, J.C.G., 1989. The $\delta^{18}O$ record of Phanerozoic abiotic marine calcite cements. Geophysical Research Letters 16, 319–322. doi:10.1029/GL016i004p00319.

Lonnee, J., Machel, H.G., 2006. Pervasive dolomitization with subsequent hydro- thermal alteration in the Clarke Lake gas field, Middle Devonian Slave Point Formation, British Columbia, Canada. American Association of Petroleum Geologists Bulletin 90, 1739–1761.

Lorens, R.B., 1981. Sr, Cd, Mn, and Co distribution coefficients in calcite as a function of calcite precipitation rate. Geochimica et Cosmochimica Acta 45, 553–561. https://doi.org/10.1016/0016-7037(81)90188-5

Lowenstern, J.B., Janik, C.J., 2003. The origins of reservoir liquids and vapors from the geysers geothermal field, California. Society of Economic Geologists, Special Publication 10, 181–196.

Machel, H. G., 2004. Concepts and models of dolomitization: a critical reappraisal. Geological Society, London, Special Publications 235(1), 7–63.

Machel, H. G., Mountjoy, E. W., 1986. Chemistry and environments of dolomitization—a reappraisal. Earth-Science Reviews 23(3): 175–222.

Machel, H.G., Mountjoy, E.W., 1990. Coastal mixing zone dolomite, forward modeling, and massive dolomitization of platform-margin carbonate; Discussion. Journal of Sedimentary Petrology 60, 1008–1012.

Machel, H.G., Burton, E.A., 1991. Factors governing cathodoluminescence in calcite and dolomite, and their implications for studies of carbonate diagenesis. Luminescence microscopy and spectroscopy, qualitative and quantitative applications. SEPM Short course 25, 37–57.

Maloof, A.C., Schrag, D.P., Crowley, J.L., Bowring, S.A., 2005. An expanded record of Early Cambrian carbon cycling from the Anti-Atlas Margin, Morocco. Canadian Journal of Earth Sciences 42, 2195–2216.

Maloof, A.C., Porter, S.M., Moore, J.L., Dudás, F.Ö., Bowring, S.A., Higgins, J.A., Fike, D.A., Eddy, M.P., 2010. The earliest Cambrian record of animals and ocean geochemical change: Geological Society of America Bulletin 122, 1731–1774, https:// doi .org /10 .1130 /B30346.1.

Marshall, D.J., 1988, Cathodoluminescence of Geological Materials: Boston, Unwin Hyman, 146.

Maruyama, S., Sawaki, Y., Ebisuzaki, T., Ikoma, M., Omori, S., Komabayashi, T., 2014. Initiation of leaking Earth: an ultimate trigger of the Cambrian explosion. Godwana Res. 25, 910–944.

Mazzullo, S.J., Chilingarian, G.V., 1996. Dolomite reservoirs: geochemical techniques for evaluating origin and distribution, by Allen, J.R., Wiggins, W.D., AAPG continuing education course note No 36. J. Pet. Sci. Eng. 14, 262–263.

McKirdy, D.M., Burgess, J.M., Lemon, N.M., Yu, X., Cooper, A.M., and Gostin, V.A., Jenkins, R.J., Both, R.A., 2001. A chemostratigraphic overview of the Late Cryogenian interglacial sequence in the Adelaide Fold Thrust Belt, South Australia. Precambrian Res. 106, 149–186.

McLennan, S. M., 1989. Rare earth elements in sedimentary rocks: influence of provenance and sedimentary processes. Geochemistry and Mineralogy of Rare Earth Elements, Reviews in Mineralogy 21, 169–200.

McLennan, S. M., 2001. Relationships between the trace element composition of sedimentary rocks and upper continental crust. Geochemistry, Geophysics, Geosystems, 2(4).

Miller, J.F., Evans, K.R., Freeman, R.L., Ripperdan, R.L., Taylor, J.F., 2011. Proposed stratotype for the base of the Lawsonian Stage (Cambrian Stage 10) at the first appearance datum of Eoconodontus notchpeakensis (Miller) in the House Range, Utah, USA. Bulletin of Geosciences 86,595–620.

Misi, A., Kaufman, A.J., Veizer, J., Powis, K., Azmy, K., Boggiani, P.C., Gaucher, C., Teixeira, J.B.G., Sanches, A.I., Iyer, S.S., 2007. Chemostratigraphic correlation of Neoproterozoic successions in South America. Chemical Geology 237, 161–185.

Montañez, I.P., Oslegger, D.A., Banner, J.I., Mack, L.E., Musgrove, M., 2000. Evolution of the Sr and C isotope composition of Cambrian oceans. GSA Today 10, 1–7.

Morel, F.M.M., Milligan, A.J., Saito, M.A., 2004. Marine bioinorganic chemistry: The role of trace metals in the oceanic cycles of major nutrients. The Oceans and Marine Geochemistry, Treatise on Geochemistry 6,113–143.

Murphy, A.E., Sageman, B.B., Hollander, D.J., Lyons, D.J., Brett C.E., 2000. Black shale deposition and faunal overturn in the Devonian Appalachian basin: clastic starvation, seasonal water-column mixing, and efficient biolimiting nutrient recycling. Paleoceanography 15, 280–291. https://doi.org/10.1029/1999PA000445

Neilson, J.E., Brasier, A.T., North, C.P., 2016. Primary aragonite and high-Mg calcite in the late Cambrian (Furongian). Potential evidence from marine carbonates in Oman. Terra Nova 28(5), 306–315.

Norman, D. I., Musgrave, J. A., 1994. N_2-Ar-He compositions in fluid inclusions: Indicators of fluid source. Geochimica et Cosmochimica Acta 58(3), 1119–1131.

Norman, D.I., Moore, J.N., 1999. Methane and excess N_2 and Ar in geothermal fluid inclusions. In: proceedings: Twenty-fourth workshop of Geothermal Reservoir Engineering. Stanford University, Stanford California, 233–240.

Norman, D.I., Blamey, N.J.F., 2001. Quantitative analysis of fluid inclusion volatiles by a two-mass spectrometer system. In: Noronha, F., Doria, A., Guedes, A. (Eds), European Current Research On Fluid Inclusions, Porto 2001 (XVI ECROFI): Faculdidade de Ciencias do Porto, Departmento de Geologia, Memoria no. 7, 341–344.

Norman, D.I., Moore, J.N., 2003. Organic species in Geothermal Waters in light of Fluid inclusion gas analyses. In: Proceedings, Twenty-eighth workshop on Geothermal Reservoir Engineering. Stanford University, Stanford, California. SGP–TR–173.

Norman, D.I., Moore, J.N., Yonaka, B., Musgrave, J., 1996. Gaseous species in fluid inclusions: A tracer of fluid and in indicator of fluid processes. In: Proceedings: Twenty-first workshop of geothermal reservoir engineering. Stanford University, Stanford, California, 233–240.

Norman, D.I., Moore, J.N., Musgrave, J., 1997. More on the use of fluid inclusion gaseous species as tracers in geothermal systems. In: Twenty-second workshop on geothermal reservoir engineering. Stanford University, Stanford, California, 419–426.

Norman, D.I., Blamey, N.J.F., Moore, J.N., 2002. Interpreting geothermal processes and fluid sources from fluid inclusion organic compounds and CO_2/N_2 ratios. In:

Proceedings, Twenty-seventh workshop on geothermal reservoir engineering. Stanford University, Stanford, California, 419–426.

North, F.K., 1971. The Cambrian of Canada and Alaska: in Holland, C.H ed., Cambrian of the New World, Wiley-Interscience, New York, 219–324.

Nothdurft, L.D., Webb, G.E., Kamber, B.S., 2004. Rare earth element geochemistry of Late Devonian reefal carbonates, Canning Basin, Western Australia: confirmation of a seawater REE proxy in ancient limestones. Geochim. Cosmochim. Acta 68, 263–283.

Olanipekun, B. J., Azmy, K., Brand, U., 2014. Dolomites of the Boat Harbour Formation in the Northern Peninsula, western Newfoundland, Canada: Implications for dolomitization history and porosity control. AAPG bulletin 98(4), 765–791.

Pagès, A., Schmid, S., 2016. Euxinia linked to the Cambrian Drumian carbon isotope excursion (DICE) in Australia: Geochemical and chemostratigraphic evidence. Palaeoegeography, Palaeoclimatology, Palaeoecology 461,65–76.

Palmer, A.R., 1969. Cambrian trilobite distributions in North America and their bearing on Cambrian paleogeography of Newfoundland: American Association of Petroleum Geologists Memoir 12, 139–144.

Palmer, A.R., James, N.P., 1979. The Hawke Bay Event: a circum-Iapetus regression near the Lower-Middle Cambrian boundary: I.G.CP. Meeting, Blacksburg, Virginia, A3.

Parry, W.T., Blamey, N.J.F., 2010. Fault fluid composition from fluid inclusion measurements, Laramide age Uinta thrust fault, Utah, Chemical Geology 278, 105–119.

Pattan, J. N., Mir, I. A., Parthiban, G., Karapurkar, S. G., Matta, V. M., Naidu, P. D., Naqvi, S. W. A., 2013. Coupling between suboxic condition in sediments of the western Bay of Bengal and southwest monsoon intensification: A geochemical study. Chemistry Geology 343, 55 –66. https://doi.org/10.1016/j.chemgeo.2013.02.011

Peng, S., Babcock, L.E., Zuo, J.X., Lin, H.L., Zhu, X.J., Yang, XF., Robison, R.A., Chi, Y.P., Bagnoli, G., Chen, Y., 2009. The Global boundary Stratotype Section and Point (GSSP) of the Guzhangian Stage (Cambrian) in the Wuling Mountains, northwestern Hunan, China: Episodes 32, 41–55.

Peng, S., Babcock, L.E., Cooper, R.A., 2012. The Cambrian period In The Geologic Time Scale 2012 (eds F.M. Gradstein, J.G. Ogg, M. Schmitz and G. Ogg). Oxford, UK: Elsevier, 437–88.

Piper, D. Z., Calvert, S. E., 2009. A marine biogeochemical perspective on black shale deposition. Earth- Science Reviews 95, 63–96. https://doi.org/10.1016/j.earscirev.2009.03.001

Pulsipher, A.P., Schiffbauer, J.D., Jeffrey, M.J., Huntley, J.W., Fike, D.A., Shelton, K.L., 2021. A meta-analysis of the Steptoean positive carbon isotope excursion: The SPICEraq database. Earth-Science Reviews, 103442.

Radke, B. M., Mathis, R. L., 1980. On the formation and occurrence of saddle dolomite. Journal of Sedimentary Research 50(4), 1149–1168.

Rameil, N., 2008. Early diagenetic dolomitization and dedolomitization of Late Jurassic and earliest Cretaceous platform carbonates: a case study from the Jura Mountains (NW Switzerland, E France). Sedimentary Geology 212, 70–85.

Rodgers, J., 1968. The eastern edge of the North American continent during the Cambrian and Early Ordovician: in Studies of Appalachian geology: Northern and Maritime, John Wiley & Sons, New York, 141–150.

Rong, H., Jiao, Y.Q., Wu, L.Q., Gu, Y., Zhang, L.Y., 2012. Relationship between heterogeneity and seismic velocities of the Yudongzi Triassic oolitic reservoirs in the Erlangmiao area, northwest Sichuan Basin, China. J. Pet. Sci. Eng. 100, 81–98.

Rowell, A.J., Brady, M.J., 1976. Brachiopods and Biomeres. Bringham Young University Geology Studies 23, 165–180.

Rush, P.F., Chafetz, H.S., 1990. Fabric retentive, non-luminescent brachiopods as indicators of original $\delta^{13}C$ and $\delta^{18}O$ compositions: a test. Journal of Sedimentary Petrology 60, 968–81.

Saltzman, M.R., Runnegar, B., Lohmann, K.C., 1998: Carbon isotope stratigraphy of Upper Cambrian (Steptoean Stage) sequences of the eastern Great Basin: record of a global oceanographic event. Geological Society of America Bulletin 110, 285–297.

Saltzman, M.R., Ripperdan, R.L., Brasier, M.D., Ergaliev, G.K., Lohmann, K.C., Robison, R.A., Chang, W.T., Peng, S., Runnegar, B., 2000. A global carbon isotope excursion during the Late Cambrian: relation to trilobite extinctions, organic matter burial and sea level. Palaeogeography, Palaeoceanography, Palaeoclimatology 162, 211–23.

Saltzman, M. R., Cowan, C. A., Runkel, A. C., Runnegar, B., Stewart, M. C., Palmer, A. R., 2004. The Late Cambrian SPICE ($\delta^{13}C$) event and the Sauk II-Sauk III regression: new evidence from Laurentian basins in Utah, Iowa, and Newfoundland. Journal of Sedimentary Research 74(3), 366–377.

Sanchez-Roman, M., McKenzie, J.A., de Luca Rebello Wagner, A., Romanek, C.S., Sanchez-Navas, A., Vasconcelos, C., 2011. Experimentally determined biomediated Sr partition coefficient for dolomite: significance and implication for natural dolomite. Geochem. Cosmochim. Acta 75, 887–904.

Schmid, S., 2017. Chemostratigraphy and palaeoenvironmental characterization of the Cambrian stratigraphy in the Amadeus Basin, Australia. Chemical Geology 451, 169–82.

Schuchert, C., Dunbar, C.O., 1934. Stratigraphy of western Newfoundland: Geological Society of America, Memoir 1, 123.

Scotese, C.R., Bambach, R.K., Van der Voo, R., Zeigler, A.M., 1979. Paleozoic base maps: Journal of Geology 87, 217–268.

Shembilu, N., Azmy, K., Blamey, N., 2021. Origin of Middle–Upper Cambrian dolomites in eastern Laurentia: a case study from Belle Isle strait, western Newfoundland. Marine and Petroleum Geology 125, 104858.

Shembilu, N., Azmy, K., 2021. Carbon-isotope stratigraphy of the Middle–Upper Cambrian in eastern Laurentia: implications for global correlation. Marine and Petroleum Geology 128, 105052

Shepherd, T.J., Rankin, A.H., Alderton, D.H.M., 1985. A Practical Guide to Fluid Inclusions. Blackie, London.

Shields, G., Stille, P., 2001. Diagenetic constraints on the use of cerium anomalies as palaeoseawater redox proxies: an isotopic and REE study of Cambrian phosphorites. Chemical Geology 175 (1-2), 29–48.

Sholkovitz, E.R., Shen, G.T., 1995. The incorporation of rare-earth elements in modern coral. Geochim. Cosmochim. Acta 59, 2749–2756.

Sholkovitz, E.R., Landing, W.M., Lewis, B.L., 1994. Ocean particle chemistry: the fractionation of rare earth elements between suspended particles and seawater. Geochim. Cosmochim. Acta 58, 1576–1580.

Sibley, D.F., 1982. Origin of common dolomite fabrics: clues from the Pliocene. Journal of Sedimentary Petrology 52, 1087–1100.

Śliwiński, M.G. Whalen, M.T., Day, J., 2010. Trace element variations in the Middle Frasnian Punctata Zone (Late Devonian) in the western Canada sedimentary basin- Changes in oceanic bioproductivity and paleoredox spurred by a pulse of terrestrial afforestation? Geologica Belgica 4, 459–482.

Sperber, C.M., Wilkinson, B.H., Peacor, D.R., 1984. Rock composition, dolomite stoichiometry, and rock/water reactions in dolomitic carbonate rocks. Journal of Geology 92 (6), 609–622.

Stouge, S., Boyce, W.D., 1983. Fossils of northwestern Newfoundland and southeastern Labrador: conodonts and trilobites: Mineral Development Division, Department of Mines and Energy, Government of Newfoundland and Labrador, Report 83-3, 55.

Sun, S.Q., 1995. Dolomite reservoir: porosity evolution and reservoir characteristics. AAPG Bull. 79, 186–204.

Tribovillard, N., Algeo, T. J., Lyons, T., Riboulleau, A., 2006. Trace metals as paleoredox and paleoproductivity proxies: An update. Chemical Geology 232, 12–32. https://doi.org/10.1016/j.chemgeo.2006.02.012

Tripathy, G. R., Singh, S. K., Ramaswamy, V., 2014. Major and trace element geochemistry of Bay of Bengal sediments: Implications to provenances and their controlling factors. Palaeogeography, Palaeoclimatology, Palaeoecology 397, 20–30. https://doi.org/ 10.1016/j.palaeo.2013.04.012

Troelsen, J.C., 1947. Geology of the Bonne Bay-Trout River area, Newfoundland: Unpublished Ph.D. thesis, Yale University, 289.

Tucker, M.E., Wright, V.P., 1990. Carbonate Sedimentology. Blackwell Publishing, Oxford, UK., 482.

Urey, H.C., Lowenstam, H.A., Epstein, S., McKinney, C.R., 1951. Measurement of paleotemperatures and temperatures of the Upper Cretaceous of England, Denmark, and the southeastern United States. Geol. Soc. Am. Bull. 62, 399–416.

Vahrenkamp, V.C., Stewart, P.K., 1990. A new distribution coefficient for the incorporation of strontium into dolomite and its implications for the formation of ancient dolomites. Geology 18, 387–391.

Vandeginste, V., John, C.M., Flierdt, T., Cosgrove, J.W., 2013. Linking process, dimension, texture, and geochemistry in dolomite geobodies: a case study from Wadi Mistal (northern Oman). AAPG Bull. 97, 1181–1207.

Veizer, J., 1983. Chemical diagenesis of carbonates: Theory and application of trace elements technique. In Stable Isotopes in Sedimentary Geology. Edited by M.A. Arthur, T.F. Anderson, I.R. Kaplan, J. Veizer, and L.S. Land. Society of Economic Paleontologists and Mineralogists (SEPM), Short course Notes 10, 3.1–3.100.

Veizer, J., Compston, W., Clauer, N., Schidlowski, M., 1983. $^{87}Sr/^{86}Sr$ in Late Proterozoic carbonates: evidence for a “mantle” event at∼ 900 Ma ago. Geochimica et Cosmochimica Acta 47(2), 295–302.

Veizer, J., Ala, D., Azmy, K., Bruckschen, P., Bruhn, F., Buhl, D., Carden, G.A.F., Diener, A., Ebneth,S., Godderis, Y., Jasper, T., Korte, C., Pawellek, F., Podlaha,O.G., Strauss, H., 1999. $^{87}Sr/^{86}Sr$, $\delta^{18}O$ and $\delta^{13}C$ evolution of Phanerozoic seawater. Chemical Geology 161, 59–88. doi:10.1016/S00092541(99)00081-9.

Wang, G.W., Li, P.P., Hao, F., Zou, H.Y., Yu, X.Y., 2015. Origin of dolomite in the Third Member of Feixianguan Formation (Lower Triassic) in the Jiannan area, Sichuan Basin, China. Mar. Pet. Geol. 63, 127–141.

Wang, L., Azmy, K., 2020. Palaeoenvironmental changes in slope carbonates across the Late Cambrian–Early Ordovician in western Newfoundland. Geological Journal. 1–13.

Warren, J., 2000. Dolomite: occurrence, evolution, and economically important associations. Earth-Science Reviews 52, 1–81.

Weaver, F.J., Macko, S.A., 1988. Source rocks of western Newfoundland. Organic Chemistry in Petroleum Exploration 13 (1-3), 411–421.

Webb, G.E., Kamber, B.S., 2000. Rare earth elements in Holocene reefal microbialites: a new shallow seawater proxy. Geochim. Cosmochim. Acta 64, 1557–1565.Webb, G.E., Nothdurft, L.D., Kamber, B.S., Kloprogge, J.T., Zhao, J.-X., 2009. Rare earth element geochemistry of scleractinian coral skeleton during meteoric diagenesis: a before and after sequence through neomorphism of aragonite to calcite. Sedimentology 56, 1433–1463.

Wendler, J.E, Wendler, I., 2016. What drove sea-level fluctuations during the mid-Cretaceous greenhouse climage? Palaeogeography, Palaeoclimatology, Palaeoecology 441, 412–419.

Wendler, I., Wendler, J.E., Clarke, L.J, 2016a. Sea-level reconstruction for Turonian sediments from Tanzania based on integration of sedimentology, microfacies, geochemistry and micropaleontology. Palaeogeography, Palaeoclimatology, Palaeoecology, 441, 578–564.

Wendler, J.E., Wendler, I., Vogt, C., Kuss, J., 2016b. Link between cyclic eustatic sea-level change and continental weathering: evidence for aquifer-eustasy in the Creatacous. Palaeogeography, Palaeoclimatology, Palaeoecology, 441, 430–437.

Whittington, H.B., Kindle, C.H., 1969. Cambrian and Ordovician stratigraphy of western Newfoundland: In North Atlantic Geology and Continental Drift (ed., M. Kay) American Association of Petroleum Geologists Memoir 12, 655–664.

Wignall, P. B., Twitchett, R. J., 1996. Oceanic anoxia and the end Permian mass extinction. Science 272, 1155–1158. https://doi.org/10.1126/science.272.5265.1155

Wignall, P.B. Zonneveld, J.P., Newton, R.J., Amor, K., Sephton, M.A., Hartley, S., 2007. The end Triassic mass extinction record of Williston Lake, British Columbia. Palaeogeography, Palaeoclimatology, Palaeoecology, 253, 385–406. https://doi.org/10.1016/j.palaeo.2007.06.020

Williams, H., 1976. Tectonic stratigraphic subdivision of the Appalachian Orogen (abstract). Geological Society of America 8, 300.

Williams, H., 1979. Appalachian Orogen in Canada. Canadian Journal of Earth Science 16, 792–807.

Williams, H., Stevens, R. K., 1974. The ancient continental margin of eastern North America. In The geology of continental margins, Springer, Berlin, Heidelberg, 781–796.Woods, M.A., Wilby, P.R., Leng, M.J., Rushton, A.W.A., Williams, M., 2011. The Furongian (late Cambrian) Steptoean Positive Carbon Isotope Excursion (SPICE) in Avalonia. Journal of the Geological Society, London 168, 851–61.

Wotte, T., Skovsted, C.B., Whitehouse, M.J., Kouchinsky, A., 2019. Isotopic evidence for temperate oceans during the Cambrian explosion. Scientific Reports 9(1), 1–9. https://doi.org/10.1038/s4518-019-42719-4.

Xiong, D., Azmy, K., Blamey, N., 2015. Origin of Carbonate Cements in Flemish Pass Basin Sandstone Reservoirs: Controls on Porosity Development. Atlantic Geology 51, 232. doi:10.4138/atlgeol.2015.008

Xiong, D., Azmy, K., Blamey, N.J.F., 2016. Diagenesis and origin of calcite cement in the Flemish Pass Basin sandstone reservoir (Upper Jurassic): Implications for porosity development. Marine and Petroleum Geology 70, 93118.

Zhang, S., Barnes, C. R., 2004. Arenigian (Early Ordovician) sea-level history and the response of conodont communities, western Newfoundland. Canadian Journal of Earth Sciences 41(7), 843–865.

Zhang, X.F., Hu, W.X., Jin, Z.J., Zhang, J.T., Qian, Y.X., Zhu, J.Q., Zhu, D.Y., Wang, X.L., Xie, X.M., 2008. REE compositions of Lower Ordovician dolomites in Central and North Tarim Basin, NW China: a potential REE proxy for ancient seawater. Acta Geol. Sin. 82, 610–621.

Zhang, J., Hu, W., Qian, Y., Wang., X., Cao, J., Zhu, J., Li, Q., Xie, X., 2009. Formation of saddle dolomites in Upper Cambrian carbonates, western Tarim Basin (northwest China): Implications for fault-related fluid flow. Marine and Petroleum Geology 26, 1428–1440.

Zhang, L., Jiao, Y., Rong, H., Li, R., Wang, R., 2017. Origins and Geochemistry of oolitic dolomite of the Feixianguan Formation from the Yudongzi Outcrop, Northwest Sichuan Basin, China. Minerals 7, 120.

Zhong, S., Mucci, A., 1995. Partitioning of rare earth elements (REEs) between calcite and seawater solutions at 25 ^{o}C and 1 atm, and high dissolved REE concentrations. Geochim. Cosmochim. Act 59 (3), 443–453.

Zhu, M.-Y., Zhang, J.-M., Li, G.-X., Yang, A.-H., 2004. Evolution of C isotopes in the Cambrian of China: implications for Cambrian subdivision and trilobite mass extinctions. Geobios 37, 287–301.

Zhu, M.-Y., Babcock, L.E., Peng, S.C., 2006. Advances in Cambrian stratigraphy and paleontology: integrating correlation techniques, paleobiology, taphonomy and paleoenvironmental reconstruction. Paleoworld 15, 217–222.

Appendix 1 Samples IDs, description, Formation, and isotopic and elemental compositions of Belle Isle dolomites.

Sample id NF-02	Formation	Dolomite Phase	δ^{13}C$_{VPDB}$ ‰	δ^{18}O$_{VPDB}$ ‰	CaCO$_3$ %	MgCO$_3$ %	Sr (ppm)	Fe (ppm)	Mn (ppm)	Al (ppm)	P (ppm)	Ni (ppm)	Cu (ppm)	Th (ppm)	U (ppm)	V (ppm)	Mo (ppm	La (ppm)	Ce (ppm)	Pr (ppm)	Nd (ppm)	Sm (ppm)	Eu (ppm)	Gd (ppm)	Tb (ppm)	Dy (ppm)	Ho (ppm)	Er (ppm)	Tm (ppm)	Yb (ppm)	Lu (ppm)	∑REE (ppm)
2.25	Petit Jardin	D1	-0.6	-4.8	55.2	44.8	94	4087	515	1879	44	4.6	1.9	0.15	0.40	4.04	0.24	2.36	4.87	0.51	1.89	0.31	0.08	0.30	0.04	0.21	0.04	0.11	0.02	0.10	0.01	10.85
3.95	Petit Jardin	D1	-0.9	-6.4	55.7	44.3	120	9681	1215	9002	261	9.8	2.4	1.95	1.10	17.07	0.42	31.14	77.59	7.40	25.86	3.61	0.70	3.24	0.39	1.82	0.35	0.95	0.14	0.96	0.14	154.32
6.15	Petit Jardin	D1	-0.6	-6.1	55.0	45.0	68	4490	476	1048	96	3.0	0.9	0.03	0.36	3.16	0.21	2.00	4.39	0.47	1.76	0.30	0.08	0.30	0.04	0.21	0.04	0.10	0.01	0.07	0.01	9.78
6.36	Petit Jardin	D1	-0.8	-6.1	49.8	50.2	57	8592	552	872	45	5.8	1.7	0.17	0.52	4	0.60	2.22	5.22	0.56	2.20	0.38	0.09	0.42	0.00	0.25	0.00	0.11	0.00	0.08	0.00	11.53
10.88	Petit Jardin	D1	-0.5	-5.5	55.6	44.4	78	8356	887	3501	142	5.1	1.5	0.30	0.68	10.14	0.15	4.53	11.17	1.23	4.75	0.92	0.24	0.89	0.14	0.73	0.14	0.35	0.05	0.32	0.04	25.48
14.04	Petit Jardin	D1	-0.5	-7.1	55.4	44.6	78	6307	596	2598	63	4.2	3.5	0.23	0.59	4.24	0.14	2.72	6.63	0.71	2.74	0.51	0.13	0.51	0.08	0.39	0.08	0.20	0.03	0.17	0.02	14.91
20.97	Petit Jardin	D1	-0.3	-6.7	55.7	44.3	94	12891	1587	4547	104	6.3	0.9	0.73	0.78	13.78	0.00	5.33	13.73	1.57	6.22	1.28	0.36	1.31	0.22	1.21	0.23	0.59	0.08	0.47	0.07	32.67
23.81	Petit Jardin	D1	-0.5	-5.3	55.1	44.9	112	9648	1119	13124	251	12.4	4.3	1.81	0.43	12.22	0.19	10.73	28.23	2.70	10.67	1.99	0.52	2.00	0.29	1.55	0.31	0.80	0.12	0.73	0.11	60.74
26.83	Petit Jardin	D1	-0.7	-4.1	55.4	44.6	114	15884	881	23058	274	11.1	6.5	6.39	0.87	19.49	0.44	13.97	30.56	3.38	12.61	2.18	0.49	2.10	0.30	1.61	0.33	0.90	0.13	0.85	0.12	69.53
29.49	Petit Jardin	D1	-1.7	-4.3	50.4	49.6	85	10245	736	4706	133	8.7	6.8	0.99	2.13	13	1.29	5.79	12.66	1.39	5.25	0.91	0.20	0.96	0.12	0.63	0.11	0.30	0.00	0.27	0.00	28.58
33	Petit Jardin	D1	-1.5	-4.7	51.8	48.2	128	37967	632	40680	510	25.2	1.1	6.53	0.81	42.80	0.17	17.30	37.27	4.30	16.54	2.87	0.75	2.69	0.36	1.82	0.35	0.94	0.14	0.90	0.13	86.36
33.8	Petit Jardin	D1	-2.1	-5.1																												
34.1	Petit Jardin	D1	-2.0	-7.4	49.4	50.6	84	11816	679	3743	178	5.2	1.2	1.18	0.16	17	4.68	6.13	15.16	1.65	6.29	1.12	0.23	1.12	0.00	0.74	0.00	0.35	0.00	0.31	0.00	33.10
36.43	Petit Jardin	D1	-1.4	-4.7	46.4	53.6	201	82673	720	75238	636	39.0	11.7	9.86	1.22	69.90	0.28	22.04	46.69	5.37	20.22	3.42	0.75	3.15	0.42	2.06	0.40	1.05	0.16	1.03	0.15	106.92
40.26	Petit Jardin	D1	-1.4	-5.6	55.7	44.3	93	10439	547	18173	1086	7.1	25.0	2.53	2.02	32.49	1.81	8.40	22.89	2.84	12.08	2.33	0.52	2.24	0.29	1.44	0.27	0.71	0.10	0.69	0.10	54.89
43.78	Petit Jardin	D1	-1.5	-6.8	55.5	44.5	60	6494	555	1912	72	2.0	0.5	0.18	0.29	3.57	0.41	4.83	11.57	1.21	4.67	0.83	0.20	0.87	0.12	0.61	0.12	0.30	0.04	0.27	0.04	25.69
49.15	Petit Jardin	D1	-2.4	-8.4	57.0	43.0	53	8023	494	1293	70	4.1	1.4	0.14	0.42	11.87	0.73	3.63	8.55	0.91	3.48	0.60	0.16	0.62	0.08	0.42	0.08	0.20	0.03	0.17	0.03	18.96
50.83	March Point	D1	-2.2	-6.8	50.1	50.6	49	12883	573	1471	30	7.4	4.38	0.30	0.70	18	1.82	3.80	9.44	1.01	3.88	0.70	0.16	0.74	0.00	0.51	0.00	0.24	0.00	0.20	0.00	20.69
53.21	March Point	D1	-2.2	-7.1	54.6	45.4	106	27129	913	29695	783	30.4	35.7	3.22	0.79	36.09	0.24	13.28	35.34	4.14	17.05	3.28	0.86	3.10	0.43	2.19	0.42	1.06	0.15	0.98	0.14	82.42
55.29	March Point	D1	-2.2	-6.8	46.1	50.6	30	27670	296	37612	635	34.5	22.3	5.79	0.83	79	1.00	18.57	46.60	5.77	21.80	3.51	0.72	3.50	0.42	1.85	0.33	0.87	0.11	0.79	0.11	104.94
59.89	March Point	D1	-2.0	-6.4	50.5	50.6	81	37293	770	3821	1697	17.9	9.3	0.84	0.64	36	7.16	16.36	39.95	5.69	23.33	4.54	1.07	4.39	0.57	2.50	0.41	0.96	0.11	0.76	0.09	100.72
62.22	March Point	D1	-1.7	-6.9	53.5	46.5	46	10903	833	1557	31.1	7.3	2.2	0.32	0.60	4.28	3.01	6.10	12.52	1.66	6.14	0.99	0.24	0.92	0.13	0.63	0.12	0.30	0.04	0.26	0.04	30.07
67.97	March Point	D1	-0.8	-7.1	55.5	44.5	101	52802	855	2363	150	8.3	5.1	0.17	0.51	2.90	0.00	2.04	4.70	0.57	2.20	0.39	0.09	0.39	0.05	0.27	0.05	0.13	0.02	0.12	0.02	11.04
80.22	March Point	D1	-0.8	-8.8	54.5	45.5	43	17160	1160	3249	91	29.1	8.4	1.06	2.35	17.31	3.44	2.10	4.36	0.47	1.77	0.30	0.068	0.28	0.042	0.23	0.048	0.14	0.02	0.15	0.02	10.00
92.8	March Point	D1	-0.1	-6.4	56.4	43.6	85	23306	1480	7829	165	8.2	3.2	1.09	1.81	7.49	0.57	2.76	5.65	0.66	2.53	0.42	0.096	0.39	0.055	0.28	0.057	0.16	0.02	0.16	0.02	13.27
96.72	March Point	D1	0.3	-6.7	55.3	44.7	61	9365	443	5422	154	6.1	2.6	0.54	0.65	5.05	0.36	2.33	5.26	0.63	2.46	0.43	0.10	0.38	0.06	0.29	0.06	0.16	0.02	0.16	0.02	12.38
97.74	March Point	D1	0.2	-6.6	54.8	45.2	71	6732	397	4200	113	3.7	1.7	0.44	0.60	3.83	0.00	1.90	4.11	0.50	1.88	0.32	0.08	0.29	0.04	0.23	0.05	0.13	0.02	0.12	0.02	9.70
103	March Point	D1	-0.1	-7.0	55.4	44.6	74	19410	866	7147	140	5.9	27.4	1.58	0.31	9.19	0.31	6.64	16.59	2.25	8.77	1.56	0.37	1.40	0.20	1.02	0.19	0.48	0.07	0.43	0.06	40.03
105.34	March Point	D1	0.1	-6.7	55.8	44.2	118	36831	770	28325	363	19.4	22.7	5.68	0.69	26.54	0.70	14.58	29.52	3.41	12.98	2.25	0.54	2.06	0.28	1.46	0.28	0.75	0.11	0.74	0.11	69.06
107.34	March Point	D1	-0.6	-6.9	55.7	44.3	81	22259	1184	14491	134	5.0	1.5	1.86	0.68	13.87	0.21	8.38	19.47	2.61	9.87	1.57	0.35	1.44	0.18	0.85	0.16	0.38	0.05	0.33	0.05	45.69
114.53	March Point	D1	-0.4	-7.3	51.2	48.8	81	22550	1101	5729	135	4.9	1.4	0.98	0.31	9	0.76	6.11	13.01	1.54	5.92	1.06	0.23	1.05	0.14	0.73	0.13	0.35	0.00	0.32	0.00	30.58
116.24	March Point	D1	-0.1	-7.0	51.9	48.1	70	26951	927	7933	109	8.2	8.8	1.16	0.29	10	1.94	4.54	10.10	1.21	4.59	0.82	0.19	0.81	0.11	0.53	0.10	0.26	0.00	0.25	0.03	23.55
119.85	March Point	D1	-0.1	-6.7	56.8	43.2	86	23528	1254	10327	231	10.0	2.1	1.76	0.54	15.03	0.42	6.14	12.44	1.44	5.51	0.94	0.24	0.88	0.12	0.62	0.12	0.33	0.05	0.31	0.05	29.19
125	March Point	D1	-0.5	-7.3																												
134.42	Hawke Bay	D1	-3.9	-9.0																												
142	Hawke Bay	D1	-3.7	-10.9																												
145.03	Hawke Bay	D1	-3.6	-7.5	55.9	44.1	264	83975	2261	56847	306	21.9	6.6	10.73	2.39	48.48	0.82	27.88	55.26	5.40	17.32	2.16	0.63	2.24	0.29	1.54	0.33	1.00	0.16	1.12	0.17	115.50
175.55	Hawke Bay	D1	-3.7	-8.1																												
49.15	March Point	D2	-2.7	-9.7	53.0	47.0	40	11508	510									5.028	11.116	1.171	4.554	0.793	0.186	0.759	0.105	0.549	0.109	0.286	0.041	0.264	0.039	1.81
59.89	March Point	D2	-1.7	-6.4	55.5	44.5	101	52802	855									17.652	39.558	4.887	18.634	3.334	0.803	3.163	0.438	2.238	0.434	1.094	0.154	0.965	0.138	1.06
59.89	March Point	D2	-1.8	-6.1																												
62.22	March Point	D2	-1.3	-7.0																												
62.22	March Point	D2	-1.7	-6.9	53.5	46.5	46	10903	833									6.096	12.517	1.657	6.137	0.985	0.243	0.924	0.127	0.626	0.121	0.300	0.042	0.259	0.039	0.60
67.97	March Point	D2	-1.0	-8.1	52.3	47.7	54	4523	334									3.550	7.577	0.897	3.391	0.562	0.116	0.504	0.067	0.336	0.063	0.163	0.024	0.156	0.024	0.57
80.22	March Point	D2	-0.8	-8.8	54.5	45.5	43	17160	1160									2.099	4.360	0.465	1.769	0.302	0.068	0.282	0.042	0.233	0.048	0.137	0.022	0.152	0.023	2.35
92.8	March Point	D2	-0.1	-6.4	56.4	43.6	85	23306	1480									2.759	5.653	0.662	2.533	0.419	0.096	0.386	0.055	0.281	0.057	0.158	0.024	0.158	0.025	1.81
97.74	March Point	D2	0.3	-7.0																												
107.34	March Point	D2	-0.6	-7.9	55.7	44.3	81	22259	1184									8.383	19.469	2.610	9.867	1.574	0.348	1.438	0.185	0.854	0.156	0.380	0.052	0.329	0.048	0.68
119.85	March Point	D2	-0.1	-6.7	56.8	43.2	86	23528	1254									6.138	12.439	1.442	5.508	0.937	0.242	0.880	0.120	0.621	0.123	0.330	0.049	0.312	0.048	0.54
134.42	Hawke Bay	D2	-4.2	-9.5																												
134.42	Hawke Bay	D2	-3.8	-9.1																												
145.03	Hawke Bay	D2	-3.5	-7.1	58.0	42.0	90	60803	2471									6.822	16.233	1.682	6.848	1.379	0.404	1.528	0.240	1.415	0.302	0.844	0.131	0.886	0.138	0.65
20.97	Petit jardin	D3			57.2	42.8	43	22265	699									15.767	66.270	11.947	52.981	12.352	3.286	11.529	1.710	8.034	1.344	2.789	0.304	1.570	0.201	0.01
29.49	Petit jardin	D3	-1.5	-11.5																												
29.49	Petit jardin	D3	-1.5	-11.3																												
50.83	March Point	D3	-2.3	-9.2	55.5	44.5	37	22604	872									6.548	28.290	3.837	15.622	2.805	0.653	2.613	0.382	1.987	0.386	0.961	0.130	0.789	0.116	0.10
67.97	March Point	D3	-1.0	-8.8	56.6	43.4	66	12854	795									12.228	50.187	6.525	23.907	3.035	0.525	2.856	0.327	1.382	0.247	0.555	0.071	0.407	0.057	0.01
80.22	March Point	D3	-0.7	-10.3	55.6	44.4	39	15629	1121									2.821	8.926	1.150	4.442	0.691	0.102	0.586	0.076	0.354	0.066	0.168	0.025	0.167	0.026	0.62
92.8	March Point	D3	-0.3	-6.4	56.7	43.3	82	21159	1583									1.725	3.432	0.399	1.504	0.257	0.061	<LD	0.036	0.181	0.037	0.099	0.014	0.092	0.015	0.58
92.8	March Point	D3	-0.3	-7.0	56.2	43.8	34	16509	986									3.857	14.473	2.069	8.138	1.382	0.374	1.241	0.161	0.697	0.114	0.238	0.027	0.147	0.021	0.02
96.72	March Point	D3	-0.3	-9.8	55.8	44.2	44	12690	701									3.154	15.149	2.421	9.809	1.812	0.325	1.542	0.227	1.124	0.202	0.481	0.065	0.411	0.060	0.19
96.72	March Point	D3	-0.3	-9.9	54.6	45.4	40	11480	689									3.287	13.805	2.169	8.707	1.599	0.300	1.342	0.200	0.974	0.173	0.410	0.056	0.355	0.052	0.13
97.74	March Point	D3	-0.4	-11.7	56.1	43.9	38	21414	1130									3.298	21.499	3.626	14.857	2.461	0.398	2.037	0.258	1.111	0.192	0.426	0.052	0.303	0.042	0.06
97.74	March Point	D3	-0.3	-11.4																												

Appendix 2 Microthermometric measurements of two-phase fluid inclusions from the Port au Port Group carbonates in the Belle Isle strai

D2 Flinc Samples

Sample #	T_{h} (^{O}C)	$T_{m(ice)}$(^{O}C)	Freezing point depress	Eq. wt% NaCl
1	98.7	-17.3	17.3	20.4
2	89.2	-17.1	17.1	20.3
3	86.1	-17.7	17.7	20.7
4	88.3	-14.2	14.2	18.0
5	90.3	-16.3	16.3	19.7
6	87.8	-15.7	15.7	19.2
7	98.3	-13.5	13.5	17.3
8	92.9	-15.2	15.2	18.8
9	83.8	-23.9	23.9	24.9
10	88.4	-20.2	20.2	22.5
11	78.2	-23.9	23.9	24.9
12	83.8	-20.2	20.2	22.5
13	79.4	-17.9	17.9	20.9
14	97.9	-19.4	19.4	22.0
15	81.7	-21.1	21.1	23.1
16	100.2	-17.5	17.5	20.6
17	91	-19.8	19.8	22.2
18	88.4	-22.9	22.9	24.3

D3 Flinc Samples

Sample #	T_{h} (^{O}C)	$T_{m(ice)}$ (^{O}C)	Freezing point depress	Eq. wt% NaCl
1	117.4	-19.5	19.5	22.0
2	125.6	-12	12.0	16.0
3	107.9	-15.5	15.5	19.0
4	113.5	-14.9	14.9	18.6
5	107.8	-13.8	13.8	17.6
6	122.5	-24.6	24.6	25.3
7	116.4	-20.3	20.3	22.6
8	106.5	-5.6	5.6	8.7
9	116.4	-7.8	7.8	11.5
10	120.6	-7.9	7.9	11.6
11	120.6	-23.2	23.2	24.5
12	112.8	-10.1	10.1	14.0
13	106.5	-16.9	16.9	20.1
14	113.5	-16	16.0	19.4
15	114.5	-20.4	20.4	22.6
16	109.8	-16	16.0	19.4
17	98	-20.4	20.4	22.6
18	98	-20.4	20.4	22.6
19	98	-17.5	17.5	20.6
20	110	-28.3	28.3	27.6
21	95.5	-17.5	17.5	20.6
22	97.5	-20	20.0	22.4
23	105.8	-20.1	20.1	22.4
24	113.2	-20.8	20.8	22.9
25	110.8	-18.8	18.8	21.5
26	96.2	-23.6	23.6	24.7
27	106.6	-20.8	20.8	22.9
28	108.7	-21.2	21.2	23.2
29	108.7	-21.4	21.4	23.3
30	121.6	-32.8	32.8	30.5
31	97.4	-22.7	22.7	24.1
32	115.1	-26.4	26.4	26.4
33	116.7	-26.4	26.4	26.4

C3 Flinc Samples

Sample #	T_{h} (^{O}C)	$T_{m(ice)}$ (^{O}C)	Freezing point depress	Eq. wt% NaCl
1	114.4	-17.9	17.9	20.9
2	110.8	-17.4	17.4	20.5
3	110.2	-18.2	18.2	21.1
4	105.6	-19.2	19.2	21.8
5	98.5	-24.8	24.8	25.5
6	118.1	-24.7	24.7	25.4
7	110.9	-22.8	22.8	24.2
8	93.3	-20.2	20.2	22.5
9	112.9	-22.6	22.6	24.1
10	104.4	-20.7	20.7	22.8
11	100.8	-19.7	19.7	22.2
12	106.8	-21.2	21.2	23.2
13	107.6	-21.8	21.8	23.6
14	97.4	-22.3	22.3	23.9
15	97.4	-19.6	19.6	22.1
16	93.6	-20.6	20.6	22.8
17	108.1	-22.1	22.1	23.8

Appendix 3 Sample IDs with description showing results of fluid inclusion gas analysis

Sample ID	**43.78 - D1**						Weighted Mean
Lab code #	9909a	9909b	9909c	9909d	9909e	9909f	
H_2	0.0000	0.0000	0.0000	0.0031	0.0025	0.0037	0.0021
He	0.0018	0.0033	0.0015	0.0043	0.0037	0.0049	0.0036
CH_4	0.2641	0.4153	0.2821	0.6926	0.7151	0.7995	0.6001
H2O	98.8349	98.4380	98.2919	97.0956	97.3557	96.5008	97.4547
N_2	0.0257	0.0342	0.0000	0.0000	0.0014	0.0000	0.0064
O_2	0.0000	0.0009	0.0007	0.0003	0.0002	0.0007	0.0005
Ar	0.0001	0.0011	0.0006	0.0018	0.0010	0.0010	0.0011
CO_2	0.8733	1.1072	1.4233	2.2023	1.9204	2.6894	1.9315

Sample ID	**97.74 - D1**									Weighted Mean
Lab code #	9914a	9914b	9914c	9914d	9914e	9914f	9914g	9914h	9914j	
H_2	0.0069	0.0062	0.0147	0.0133	0.0152	0.0137	0.0189	0.0201	0.0268	0.0148
He	0.0054	0.0123	0.0071	0.0164	0.0123	0.0088	0.0189	0.0132	0.0164	0.0126
CH_4	20.3523	23.7069	25.3146	30.0629	34.2852	37.0644	51.0208	41.2743	43.0926	35.4172
H2O	66.3296	64.8160	61.8545	59.5419	51.9572	43.7960	27.9653	34.3717	41.1839	47.4653
N_2	9.2701	8.7518	9.0225	6.8706	9.8756	12.8460	14.9331	15.1218	11.6313	11.7333
O_2	0.0010	0.0008	0.0010	0.0006	0.0015	0.0012	0.0015	0.0018	0.0013	0.0013
Ar	0.1121	0.0998	0.0824	0.0643	0.1003	0.1530	0.1882	0.2113	0.1137	0.1419
CO_2	3.9226	2.6061	3.7032	3.4300	3.7527	6.1170	5.8535	8.9858	3.9340	5.2136

Sample ID	**62.22 - D2**								Weighted Mean
Lab code #	9911b	9911c	9911d	9911e	9911f	9911g	9911h	9911j	
H_2	0.0103	0.0114	0.0033	0.0060	0.0048	0.0107	0.0133	0.0092	0.0062
He	0.0033	0.0033	0.0018	0.0034	0.0045	0.0029	0.0062	0.0022	0.0035
CH_4	7.2993	9.1327	11.3207	16.1864	15.5373	12.2037	12.4398	12.9290	14.0083
H2O	91.9647	90.0905	88.0597	82.8275	83.4830	86.3130	86.5043	85.8962	85.0358
N_2	0.2571	0.3086	0.2791	0.3760	0.3333	0.3457	0.2612	0.3707	0.3289
O_2	0.0012	0.0000	0.0002	0.0002	0.0002	0.0004	0.0004	0.0003	0.0002
Ar	0.0016	0.0016	0.0012	0.0014	0.0013	0.0019	0.0013	0.0021	0.0014
CO_2	0.4625	0.4519	0.3342	0.5991	0.6355	1.1218	0.7736	0.7904	0.6156

Sample ID	**196.92 - D2**							Weighted
Lab code #	9916a	9916b	9916c	9916d	9916e	9916f	9916g	Mean
H_2	0.0000	0.0000	0.0033	0.0047	0.0049	0.0055	0.0048	0.0044
He	0.0000	0.0007	0.0001	0.0003	0.0002	0.0004	0.0002	0.0002
CH_4	0.1251	0.2359	0.2791	0.2874	0.3089	0.3473	0.2839	0.2973
H2O	97.2872	96.7061	94.9547	96.0151	96.6901	96.2122	96.6253	96.1907
N_2	1.0045	1.6846	2.1230	1.2947	0.8639	1.1319	1.2527	1.2737
O_2	0.0005	0.0000	0.0011	0.0004	0.0002	0.0003	0.0004	0.0004
Ar	0.0152	0.0187	0.0341	0.0211	0.0155	0.0194	0.0195	0.0209
CO_2	1.5674	1.3540	2.6047	2.3764	2.1163	2.2830	1.8132	2.2122

Sample ID	**80.22 - D3**									Weighted
Lab code #	9912a	9912b	9912c	9912d	9912e	9912f	9912g	9912h	9912j	Mean
H_2	0.0120	0.0082	0.0024	0.0085	0.0034	0.0013	0.0000	0.0053	0.0040	0.0024
He	0.0099	0.0065	0.0063	0.0075	0.0043	0.0059	0.0048	0.0061	0.0047	0.0055
CH_4	12.6296	6.8524	6.7557	8.9773	6.0888	6.0799	6.1395	9.0660	6.5236	6.6124
H2O	85.3383	92.0868	92.4940	89.9106	92.7759	93.1679	93.0962	89.7059	92.4808	92.5060
N_2	0.5705	0.2767	0.2665	0.2918	0.1930	0.2353	0.2145	0.3384	0.2086	0.2412
O_2	0.0009	0.0005	0.0002	0.0004	0.0002	0.0002	0.0002	0.0004	0.0002	0.0002
Ar	0.0041	0.0024	0.0017	0.0018	0.0021	0.0017	0.0017	0.0023	0.0019	0.0018
CO_2	1.4347	0.7666	0.4733	0.8021	0.9324	0.5078	0.5431	0.8755	0.7762	0.6305

Sample ID	**96.72 - D3**								Weighted
Lab code #	9913a	9913b	9913c	9913d	9913e	9913f	9913g	9913h	Mean
H_2	0.0087	0.0058	0.0052	0.0119	0.0048	0.0113	0.0026	0.0054	0.0050
He	0.0048	0.0021	0.0031	0.0051	0.0071	0.0094	0.0041	0.0059	0.0054
CH_4	7.1649	5.4414	11.2427	7.8356	8.8180	12.8433	9.0554	16.1114	10.2474
H2O	91.7915	93.3045	87.5324	91.1143	90.4539	85.9162	89.7073	82.4398	88.5926
N_2	0.5348	0.7225	0.7232	0.4411	0.3828	0.6042	0.5802	0.7776	0.5797
O_2	0.0006	0.0007	0.0002	0.0006	0.0002	0.0004	0.0003	0.0004	0.0004
Ar	0.0023	0.0033	0.0031	0.0020	0.0014	0.0024	0.0028	0.0030	0.0025
CO_2	0.4924	0.5197	0.4901	0.5894	0.3318	0.6129	0.6473	0.6565	0.5670